Copyright Warning & Restrictions

ABSTRACT

**A DETAILED PARAMETER STUDY INTO THE DERMAL ABSORPTION OF
CHEMICAL WARFARE AGENTS AND THE EFFECTS OF
PHARMACOKINETICS**

by

Koko Lear

Chemical warfare agents (CWAs) are substances of varying toxicity profiles. These chemicals exhibit complex dynamics and pose a serious health risk when released into the environment. A mathematical model based on Fick's second law of diffusion was developed to comprehend how these compounds were absorbed into the skin. The analysis applied to both small and large doses and, successfully, predicted experimental results. This work also includes the effects of CWA physicochemical properties on evaporation and dermal absorption through the stratum corneum. A sensitivity analysis was conducted to assess the impacts of small variations in the initial dose, environmental conditions, and key model parameters (e.g., diffusion coefficient) on the permeation kinetics. In addition, a concept-based assessment about the roles of skin metabolism and binding is also presented. Our results show that the diffusion coefficient, the ratio of the steady-state evaporation rate to the steady-state absorption rate, and the initial dose impact the cumulative amount of permeant absorbed or evaporated.

A DETAILED PARAMETER STUDY INTO THE DERMAL ABSORPTION OF CHEMICAL WARFARE AGENTS AND THE EFFECTS OF PHARMACOKINETICS

by

Koko Lear

A Dissertation
Submitted to the Faculty of
New Jersey Institute of Technology
in Partial Fulfillment of the Requirements for the Degree of
Master of Science in Pharmaceutical Engineering

Otto H. York Department of
Chemical and Materials Engineering

May 2022

APPROVAL PAGE

A DETAILED PARAMETER STUDY INTO THE DERMAL ABSORPTION OF CHEMICAL WARFARE AGENTS AND THE EFFECTS OF PHARMACOKINETICS

Koko Lear

Dr. Laurent Simon, Dissertation Advisor	Date
Professor of Chemical and Materials Engineering, NJIT	

Dr. Roman Voronov, Committee Member	Date
Associate Professor of Chemical and Materials Engineering, NJIT	

Dr. Sagnik Basuray, Committee Member	Date
Associate Professor of Chemical and Materials Engineering, NJIT	

Dr. Piero Armenante, Committee Member	Date
Distinguished Professor, Chemical & Materials Engineering, NJIT	

BIOGRAPHICAL SKETCH

Author: Koko Lear

Degree: Master of Pharmaceutical Engineering

Date: May 2022

Date of Birth:

Place of Birth:

Undergraduate and Graduate Education:

- Master of Science in Pharmaceutical Engineering,
  New Jersey Institute of Technology, Newark, NJ, 2022

- Bachelor of Science in Chemical Engineering,
  New Jersey Institute of Technology, Newark, NJ, 2021

Major: Pharmaceutical Engineering

Presentations and Publications:

Lear, K., Simon, L. (2022), **"A Method to Assess Dermal Absorption Dynamics of Chemical Warfare Agents: Finite Doses of Volatile Compounds,"** *Submitted for publication*.

DEDICATION

I dedicate my dissertation work to my close support network. Many thanks to Aris for helping me to develop key technological skills and being the best tutor I ever had. I also dedicate this dissertation to partner, Juan, who has been a constant show of support for me throughout the process of both my graduate school and life. And finally, to my friends who have reminded me about the importance of stopping to smell the roses.

I will always appreciate all they have done during this chapter of my life.

ACKNOWLEDGMENT

Throughout the writing process of this dissertation, I have received a great deal of support and assistance.

First and foremost, I would like to thank my advisor, Dr. Laurent Simon, whose proficiency, and subject knowledge was invaluable and abundant in formulating the research paper structure and theoretical sections. Your mentorship and detailed feedback pushed me out of my comfort zone and drove me to broaden my skillset to bring my work to a higher level.

I would also like to acknowledge the support I have received from each of my committee members. Dr. Roman Voronov, who is the reason this dissertation exists, has kindly extended a recommendation to my advisor about my qualifications for the collaboration. My background and theoretical understandings are owed to Dr. Piero Armenante. With his tutelage in my many graduate and undergraduate courses, I had a comprehensive prior understanding of the many topics I am covering in this dissertation. Finally, my writing prowess is thanks to Dr. Sagnik Basuray. His feedback in my past laboratory reports has provided me with an introductory understanding of scientific writing.

Finally, I would like to thank the United States Army for their financial contributions and support for this project.

TABLE OF CONTENTS

TABLE OF CONTENTS
(Continued)

LIST OF TABLES

LIST OF FIGURES

Figure   **Page**

LIST OF SYMBOLS

Symbol	Parameter Description	Unit
D_{sc}	Diffusion coefficient in the stratum coenrum	cm^2/s
D	Diffusion coefficient in the air	cm^2/s
f_{dep}	Fractional depth	-
h	Thickness of stratum corneum	cm
k_g	Gas phase mass transfer coefficient	cm/hr
K_{ow}	Octanol-water partition coefficient	-
k_p	Permeability coefficient	cm/hr
L	Characteristic length	cm
M_0	Initial finite dermal dose	-
MW	Molecular weight	g/mol
n_c	Number of carbon atoms	-
n_h	Number of hydrogen atoms	-
n_n	Number of nitrogen atoms	-
n_o	Number of oxygen atoms	-
n_{ring}	Number of ring systems	-
P_{vap}	Vapor pressure	torr
$t_{eff,abs}$	Effective time constant of absorption	hr
$t_{eff,evap}$	Effective time constant of evaporation	hr
R	Gas constant	mLTorr/ K-mmol
Sum	Sum of molecular components	-
S_w	Water solubility	mg/mL
T	Temperature	K
t	Time	hr
u	Velocity	cm/s
κ	Ratio of the steady-state evaporation rate to the steady-state dermal absorption rate	-

K_i	Inhibition constant of the second reaction for Drug A	g/L
a,b,c	Coefficients of Drug A, B, and C	-
H	Thickness of intact skin	cm
x	Distance from surface of skin	cm
B	Michaelis-Menten kinetics parameters	g/L
C	Drug concentration in the skin	g/L
ρ	Binding rate constant based on dual absorption model	-
q	Binding rate constant based on dual absorption model	L/g

LIST OF DEFINITIONS

CWA   Chemical Warfare Agent

SC   Stratum Corneum

VOC   Volatile Organic Compounds

OEL   Occupational Exposure Limit

TWA   Total Weight Average

CHAPTER 1

INTRODUCTION

1.1 Brief Background on Chemical Warfare Agents

Chemical warfare is defined as the use of toxicity of chemical compounds to kill, injure, or incapacitate an enemy in warfare and associated military operations (Chauhan et al., 2008). Chemical warfare agents (CWAs) have historically been used since ancient times with the usage of poisoned arrows and other crude chemicals in various weapon apparatuses (Black, 2016). Another instance of ancient usage dates back to 600 B.C. where the biological warfare agent, Helleborus root, was used to contaminate the water supplies in the siege of Kirrha (Chauhan et al., 2008). The usage of chemicals as a means to either combat against foes in defensive or offensive maneuvers has thus been long acknowledged as a key tactical advantage.

As time passed, designs for the release of chemicals have become more sophisticated than the previous iterations. However, the most explosive time period for CWAs has been the twentieth century as it has seen the full capabilities of CWAs in a world war, a regional conflict, and the first instance of their use by terrorists (Coleman, 2005). WWI marked an important turning point for the culture of the battlefield and the views and capabilities of CWAs. Between Germany, France, Britain, the US, Austria, Italy, and Russia, it is reported that forty-six different gases were created and used in the war leading to the famous nickname for WWI being "The Chemists' War" (Freemantle, 2015). The tumultuous start of a mass scale usage of CWAs can be attributed to the German designer, Fritz Haber. Haber's creation of Germany's poison-gas weapon system started as

a response to trench warfare. Due to his work in the field of weaponized chemicals, he is now regarded as the father of modern chemical warfare (Freemantle, 2015). As a result of Haber making chemical weapons better-known from his WWI involvement, many countries soon adopted and employed similar tactics.

As such, a surge in manufacturing and delivery systems has arisen across the globe for countries to match defense systems against other nations. With this climate change, tensions have stirred for how best to contain and handle CWAs during storage and stockpiling and how to mitigate the effects of exposure. A multilateral treaty stated that every ten years CWA stockpiles much be destroyed (Chauhan et al., 2008). This legislation, enacted from the chemical weapons convention, was created to regulate better and contain CWAs to minimize harm.

Presently, methods to counteract the spread of the effects caused by exposure to various CWAs have been a growing research topic. However, choosing one simulant to represent all those CWAs is difficult because of their numerous innate properties. As a result, multiple simulants need to be chosen (Cao et al., 2020). A classification system was created to group compounds of similar properties to treat exposed victims better. CWAs are defined as one of eight different classes: nerve agents, vesicants (also known as blistering agents), blood agents, lung injurants, riot-control agents, psychotomimetic agents, toxins, and vomiting agents (K Ganesan et al., 2010). Nerve agents target the body's nervous system with typical entrance routes of either inhalation or dermal contact (Wexler & Anderson, 2014). Vesicants are defined as compounds that create severe chemical burns that may result in painful blisters and lesions to the skin (Hilmas & Hilmas, 2009). This class of CWAs is said to enter through inhalation, dermal, or ocular routes (Goswami et

al., 2018). Blood agents enter the bloodstream, typically, by inhalation or ingestion, with nausea and dizziness being the early signs of exposure. Lung injurants, also commonly called choking agents, compromise the respiratory tract, leading to victims losing breath and choking (K. Ganesan et al., 2010). Riot-control agents are the most commonly used CWA in times of war. They are applied to temporarily disarm a person when the compound contacts the eyes, skin, or is inhaled (Wexler & Anderson, 2005). As such, these agents are typically deployed for use as crowd control. Psychomimetic agents create hallucinations and are meant to incapacitate an individual by harming the central nervous system (K. Ganesan et al., 2010). Toxins are biological substances that are found in nature. They have poisonous or toxic effects (Janik et al., 2019).

Physical or chemical decontamination is usually the primary initial response to treating dermal exposure. Defining a chemical's properties increases the efficacy of decontamination to the skin's surface and back-extract chemicals from the stratum corneum's reservoir to reduce the penetration and systemic absorption of the compound (Cao et al., 2020). Research for assisting decontamination methods for chemical weapons has focused on parameter studies' importance to help create mathematical models. Current methodologies to estimate the rate of dermal absorption are based on Fick's second law, which was proven to predict and model transport through the skin successfully (Kasting & Miller, 2006). Therefore, an application utilizing computational programming can help improve risk assessment and estimate the time window to respond to chemical exposure.

1.2 Literature Review

The skin is a crucial organ to study when considering how compounds can freely interact with it. As the largest and most complex organ of the human body (Mueller, 2017), the

skin is comprised of various protective layers and mechanical barriers like hair follicles (Gorzelanny et al., 2020), which serve as protection from the environment. The stratum corneum (SC) is the outermost layer of the skin and thus the first barrier that guards against external threats. The stratum corneum is regarded as the major barrier for most permeants and, as such, is the focus of many steady-state and transient models (Dancik et al.). This layer has a rate-limiting mechanism for transdermal uptake as it delays penetration into the viable epidermis and below (Gorzelanny et al., 2020).

Another important aspect of dermal investigation lies in the skin layer's thickness. The hydration of the skin layer varies significantly from person to person. The stratum corneum is estimated to be $10 - 15$ µm thick (Andrews et al., 2013). A partially hydrated stratum corneum differs from a fully hydrated one in the way compounds are absorbed or evaporated. As humans age, their skin changes texture and appearance. Wrinkles, elasticity, and moisturization will vary from a teen to an older person (Boireau-Adamezyk et al., 2014). A linear regression, performed using a sample group of ages 18-30, 30-40, 40-55, and 55-70, showed that the stratum corneum thickness depended on chronological aging (Boireau-Adamezyk et al., 2014). Other contributing factors that influence the thickness of the skin are related to environmental conditions. In an animal study, it was found that the SC thickness increases in low humidity (Denda et al., 1998). Likewise, exposure to higher temperatures results in a thinner SC due to moisture loss through evaporation (Blank, 1952). As such, dermal absorption can vary from person to person, especially over different environments.

1.3 Purpose of Study

An analysis of various aqueous solutions of chemical warfare agents and their associated dermal absorption rates was conducted using published equations (Frasch & Bunge, 2015). The work includes large and small dose absorption (Kasting & Miller, 2006). In these cases, the prediction accuracy depended, in part, on the accuracy of the estimated parameters. This research aims to build upon the relationships previously discussed. First, the sensitivity of the parameters will be tested to determine which ones have the most significant impact on absorption and evaporation rates through the stratum corneum only. Then, the most sensitive parameters will be used to hypothesize about external factors contributing to the release mechanism. The kinetics of small and large doses and their impacts on dermal absorption will be analyzed. Finally, the work will discuss how skin metabolism and binding influence the transport mechanism.

The thesis examines the external factors influencing the dermal absorption and evaporation of CWAs. The results will help improve monitoring methods and provide significant insight into these compounds' complex nature and how they travel through this biological barrier. In addition, the approach can lead to better risk prevention strategies. For instance, decontamination is crucial to prevent harmful toxins from spreading to the body. However, current decontamination procedures may limit the amount of chemicals that can be effectively removed. Research on pharmacokinetics could potentially prove instrumental in improving conventional methods or developing new ones.

1.4 Risks from Exposure to Chemical Warfare Agents

Regularly, the human skin is exposed to many chemicals throughout the day. Whether it be particulates through the air, topical moisturizing lotions, or fibers from clothing, the skin is vulnerable to foreign exposure. Clothing and lotions are materials that come in contact

with the skin and may pose low or high risks depending on their characteristics. A lack of knowledge of how chemicals from these materials are absorbed and diffused through the dermal layer can be detrimental.

Many people live in an area where the air is clean enough that particle pollution is not a significant threat. However, individuals are more likely exposed to harmful chemicals in high-risk areas where they use or transport CWAs. These agents have been deployed for biological and chemical warfare for a long time. Therefore, researchers studied their properties as they represent a severe risk to the public. Toxicological data typically list the entry route and the risk level. For example, lewisite is labeled a vesicating agent because it causes blisters on exposed skin (Bakshi et al., 2000).

This report will analyze the effects of CWA characteristics on dermal absorption and evaporation rates. According to relationships published in (Kasting & Miller, 2006), most CWAs, even those that mostly evaporate, pose a dermal absorption risk because of their intrinsic properties. Therefore, it is essential to fully understand these features and their implications to better leverage the information for emergency management or planned mitigation responses. In addition, the role of environmental conditions on the effects on kinetics deserves careful consideration.

1.5 Introduction to the Model Parameters

According to (Wartell et al., 1999), meteorological patterns local to the army's position were used to predict the movement of the gas clouds in WWI. Even though this method was largely ineffective, it shows an early understanding of the effects of input parameters on transdermal absorption. This research explored the direct impact of the diffusion

coefficient, the ratio κ, and exposure concentration on the skin's absorption rate. The knowledge of environmental conditions and physicochemical properties can provide crucial insight into transdermal toxicity. Even though the model can capture the complex physics and mechanisms of mass transport, its accuracy still relies on users' specifications. A lack of understanding of how to estimate the needed parameters and how they affect the outputs may lead to sub-optimum preventive measures. Such a disconnect could prove to be lethal.

The diffusion depends primarily on the chemical composition of the chemical warfare agent itself, as seen in Eq. (34). The molecular weight of the agent contributes to the diffusion coefficient. A large molecular weight yields a lower diffusion value, thus increasing the effective time constant of either absorption or evaporation. The composition of elements in a molecule is the main factor that affects molecular weight. Elements, such as carbon, hydrogen, nitrogen, and oxygen, impact the molecular weight amount and the diffusivity through the air. Furthermore, the geometry of the molecule matters as well. For instance, the presence of a larger ring system can decrease the diffusion through the air. Its value is directly proportional to the gas-phase mass transfer coefficient.

The ratio κ, defined in Kasting's work as equation 39 (Kasting & Miller, 2006), relates the ratio of evaporation to dermal absorption on the gas-phase mass transfer coefficient, vapor pressure, molecular weight, temperature, permeability coefficient, and solubility. Like its predecessors, it too directly impacts the finite dose transdermal uptake of CWAs. The ratio κ is directly proportional to the vapor pressure, the molecular weight, and the gas-phase mass transfer coefficient. Conversely, κ is inversely proportional to temperature, solubility, and the permeability coefficient. The heavier a chemical compound

7

is the more it tends to evaporate over absorbing into the stratum corneum. The gas-phase mass transfer coefficient (k_g) considers the fluidic properties of the compound and its relation to the environmental surroundings. Our model is set to a constant indoor air flow of 16.5 cm/s to simulate exposures of CWAs during shipping or storage. However, the model would change drastically if the turbulent nature of outside air conditions were to be instead considered. With higher wind flows, the air directly contributes to evaporating more product away from the skin. The vapor pressure, which also depends on the temperature, impacts the ratio κ.

1.6 Small and Large Dose Absorption

The absorption rate across the skin barrier and the transport mechanism are directly related to the dose size. In addition, the exposure concentration affects the decontamination efficacy, i.e., the percentage of the initial amount of the compound that can be removed from the surface (Capoun & Krykorkova, 2019). Therefore, estimating the amount absorbed when a neutralization protocol is initiated is crucial. To that end, researchers have developed equations appropriate for large and small dose applications to facilitate an improved understanding of the effects of CWAs following a topical exposure. Their work was based on Fick's second law.

The methods presented in this contribution are applied to CWA's using the Wolfram Mathematica environment. Programs will be written to aid researchers study the effect of physicochemical parameters on the percentages of chemicals absorbed and evaporated over time. The process time constant will be evaluated in the case of small doses. Researchers can adapt the tools developed to their analyses and predict the outcome of dermal exposure scenarios.

Small-dose absorption assumes that the applied dose is lower than the saturation amount in the stratum corneum. In addition, the flux at the skin's surface is proportional to the local concentration in the skin (Kasting & Miller, 2006). For large doses, the initial amount is above saturation. However, the rate at which chemicals are removed from the surface depends on the losses by evaporation and diffusion (2006). Both models apply to neat, hydrophilic-to-moderately lipophilic liquid coming into contact with the skin (2006). As such, they can model for a variety of CWAs.

1.7 Metabolism and Binding of CWAs

As toxic molecules penetrate the skin's surface, the entire body becomes at risk. CWAs pose a significant threat if the compound has a chance to travel deeper into the skin layers (i.e., viable epidermis and dermis) (Alkilani et al., 2015). Due to both the mechanistically connected diffusion and metabolism in the viable tissue, it is essential to thoroughly understand the behavior of CWA's penetrating the skin (Boderke et al., 2000). Although this work assumes negligible skin metabolism and binding, their impact can be significant in some cases. For example, the dual absorption model has successfully described the binding permeation of steroids, verapamil, and some amino acids compared to experimental results with mouse skin (Kydonieus, 2017). Furthermore, animal studies cannot fully indicate a human's metabolic effects on the skin due to significant and unpredictable variations among species (Kydonieus, 2017). So, devising methods to explain the binding and metabolism through transdermal delivery is strongly encouraged for future research.

The skin barrier is composed of proteins and a lipid matrix (van Smeden & Bouwstra, 2016). Nerve agents are toxic because of their ability to inhibit the action of

certain enzymes (Moshiri et al., 2012). The extent of skin binding depends on the compound. While metabolism occurs in the viable skin, binding occurs in the stratum corneum (Tojo, 1987). *In-vivo* studies use nonlinear saturation kinetic models to predict, more accurately, the metabolism effect (Boderke et al., 2000). A bioburden relationship between the binding rate constants, Michaelis-Menten kinetics, and the concentration of the compound was established by Tojo (1987). The fundamentals of these equations will be provided to facilitate research on the effects on metabolism and binding in the skin.

1.8 List of CWAs to be Studied

CWAs fall into eight classes: nerve agents, vesicants, blood agents, lung injurants, riot-control agents, psychotomimetic agents, toxins, and vomiting agents. This classification is based on the physiological effects of the CWAs. The following compounds will be selected for the skin absorption study: VX, sulfur mustard, hydrogen sulfide, phosgene, ethyl iodoacetate, 3-quinuclidinyl benzilate, colchicine, and adamsite. The dynamic behavior of other CWAs will be provided in the Appendix.

1.9 Proposed Work

The thesis includes a detailed introduction to CWAs and the development of a mathematical model to estimate the amount of a chemical compound that can be absorbed into the skin. The literature review section contains the usage of CWAs, the health risks they pose, and how the skin is a significant exposure route for these toxic chemicals. In addition, the compounds used in the study were selected from eight categories. The methodology was tested on published data. A discussion on small and large dose absorption

and parameter sensitivity is included. Insights into skin binding and metabolism are provided based on the absorption and evaporation results.

CHAPTER 2

THEORY

Previously, a method was developed to study the skin disposition of volatile compounds (Kasting & Miller, 2006). When a chemical warfare agent's dose is large, the permeant forms a saturated concentration at the upper layer of the stratum corneum. Section 2.1 outlines a solution procedure where the process is divided into two stages. One stage describes the stratum corneum (SC) when the upper tenth of the SC (f_{dep}) is saturated with the CWA and the other stage starts when this upper region is below saturation. The small-dose case is discussed in Section 2.2.

2.1 Large Doses: $M_0 > M_{sat}$

For large doses, the initial amount is greater than the saturated amount. The saturated amount (M_{sat}) can be determined by Eq. (25) in (H. F. Frasch, 2012).

Phase 1

Phase 1 describes the point where the pool saturates the stratum corneum's upper layer and absorption of the compound into the cell layers. The initial amount on the surface (M_{surf}) equals the dose minus the saturated amount:

$$M_{surf}\left(0\right) = M_{surf\,0} = M_0 - M_{sat} \tag{1}$$

Equation (2) represents Fick's second law of diffusion through the stratum corneum of thickness h_{sc} :

$$\frac{\partial C_{sc}}{\partial t} = D_{sc} \frac{\partial^2 C_{sc}}{\partial z^2} \tag{2}$$

where C_{SC} is the concentration of the stratum corneum with respect to time (t) and position (z), D_{sc} is the diffusion coefficient of the stratum corneum. The initial condition is represented by

$$C_{sc}(z,0) = C_{sc0}(z) = \{0; \quad f_{dep}h_{sc} < z \le h_{sc} \tag{3}$$

The boundary condition at the surface is

$$\frac{dM_{surf}}{dt} = -k_{evap}\rho - D_{sc} \left. \frac{\partial C_{sc}}{\partial z} \right|_{z=f_{dep}h_{sc}} \tag{4}$$

This mass balance equation involves accumulation and losses due to evaporation and absorption; k_{evap} is the mass transfer coefficient and ρ as the permeant density.

$$\frac{dM_{surf}}{dt} = -k_{evap}\rho - D_{sc} \left. \frac{\partial C_{sc}}{\partial z} \right|_{z=f_{dep}h_{sc}} \tag{5}$$

A perfect sink condition is applied at h_{sc}:

$$C_{sc}(h_{sc},t) = 0 \tag{6}$$

Finally, the absorption flux is determined with Fick's first law represented:

$$J_{abs}(t) = -D_{sc} \left. \frac{\partial C_{sc}}{\partial z} \right|_{z=h_{sc}} \tag{7}$$

Therefore, the amount absorbed, the flux due to evaporation and the cumulative amount of compound evaporated are given by equations (8), (9) and (10), respectively:

$$M_{abs}(t) = \int_0^t J_{abs}(\tau)d\tau \tag{8}$$

$$J_{evap}(t) = k_{evap}\rho \tag{9}$$

$$Q_{evap}(t) = k_{evap}\rho t \tag{10}$$

Phase 2

Phase 2 starts when the pool has evaporated from the surface (i.e. M_{surf}=0). The stratum corneum is divided into two regions: an upper (scu) and lower (sc) part. Again, Equation (11) and (12) apply Fick's second law of diffusion to both regions:

$$\frac{\partial C_{scu}}{\partial t} = D_{sc}\frac{\partial^2 C_{scu}}{\partial z^2} \tag{11}$$

$$\frac{\partial C_{sc}}{\partial t} = D_{sc}\frac{\partial^2 C_{sc}}{\partial z^2} \tag{12}$$

Equations (13) and (14) are the boundary conditions at $z = 0$ and $z = f_{dep}h_{sc}$:

$$\left.\frac{\partial C_{scu}}{\partial z}\right|_{z=0} = \frac{\kappa}{h_{sc}}C_{scu}(0,t) \tag{13}$$

$$\left.\frac{\partial C_{scu}}{\partial z}\right|_{z=f_{dep}h_{sc}} = \left.\frac{\partial C_{sc}}{\partial z}\right|_{z=f_{dep}h_{sc}} \tag{14}$$

The equilibrium partition condition at $z = f_{dep}h_{sc}$ is

$$C_{scu}(f_{dep}h_{sc},t) = C_{sc}(f_{dep}h_{sc},t) \tag{15}$$

The perfect sink condition is still valid:

14

$$C_{sc}\left(h_{sc},t\right)=0 \tag{16}$$

In addition, the initial conditions are

$$C_{scu}\left(z,0\right)=C_{sat} \tag{17}$$

$$C_{sc}\left(z,0\right)=C_{sc}\left(t_{p1}\right) \tag{18}$$

Finally, the amount evaporated and absorbed can be found by:

$$M_{abs}\left(t\right)=\int_{0}^{t}J_{abs}\left(\tau\right)d\tau \tag{19}$$

$$M_{evap}\left(t\right)=\int_{0}^{t}J_{evap}\left(\tau\right)d\tau \tag{20}$$

And with the fluxes:

$$J_{abs}\left(t\right)=-D_{sc}\left.\frac{\partial C_{sc}}{\partial z}\right|_{z=h_{sc}} \tag{21}$$

$$J_{evap}\left(t\right)=D_{sc}\left.\frac{\partial C_{scu}}{\partial z}\right|_{z=0} \tag{22}$$

The total amount absorbed and evaporated can be found by using the equations for phases 1 and 2.

2.2 Small Dose

A small amount of a compound can also be in direct contact with the skin barrier. Even though the dose size is below saturation, the absorption can still reach a critical amount

depending on a number of parameters. The sensitivity of these parameters and their effects will be studied in more detail in the next section.

Similar to the large dose, the starting point for the mathematical model is with Fick's second law of diffusion, represented in equation (23). Fick's second law is used to study permeation through skin because it helps predict how the concentration gradient changes with time through diffusion (Couto et al., 2014).

$$\frac{\partial C_{SC}}{\partial t} = D_{SC} \frac{\partial^2 C_{SC}}{\partial z^2} \tag{23}$$

where C_{SC} is the chemical concentration in the stratum corneum, t is the time, D_{SC} is the diffusion through the stratum corneum, and z represents the length. The location where z equal to zero denotes the position of the skin surface, while the bottom of the stratum corneum is where z is equal to h (i.e., the layer thickness). Eq. (24) is applied at $z=0$ and accounts for the loss through evaporation (H. Frasch, 2012):

$$\left.\frac{\partial C_{sc}}{\partial z}\right|_{z=0} = \frac{\kappa}{h} C_{sc}(0,t) \tag{24}$$

where κ is the ratio of the steady-state evaporation rate to the steady-state absorption rate. A perfect skin condition is imposed at $z = h$:

$$C_{SC}(h,t) = 0 \tag{25}$$

The initial condition is (H. Frasch, 2012)

$$C_{SC}(z,0) = C_{SC_0}(z) = \begin{cases} \dfrac{m_0}{f_{dep} \times h} & 0 \leq z \leq f_{dep}h \\ 0 & f_{dep}h < z \leq h \end{cases} \tag{26}$$

The parameters m_0 and f_{dep} are the initial finite dermal dose and the fractional depth through which the CWA is deposited at $t = 0$; f_{dep} is set to 0.1 and h is set at 0.00134 cm (Kasting et al., 2008). Although the system given by Eqs. (23) to (26) can be solved analytically (H. Frasch, 2012), an orthogonal collocations-based method is employed to provide a numerical solution to the partial differential equations. The technique converts the partial differential equations to a system of ordinary differential equations (ODE's) that is then solved using Mathematica. The selected approach also facilitates the integration of multiple skin layers and the effect of skin binding or metabolism into the study.

The cumulative amount of CWA absorbed and evaporated are given by

$$m_{abs}(t) = \int_0^t J_{abs}(\tau)d\tau \tag{27}$$

$$m_{evap}(t) = \int_0^t J_{evap}(\tau)d\tau \tag{28}$$

respectively, with the fluxes $J_{abs}(t)$ and $J_{evap}(t)$ defined by

$$J_{abs}(t) = -D_{SC} \left. \frac{\partial C_{SC}}{\partial z} \right|_{z=h} \tag{29}$$

and

$$J_{evap}(t) = D_{SC} \left. \frac{\partial C_{SC}}{\partial z} \right|_{z=0} \tag{30}$$

Note that m_0 is the sum of the amount of CWA absorbed ($m_{abs}(\infty)$) and evaporated ($m_{evap}(\infty)$) because binding and metabolism are not addressed in the current framework:

$$m_0 = m_{abs}(\infty) + m_{evap}(\infty) \tag{31}$$

It can be shown that the total fractions of CWA absorbed and evaporated are (H. Frasch, 2012):

$$M_{abs}(\infty) = \frac{m_{abs}(\infty)}{m_0} = \frac{2 + f_{dep}\kappa}{2 + 2\kappa} \tag{32}$$

and

$$M_{evap}(\infty) = \frac{m_{evap}(\infty)}{m_0} = \frac{2\kappa - f_{dep}\kappa}{2 + 2\kappa} \tag{33}$$

The initial applied amount m_0 is less than the M_{sat}, the mass (per unit area) of chemical necessary to saturate the top fraction of the stratum corneum (H. Frasch, 2012).

2.3 Parameter Sensitivity

A sensitivity analysis can be studied directly by using Equations (34) to (39), which are derived from Frasch and Bunge's calculations (2015). A standard characteristic length is used for the skin (Frasch & Bunge, 2015). Furthermore, volatile compounds were assumed to be transported from an aqueous vehicle, through the stratum corneum and to the bloodstream. The online database, PubChem, was utilized to find most of the parameters needed (e.g., $\log(K_{ow})$ values).

Eq. (34) represents the effective diffusion coefficient of the stratum corneum in cm^2/s.

$$D_{sc} = \frac{1}{3600} h \times 10^{-2.80-0.0056MW} \tag{34}$$

The diffusion depends on the molecular weight (*MW*). Eq. (35) is used to calculate the permeability coefficient k_p (Frasch & Bunge, 2015):

$$k_p = 10^{-2.8+0.66\log(K_{ow})-0.0056MW} \tag{35}$$

The parameter k_p (cm/h) is essential to the dermal absorption since it is the rate at which a chemical penetrates the skin. Eq. (36) calculates the sum of key molecular components of each compound, i.e., the number of carbons, hydrogens, nitrogens, oxygens, and ring systems:

$$Sum = 16.5n_C + 1.98n_H + 5.69n_N + 5.48n_O - 20.2n_{ring} \tag{36}$$

The diffusivity (cm^2/s) of the compound in the air is given by:

$$D = \frac{10^{-3} \times 298^{1.75} \left(\frac{1}{29} + \frac{1}{MW} \right)^{1/2}}{\left(Sum^{1/3} + (20.1)^{1/3} \right)^2} \tag{37}$$

The gas-phase mass transfer coefficient (cm/h)

$$k_g = 3260D^{\frac{2}{3}} \sqrt{\frac{u}{L}} \tag{38}$$

is derived by considering the fluid flow characteristics (i.e., Reynolds number) and the mass transfer properties (i.e., Nusselt number) as explained in (Geankoplis, 2018). The velocity (*u*) is set at the indoor condition of 16.5 cm/s. The characteristic length (*L*) is assumed to be 13.4 μm (Frasch & Bunge, 2015). The ratio of the steady-state evaporation

rate to the steady-state absorption rate (κ), described below, combines equations (35) and (38), the molecular weight and the water solubility parameter (mg/mL):

$$\kappa = \frac{k_g P_{vap} MW}{RT} \frac{1}{k_p S_w} \tag{39}$$

The gas constant is 62.37 mL Torr/K-mmol and the absolute temperature is 298K.

The effective time constants for absorption and evaporation are represented in equations (40) and (41) which explain the speed at which the compound reaches steady state.

$$t_{eff,abs} =$$

$$\frac{1}{30 D_{sc}} \frac{\left\{ \begin{array}{l} \left(150 - 60 f_{dep}^{\,2} + 6 f_{dep}^{\,4}\right) h^2 + \left(84 + 75 f_{dep} - 80 f_{dep}^{\,2} - 15 f_{dep}^{\,3} + 12 f_{dep}^{\,4} + f_{dep}^{\,5}\right) h^2 \kappa + \\ \left(14 + 42 f_{dep} - 20 f_{dep}^{\,2} - 20 f_{dep}^{\,3} + 6 f_{dep}^{\,4} + 2 f_{dep}^{\,5}\right) h^2 \kappa^2 + \left(7 f_{dep} - 5 f_{dep}^{\,3} + f_{dep}^{\,5}\right) h^2 \kappa^3 \end{array} \right\}}{\left(12 - 4 f_{dep}^{\,2}\right) + \left(16 + 6 f_{dep} - 8 f_{dep}^{\,2} - f_{dep}^{\,3}\right)\kappa + \left(4 + 8 f_{dep} - 4 f_{dep}^{\,2} - 2 f_{dep}^{\,3}\right)\kappa^2 + \left(2 f_{dep} - f_{dep}^{\,3}\right)\kappa^3} \tag{40}$$

and

$$t_{eff,evap} =$$

$$\frac{1}{30 D_{sc}} \frac{\left\{ \begin{array}{l} \left(48 + 24 f_{dep} - 8 f_{dep}^{\,2} - 4 f_{dep}^{\,3} + f_{dep}^{\,4}\right) h^2 + \left(8 + 28 f_{dep} - 6 f_{dep}^{\,2} - 8 f_{dep}^{\,3} + 2 f_{dep}^{\,4}\right) h^2 \kappa + \\ \left(4 f_{dep} + 2 f_{dep}^{\,2} - 4 f_{dep}^{\,3} + f_{dep}^{\,4}\right) h^2 \kappa^2 \end{array} \right\}}{\left(4 + 2 f_{dep} - f_{dep}^{\,2}\right) + \left(4 + 4 f_{dep} - 2 f_{dep}^{\,2}\right)\kappa + \left(2 f_{dep} - f_{dep}^{\,2}\right)\kappa^2} \tag{41}$$

A parameter sensitivity study was conducted using the mathematical models for small and large doses. The following parameters were investigated because of their effects on the rate of absorption and evaporation: κ, D, and m_0. Mathematica was used to find a randomized set of points around nominal values of κ, D, and m_0. 10% around the mean value was used to generate the resulting profiles.

2.4 Binding and Metabolism

The effects of the diffusion coefficient binding and metabolism through the layer of the skin were studied with the relationships defined by Tojo in a bilayer (SC and viable) skin permeation model (Tojo, 1987).

$$\{1+\frac{p_a}{(1+q_aC_a)^2}\}\frac{\partial C_a}{\partial t}=\frac{\partial}{\partial x}(D_a\frac{\partial C_a}{\partial x})-\frac{M_aC_a}{B_a+C_a} \tag{42}$$

$$\{1+\frac{p_b}{(1+q_bC_b)^2}\}\frac{\partial C_b}{\partial t}=\frac{\partial}{\partial x}(D_b\frac{\partial C_b}{\partial x})+\frac{M_aC_a}{B_a+C_a}-\frac{M_bC_b}{(1+\frac{C_a}{K_i})B_b+C_b} \tag{43}$$

$$\{1+\frac{p_c}{(1+q_cC_c)^2}\}\frac{\partial C_c}{\partial t}=\frac{\partial}{\partial x}(D_c\frac{\partial C_c}{\partial x})+\frac{M_bC_b}{(1+\frac{C_a}{K_i})B_b+C_b} \tag{44}$$

Equations (42) through (44) are based on the Langmuir isotherm, which is a simple type of adsorption equilibrium model that relates the area covered by the adsorbate molecules on the surface of solid adsorbents as a function of partial pressure or concentration at a fixed temperature (Ye et al., 2021). Drug A is converted into Drug B and Drug C, which can either be an active or nonactive metabolite, for transdermal metabolism (Tojo, 1987). Where K_i is the inhibition constant of the second reaction for Drug A; B_b & B_a are the Michaelis-Menten kinetics parameters for Drug B and A, respectively; C is the drug concentration in the skin, and ρ and q are the binding rate constants based on dual absorption model (Tojo, 1987). These mass balances over differential skin volume are applied to the SC without metabolism ($0 \leq x \leq h$) and to the viable skin without drug binding ($h < x \leq H$, and $\rho=q=0$) (Tojo, 1987). The equations (42) through (44) can be simplified to equations (45) through (47) at a low concentration of Drug A.

$$\{1+\frac{p_a}{(1+q_aC_a)^2}\}\frac{\partial C_a}{\partial t}=\frac{\partial}{\partial x}(D_a\frac{\partial C_a}{\partial x})-k_1C_a \tag{45}$$

$$\{1+\frac{p_b}{(1+q_bC_b)^2}\}\frac{\partial C_b}{\partial t}=\frac{\partial}{\partial x}(D_b\frac{\partial C_b}{\partial x})+k_1C_a-k_2C_b \tag{46}$$

$$\{1+\frac{p_c}{(1+q_cC_c)^2}\}\frac{\partial C_c}{\partial t}=\frac{\partial}{\partial x}(D_c\frac{\partial C_c}{\partial x})+k_2C_b \tag{47}$$

where k is the rate constant of enzymatic reaction in viable skin (Tojo, 1987).

CHAPTER 3

METHODS

Mathematica was utilized to simulate the mathematical models of the small and large doses. Two different codes were created, one that applies to large quantities while the other considers small amounts. A collocation method converted the partial differential equations (PDEs) into ordinary partial differential equations (ODEs). Then, the simulations yielded absorption and evaporation profiles based on the ratio κ. Other key model parameters were the stratum corneum thickness, the fractional depth and the dose size. The algorithm also helped conduct a parameter sensitivity analysis. The program generated random κ, D_{SC} and M_0 values corresponding to a deviation of 10% around the mean value. Equations (39) were applied to determine how the effects of parameter uncertainty on the calculation of κ.

CHAPTER 4

RESULTS AND DISCUSSION

4.1 Effects of Model Parameters on the Cumulative Amount of CWA Absorbed and Evaporated

A study was conducted to assess the effects of the model parameters on process dynamics for a small dose application. As referenced in Eq. (39), the ratio κ is the ratio of the steady-state evaporation rate to the steady-state absorption rate, i.e., a crucial property in determining the fate of the CWA. Therefore, it was chosen to be one of the inputs to vary. The diffusion coefficient was the next important property. Its value can significantly contribute to accelerating the amount of chemicals absorbed into the body or the evaporation from the skin barrier for compounds that have a higher tendency to evaporate from the skin's surface. Finally, the investigation also considered the dose's influence on the skin's surface M_0. Even below M_{sat}, a large or small dose can modify the ability of a CWA to diffuse through the skin or evaporate.

CWAs can travel through the environment when released. It is pertinent to understand the significance of parameter changes because they can drastically affect transdermal transport and tissue concentrations. One of the causes of a larger κ could be a small temperature. Different surroundings (particularly outdoors) can lower or increase its value. For instance, if the climate is more tropical, a lower κ is expected. The analysis of the effects of the diffusion coefficient and κ have been conducted for both small- and large-dose concentration models. The results are summarized in Figures 4.1.1-4.1.12 for the small dose model and Figures 4.1.13-4.1.24 for the large dose model. VX, adamsite, and

colchicine were used as reference compounds. Similar studies were pursued for the remaining CWA's (See the Appendix).

Small Dose:

Mabs
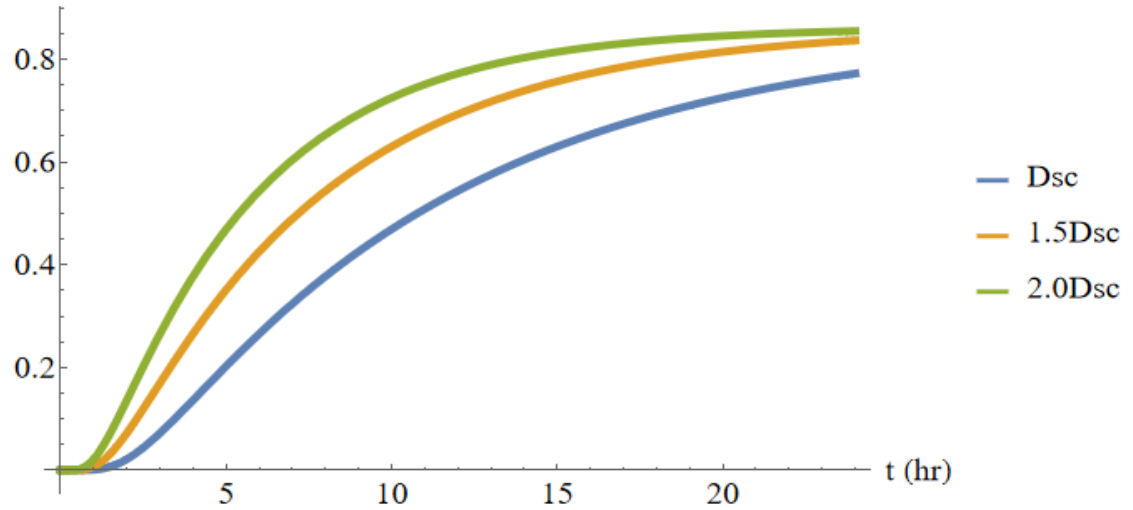
Figure 4.1.1 Graphical representation of the effect of the diffusion coefficient for the absorption profile using VX as a reference compound.

Mevap
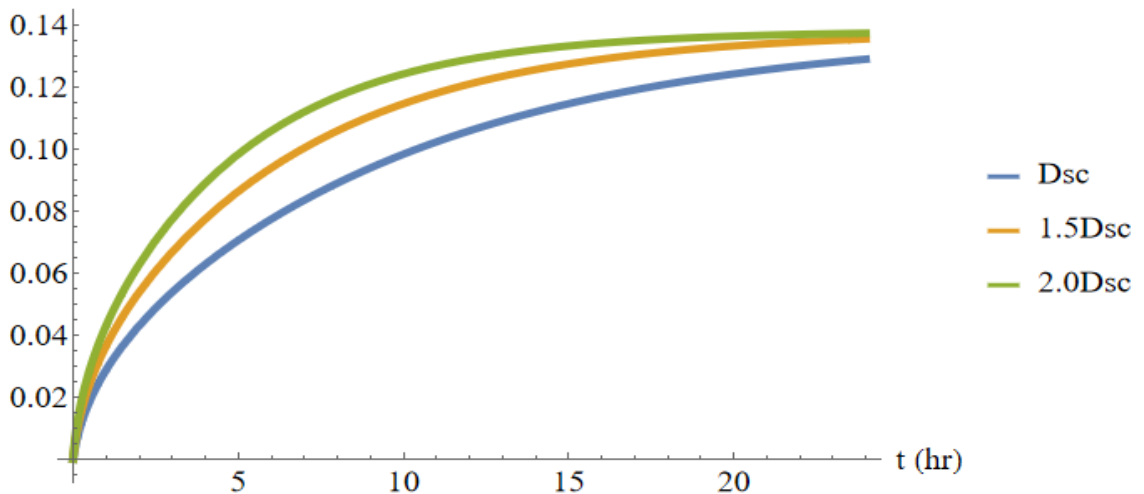
Figure 4.1.2 Graphical representation of the effect of the diffusion coefficient for the evaporation profile using VX as a reference compound.

Mabs
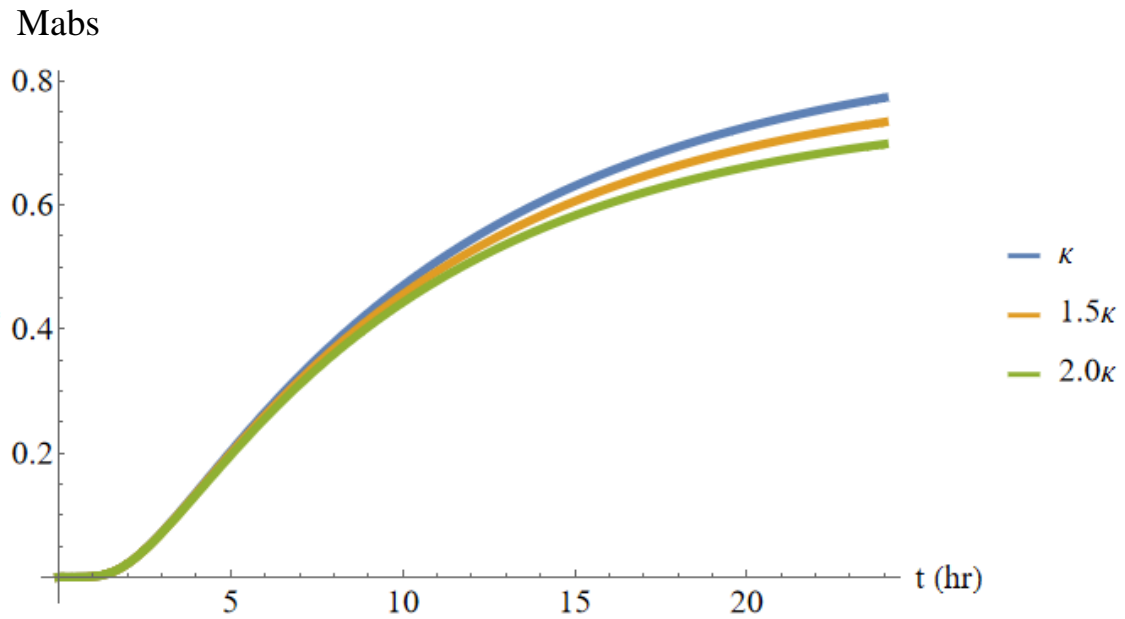
Figure 4.1.3 Graphical representation of the effect of the ratio κ for the absorption profile using VX as a reference compound.

Mevap
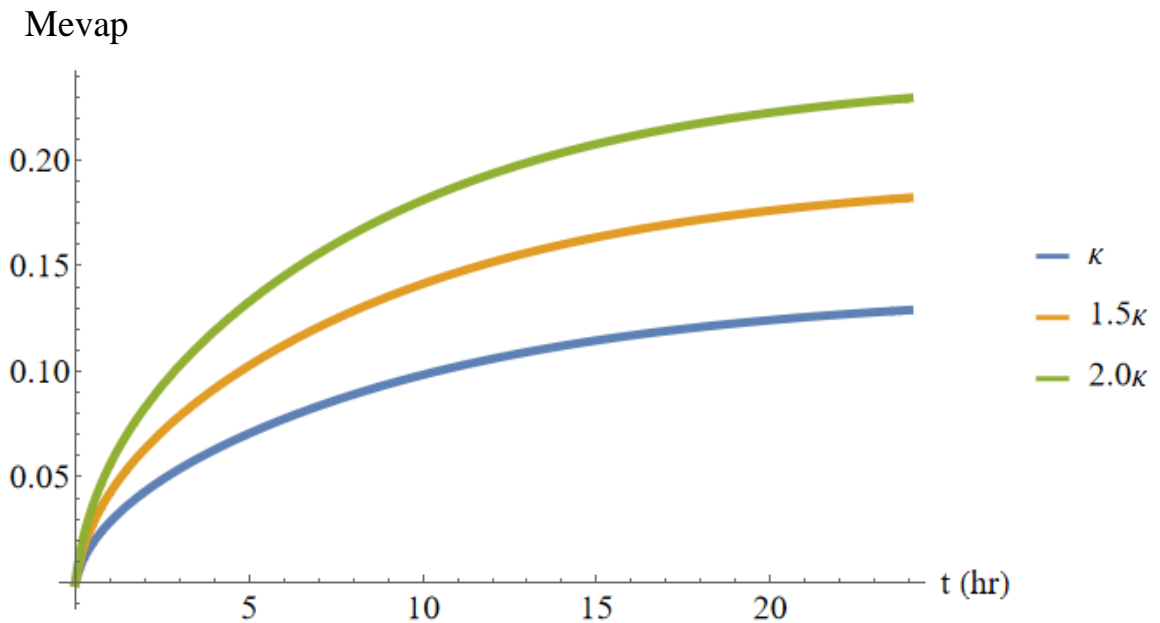
Figure 4.1.4 Graphical representation of the effect of the ratio κ for the evaporation profile using VX as a reference compound.
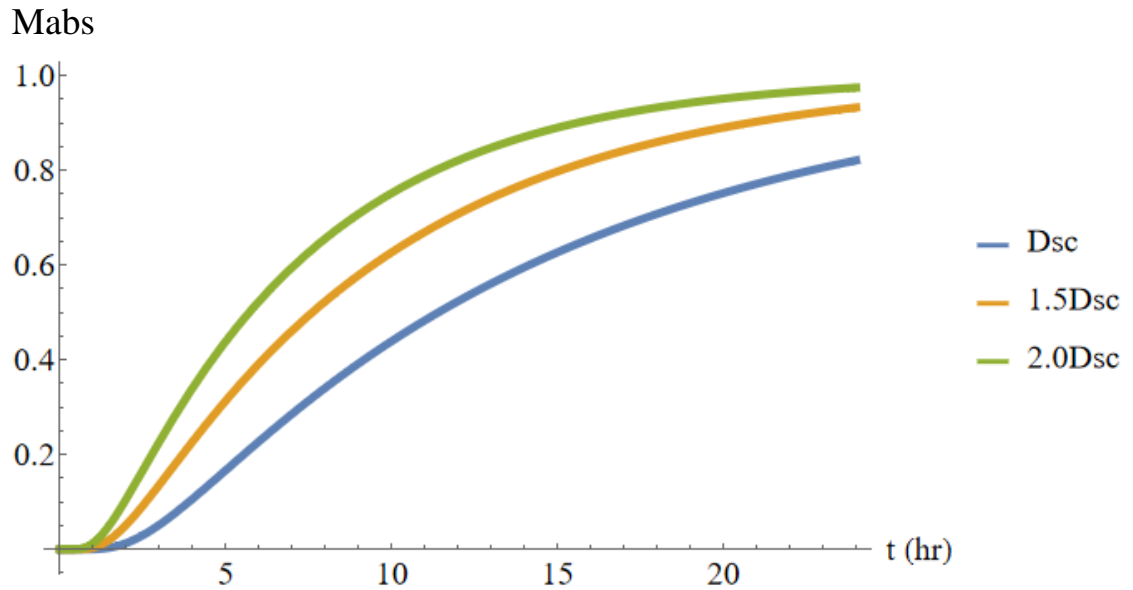
Figure 4.1.5 Graphical representation of the effect of the diffusion coefficient for the absorption profile using adamsite as a reference compound.
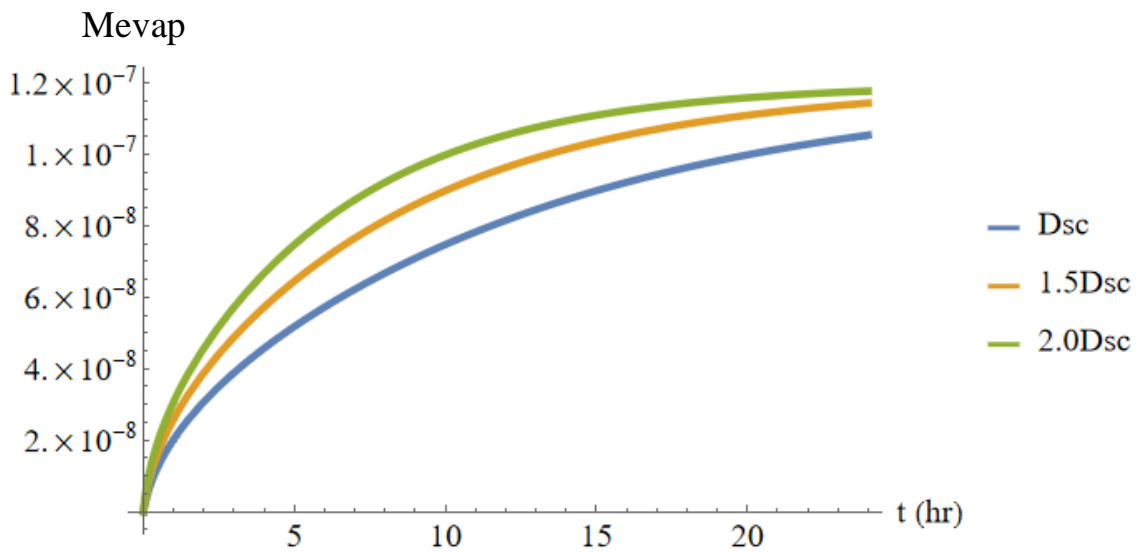
Figure 4.1.6 Graphical representation of the effect of the diffusion coefficient for the evaporation profile using adamsite as a reference compound.

27
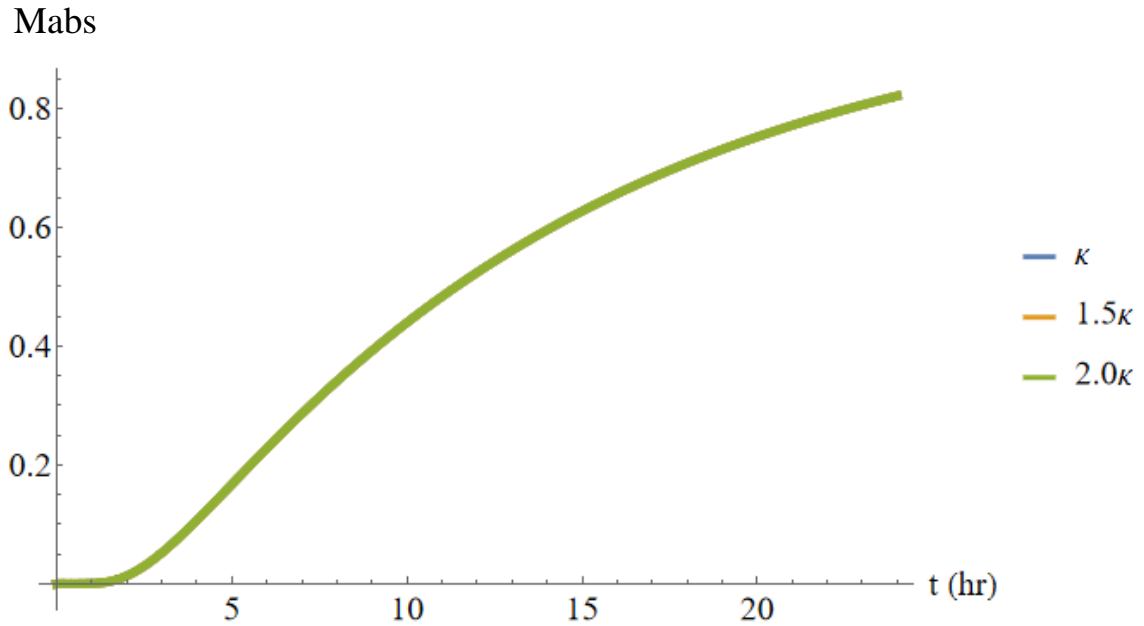
Figure 4.1.7 Graphical representation of the effect of the ratio κ for the absorption profile using adamsite as a reference compound.
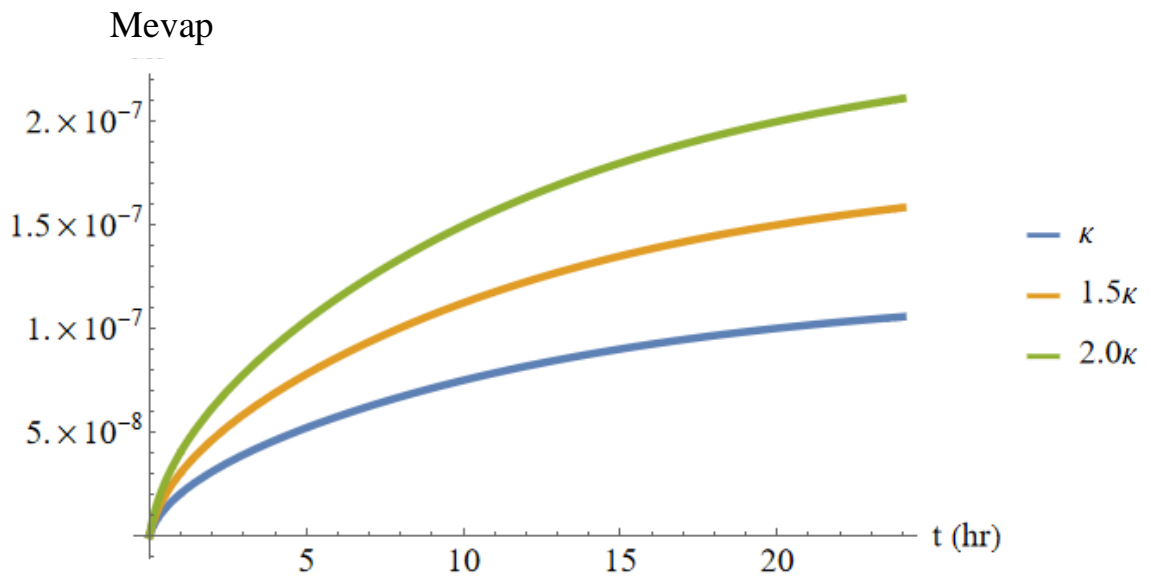
Figure 4.1.8 Graphical representation of the effect of the ratio κ for the evaporation profile using adamsite as a reference compound.
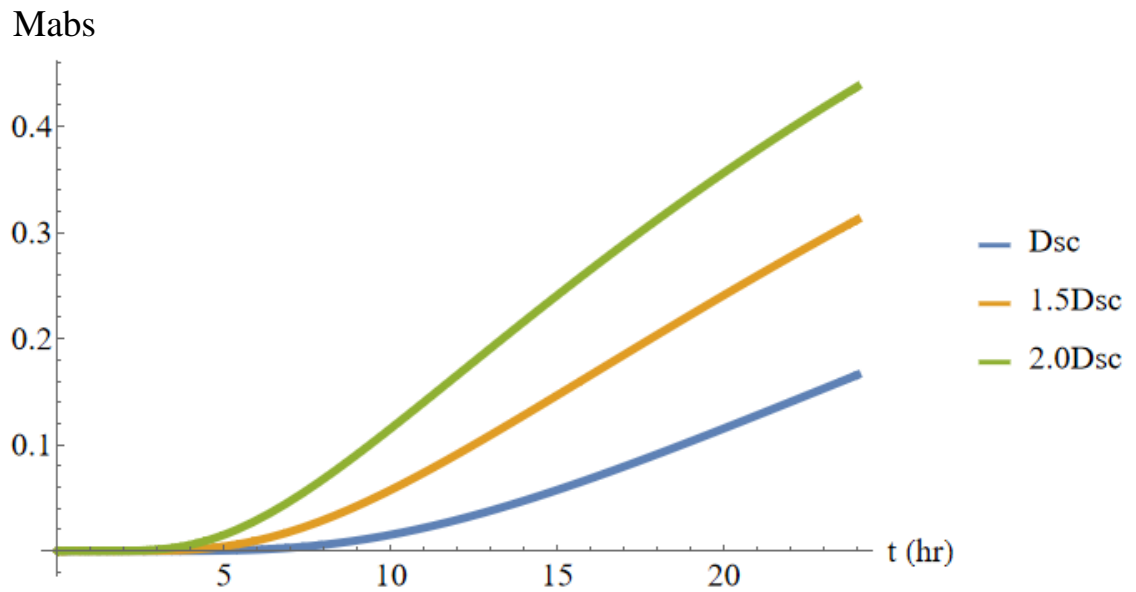
Figure 4.1.9 Graphical representation of the effect of the diffusion coefficient for the absorption profile using colchicine as a reference compound.
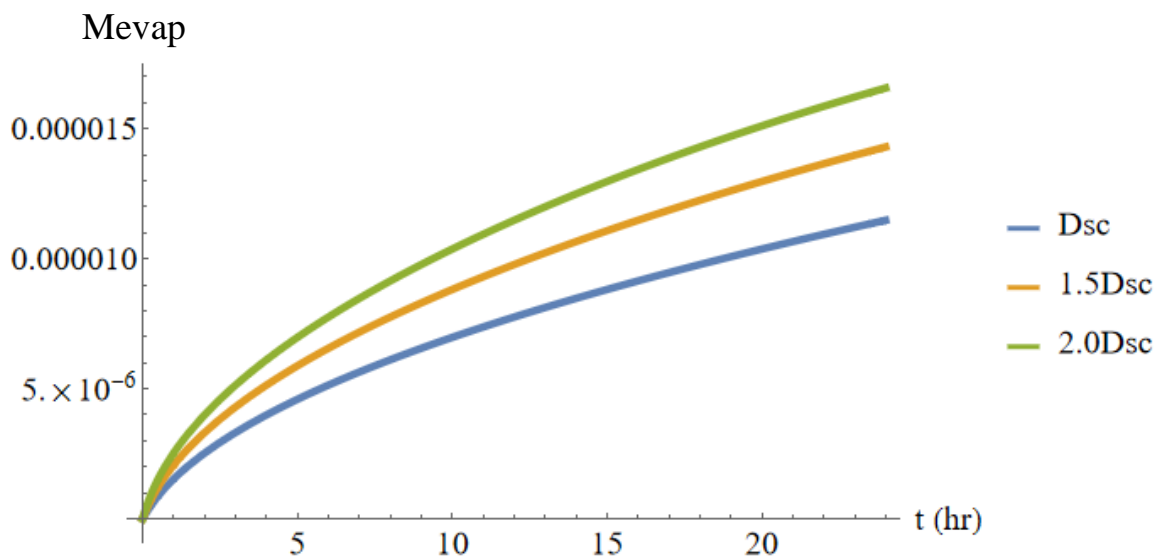
Figure 4.1.10 Graphical representation of the effect of the diffusion coefficient for the evaporation profile using colchicine as a reference compound.

Mabs
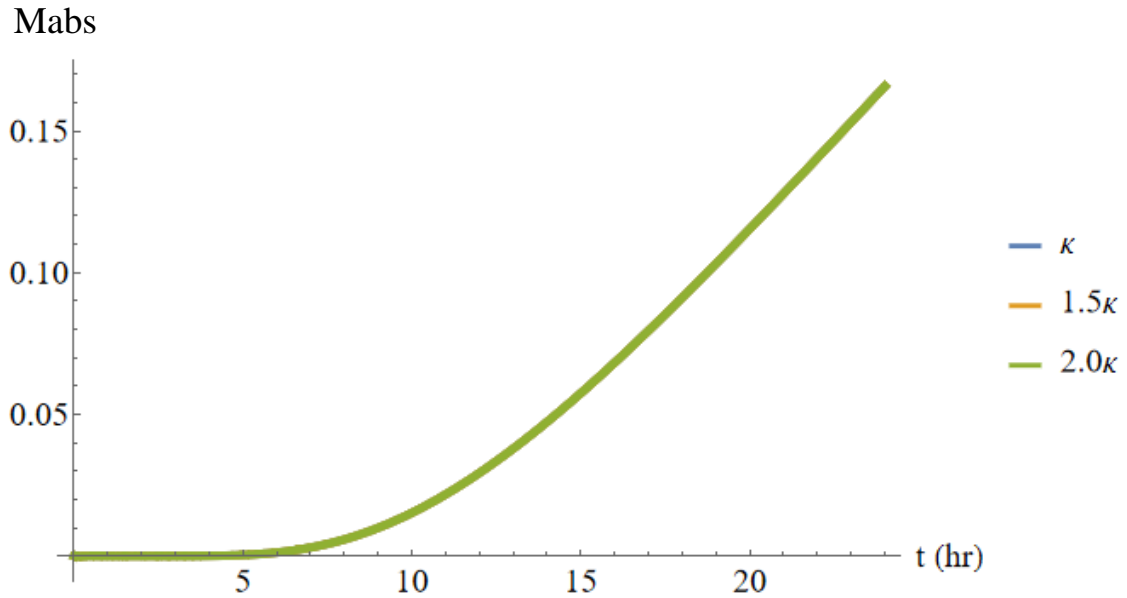
Figure 4.1.11 Graphical representation of the effect of the ratio κ for the absorption profile using colchicine as a reference compound.

Mevap
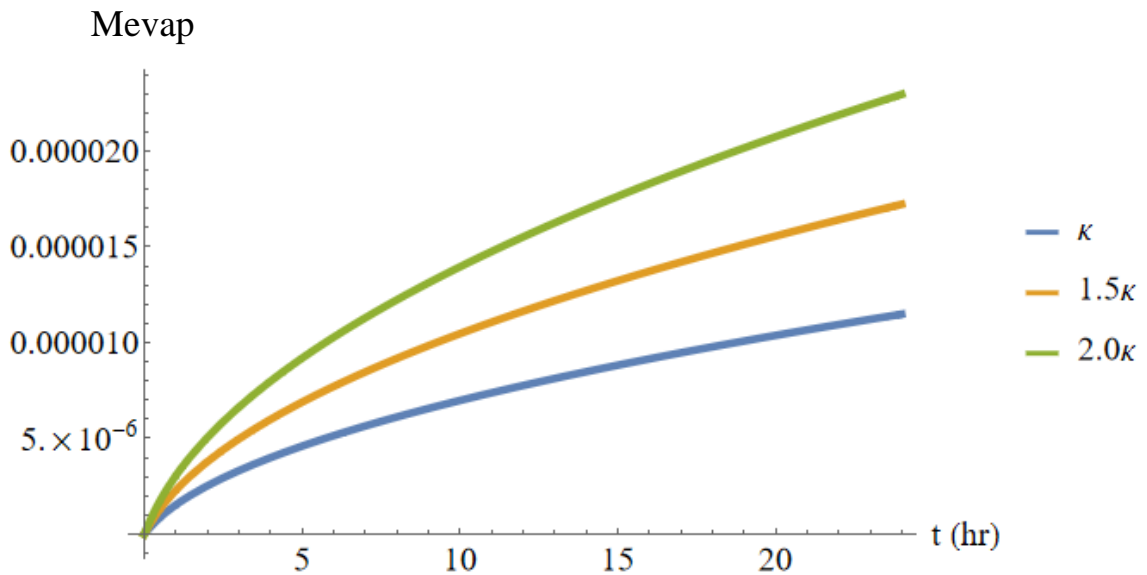
Figure 4.1.12 Graphical representation of the effect of the ratio κ for the evaporation profile using colchicine as a reference compound.

Large Dose:
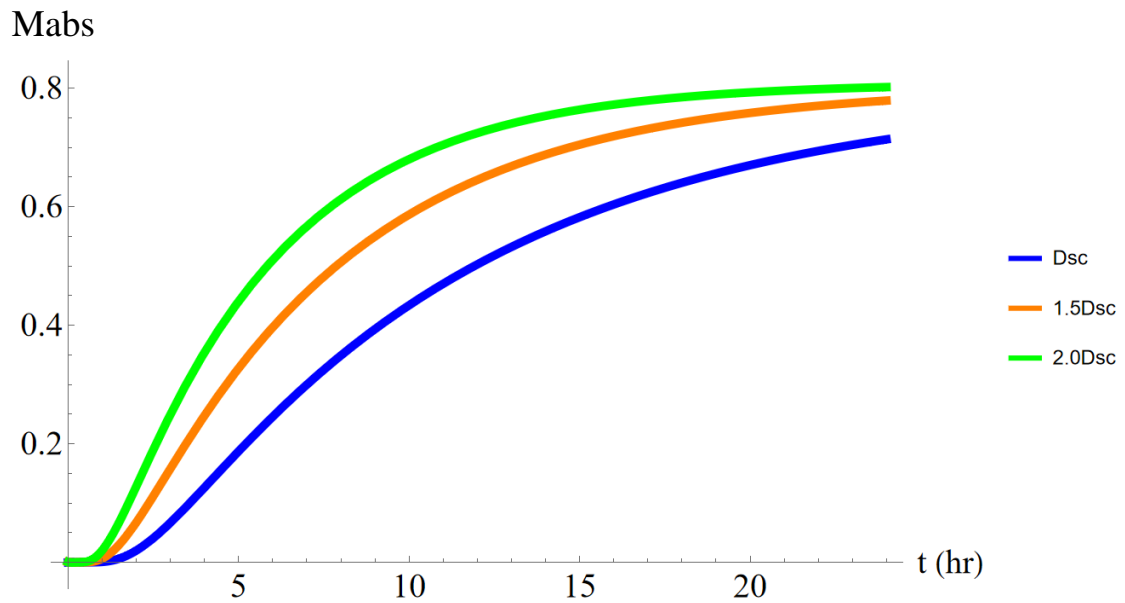
Figure 4.1.13 Graphical representation of the effect of the diffusion coefficient for the absorption profile using VX as a reference compound.
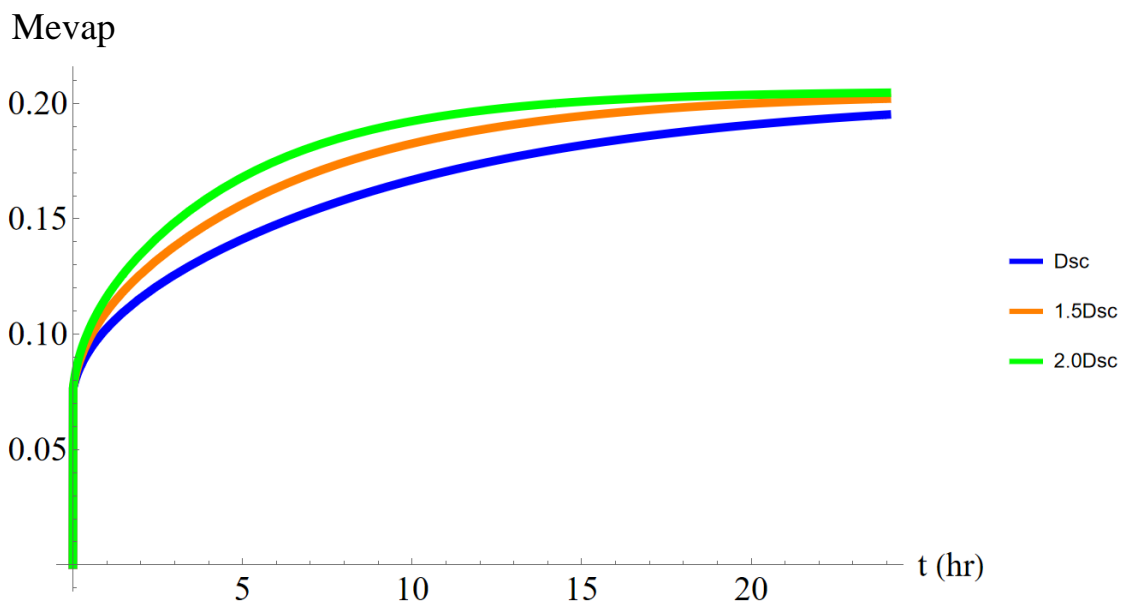
Figure 4.1.14 Graphical representation of the effect of the diffusion coefficient for the evaporation profile using VX as a reference compound.
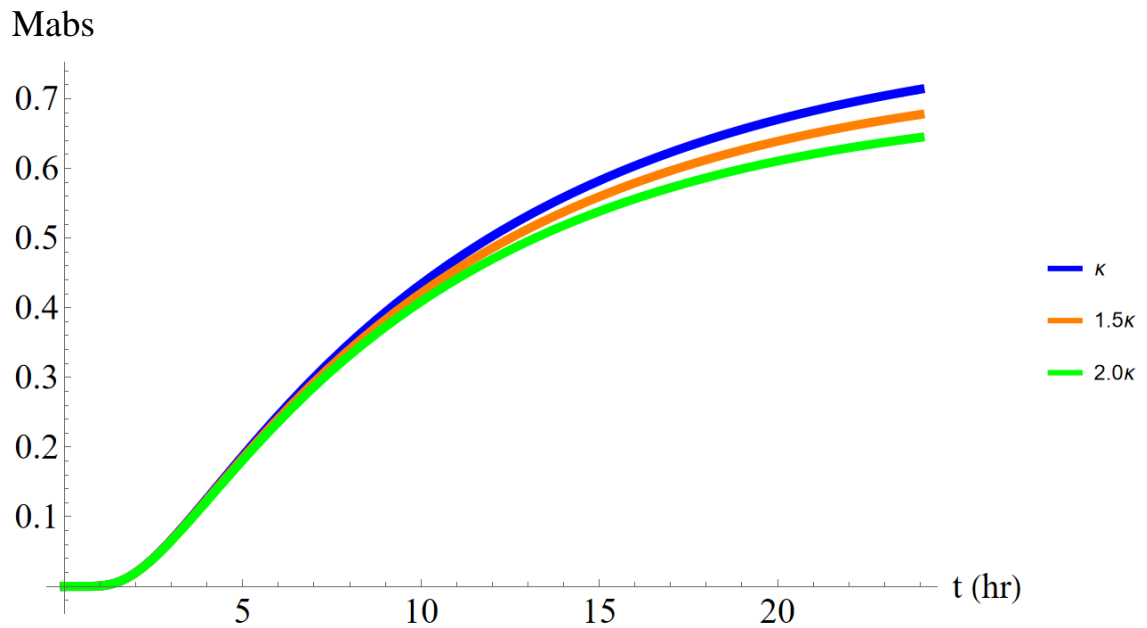
Figure 4.1.15 Graphical representation of the effect of the ratio κ for the absorption profile using VX as a reference compound.
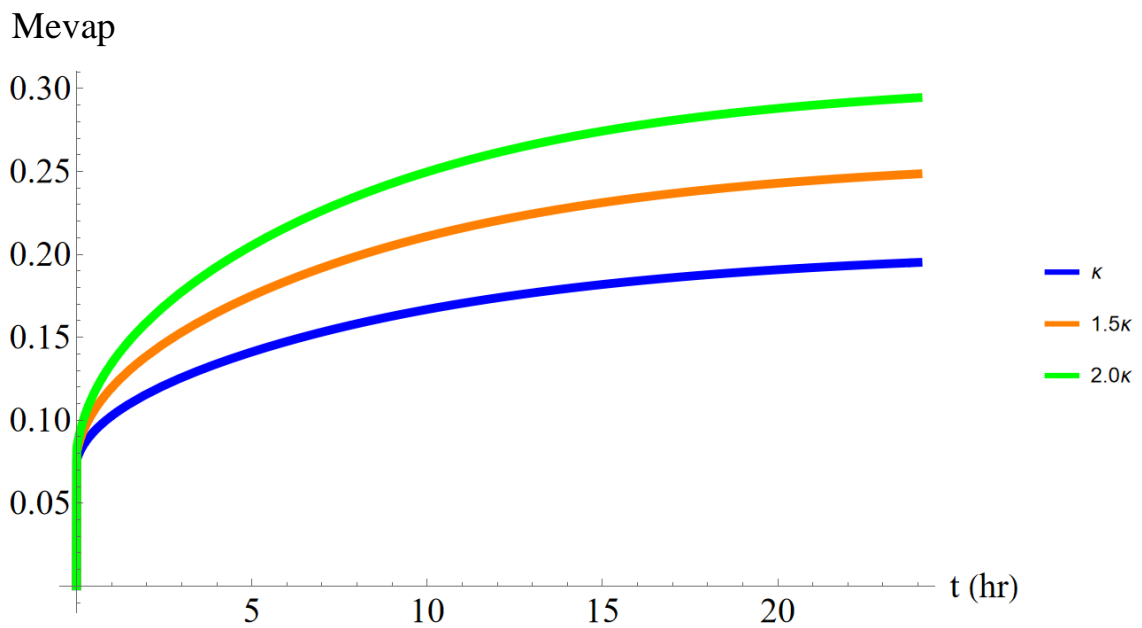
Figure 4.1.16 Graphical representation of the effect of the ratio κ for the evaporation profile using VX as a reference compound.

Mabs
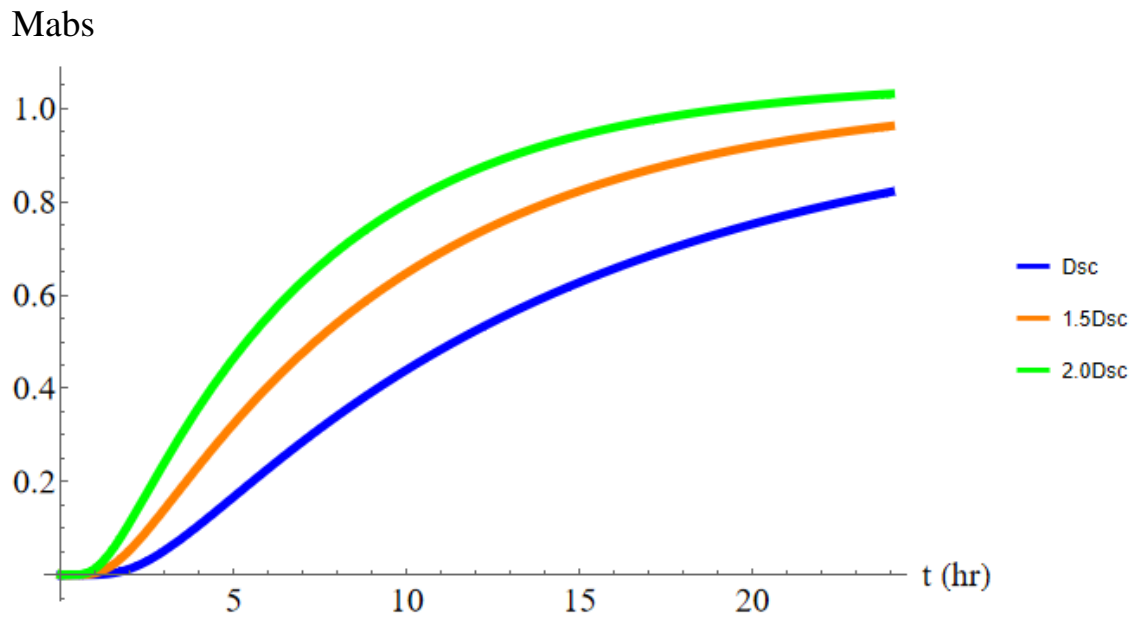
Figure 4.1.17 Graphical representation of the effect of the diffusion coefficient for the absorption profile using adamsite as a reference compound.

Mevap
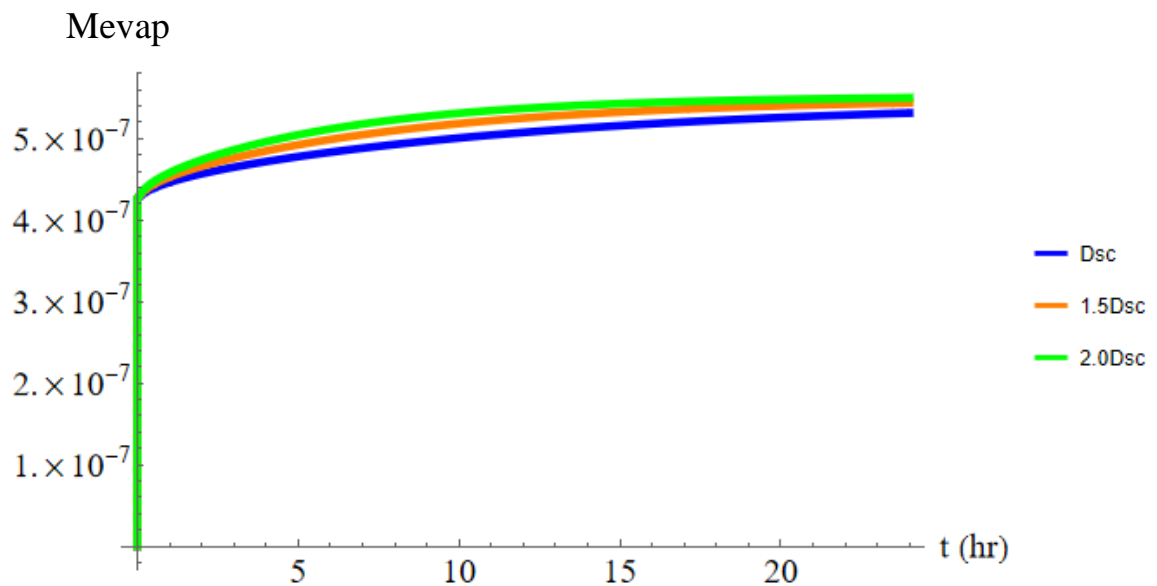
Figure 4.1.18 Graphical representation of the effect of the diffusion coefficient for the evaporation profile using adamsite as a reference compound.
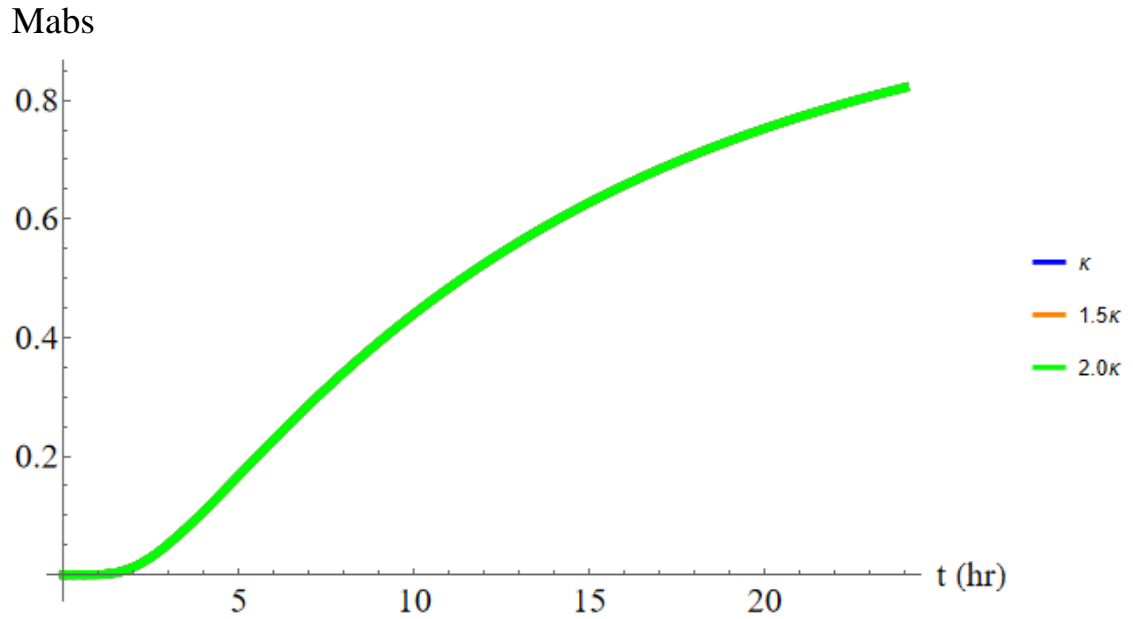
Figure 4.1.19 Graphical representation of the effect of the ratio κ for the absorption profile using adamsite as a reference compound.
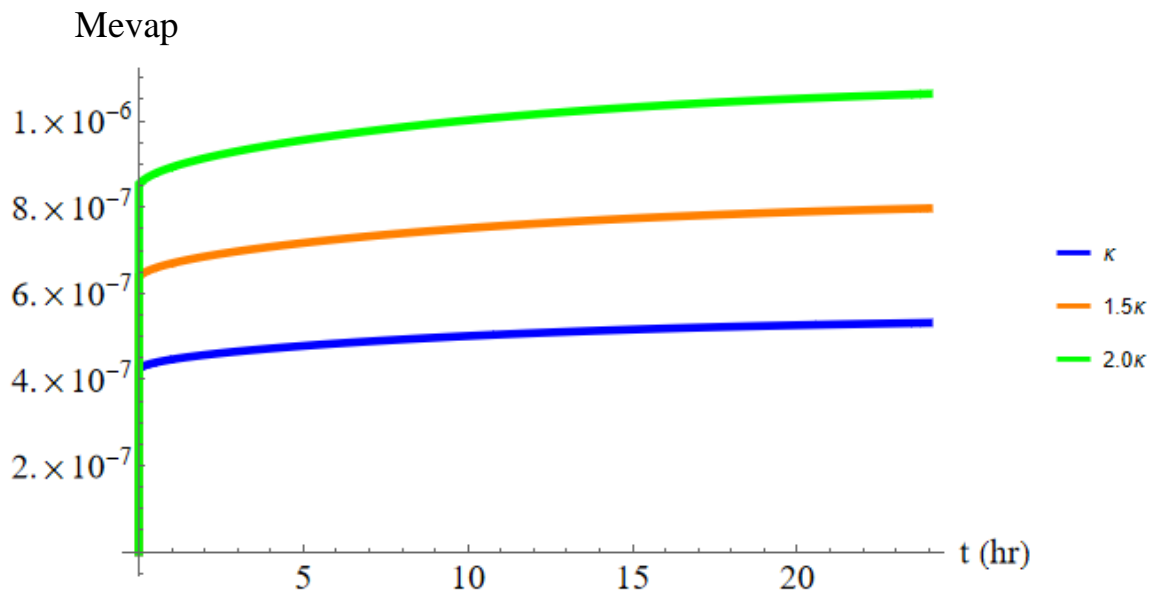
Figure 4.1.20 Graphical representation of the effect of the ratio κ for the evaporation profile using adamsite as a reference compound.

Mabs
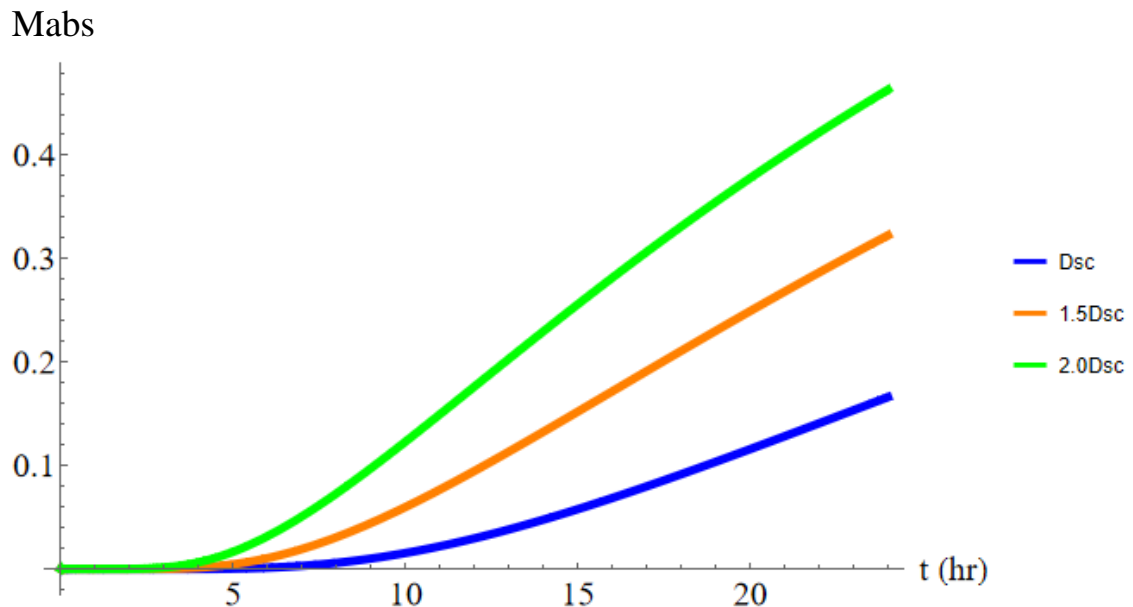
Figure 4.1.21 Graphical representation of the effect of the diffusion coefficient for the absorption profile using colchicine as a reference compound.

Mevap
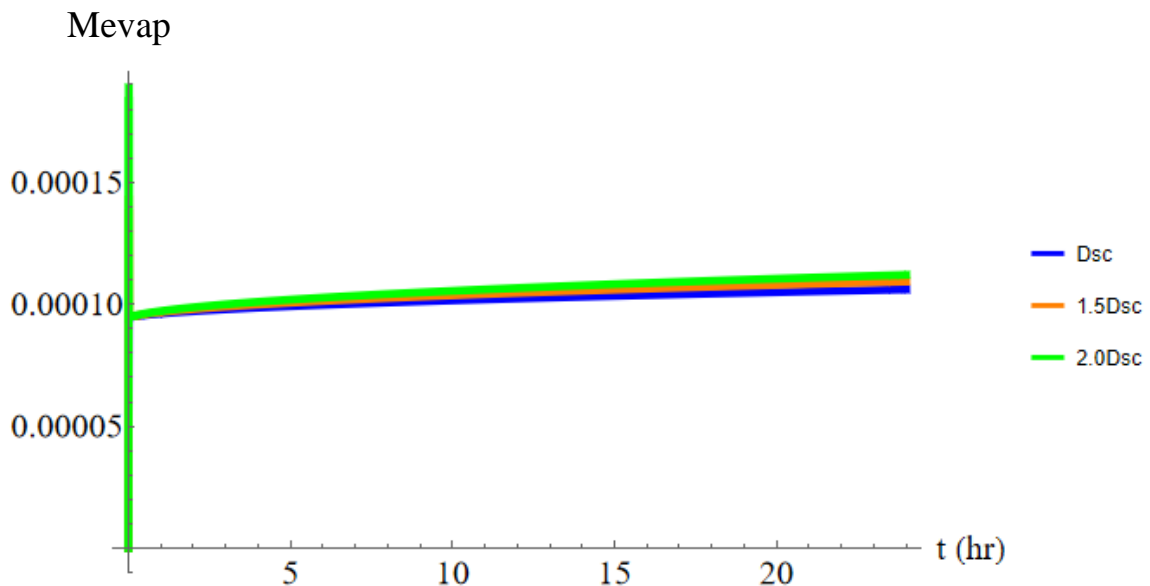
Figure 4.1.22 Graphical representation of the effect of the diffusion coefficient for the evaporation profile using colchicine as a reference compound.

Mabs
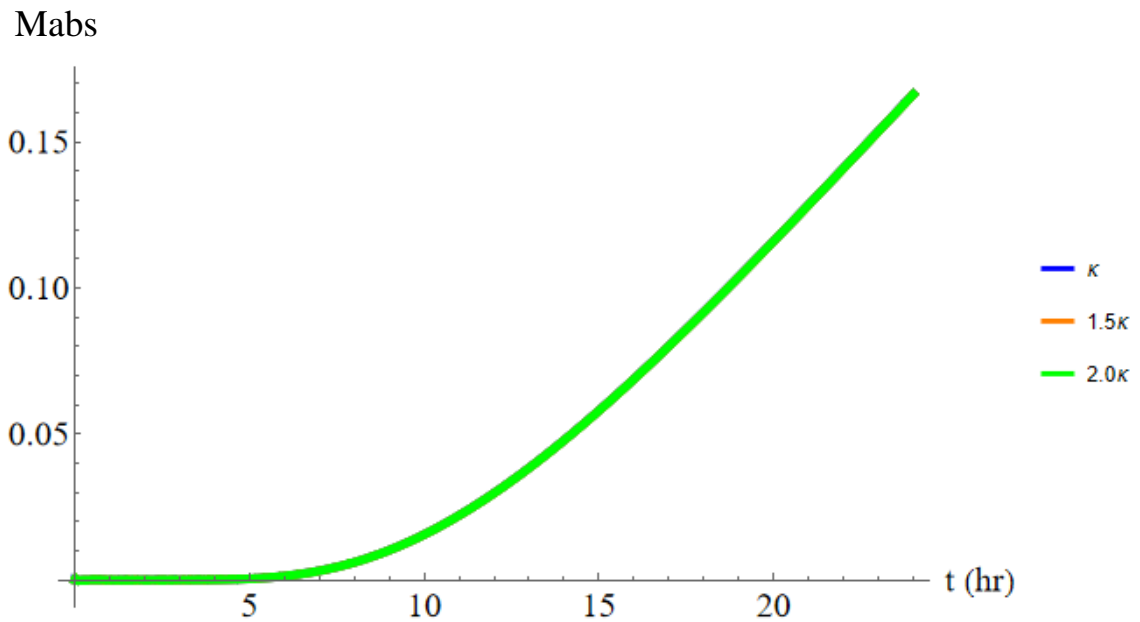
Figure 4.1.23 Graphical representation of the effect of the ratio κ for the absorption profile using colchicine as a reference compound.

Mevap
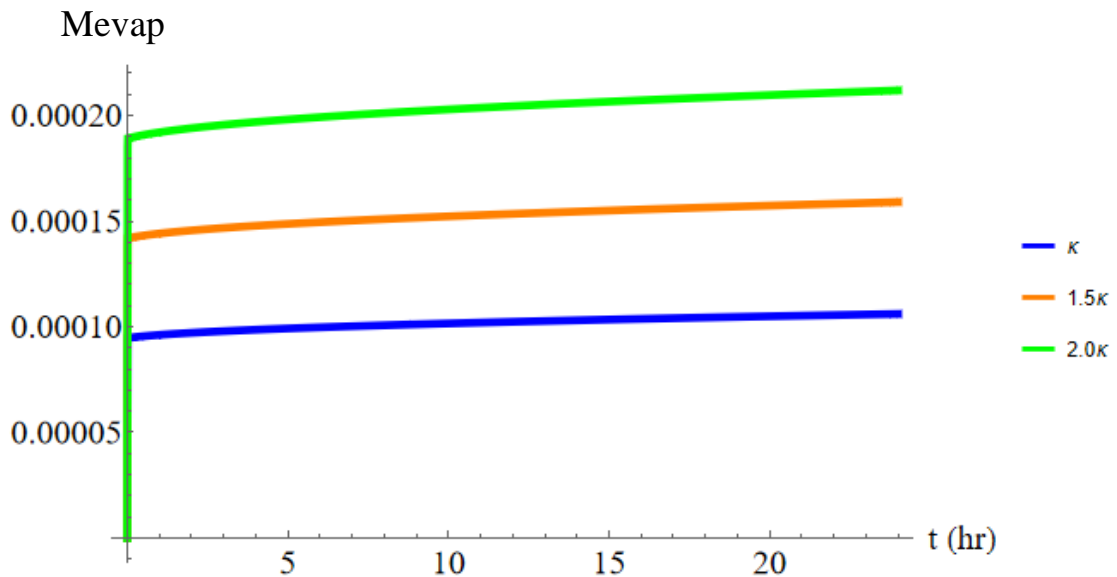
Figure 4.1.24 Graphical representation of the effect of the ratio κ for the evaporation profile using colchicine as a reference compound.

The parameters for κ and diffusion were varied with κ and D_{sc} being the values found from the analysis of the charts in the appendix. The absorption profiles of small and large doses

did not vary significantly with a change in the ratio κ. The outlier was VX in the large dose

model, in which the differences were appreciable enough to see that a higher the ratio κ

resulted in a lower absorption. Comparably, the ratio κ did significantly affect the

evaporation of the compounds. It was determined that a larger κ typically resulted in a

larger evaporation. For both large and small doses, an increase in diffusion coefficient has

led to an increase in the cumulative amount evaporated and absorbed. It was seen that of

the two parameters, the diffusion coefficient was the more significant in impact. This is

because a larger diffusion coefficient increases the speed at which it reaches steady state.

From this analysis, it can be seen that if one is concerned with the severity of CWAs being

absorbed through the skin, the diffusion coefficient has a far greater effect.

4.2 Sensitivity Analysis

A representation of the parameters' magnitude is tabularized below. Using 10% around the

mean value, the randomly collected points for the adamsite are displayed in Table 4.2.1.

Table 4.2.1 Data Points for κ, Dsc, and M_0

κ $[10^{-7}]$	Dsc $[10^{-11}]$	M_0
1.269	1.832	0.009047
1.486	1.900	0.01082
1.236	1.808	0.009992
1.328	1.585	0.01007
0.9553	1.537	0.01042
1.216	1.629	0.01066
1.049	1.418	0.008940

1.450	1.291	0.01070
1.208	1.699	0.01039
1.388	1.859	0.01071

The cumulative amount absorbed and evaporated were plotted using the values listed in Table 4.2.1. Figure 4.2.25 and Figure 4.2.26 show the results for adamsite.
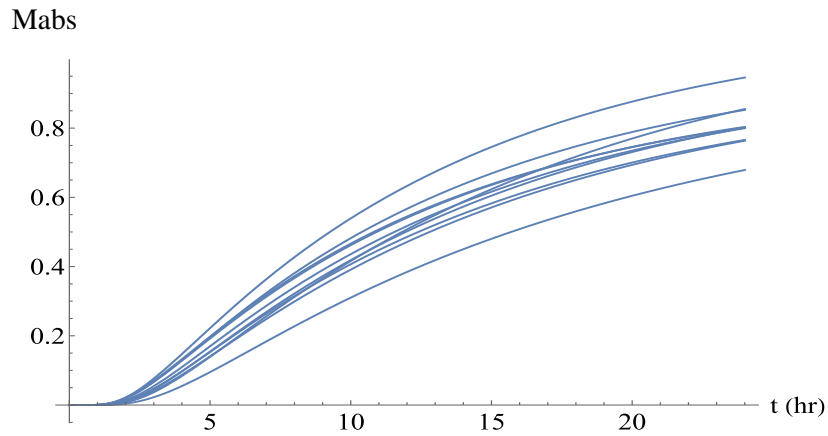
Figure 4.2.25 Effects of random changes on the cumulative amount of adamsite absorbed – small doses.
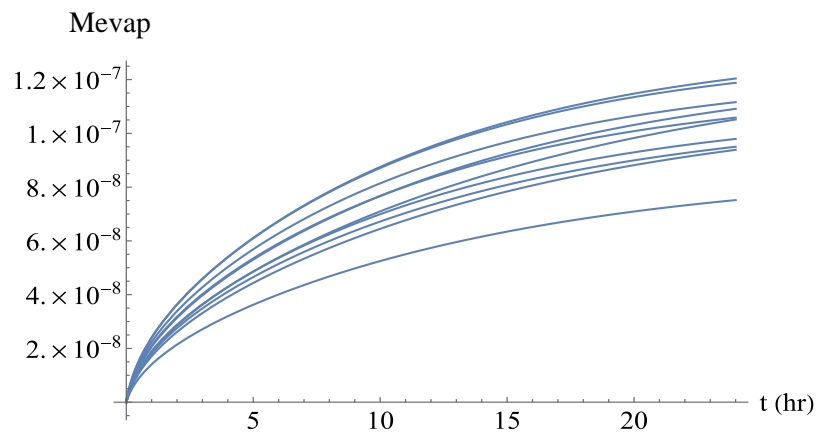
Figure 4.2.26 Effects of random changes on the cumulative amount of adamsite evaporated – small doses.
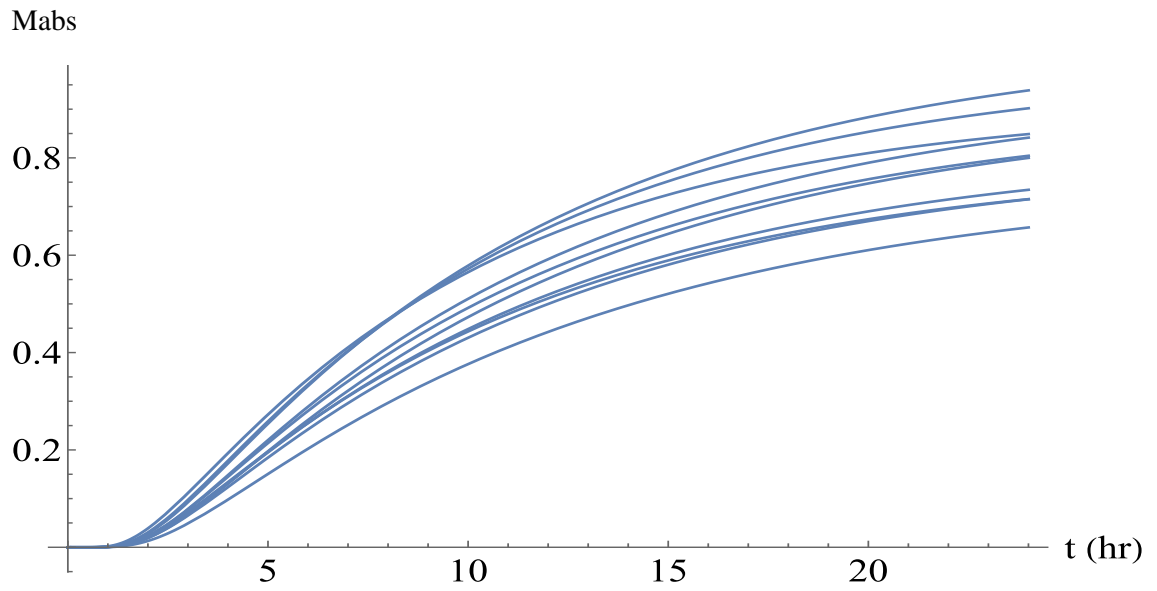
Figure 4.2.27 Effects of random changes on the cumulative amount of VX absorbed – small doses.
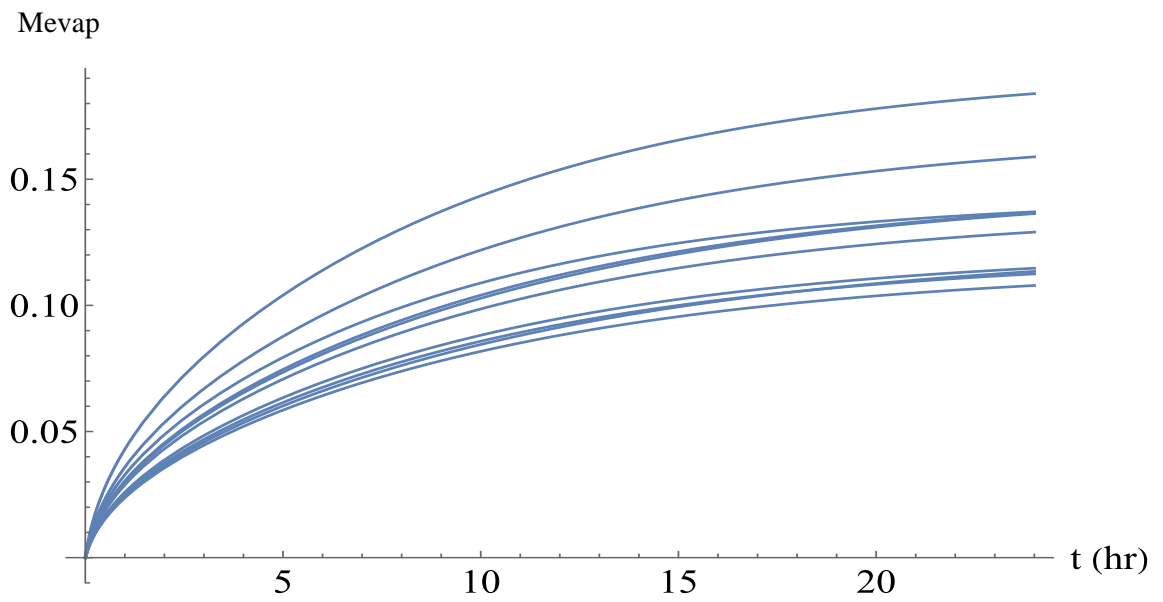
Figure 4.2.28 Effects of random changes on the cumulative amount of VX evaporated – small doses.
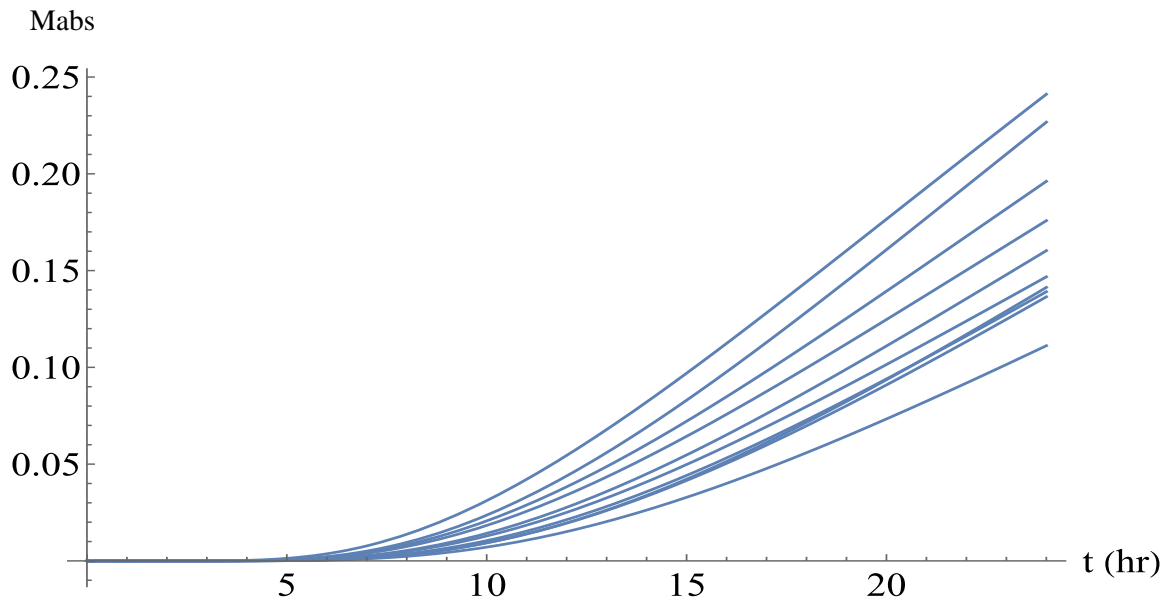
Figure 4.2.29 Effects of random changes on the cumulative amount of colchicine absorbed – small doses.
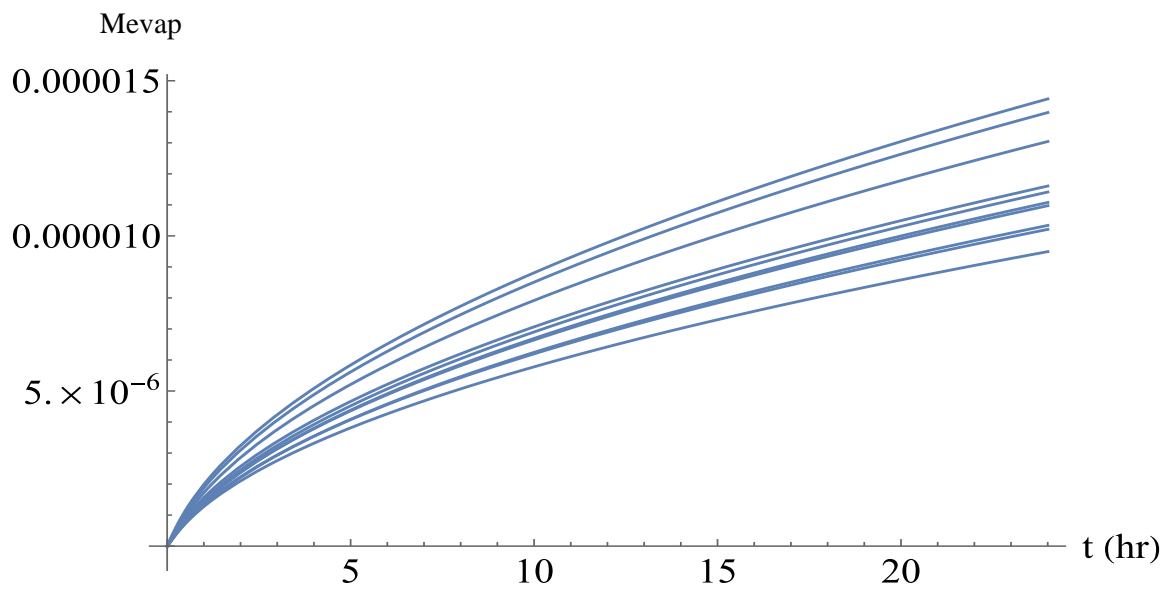
Figure 4.2.30 Effects of random changes on the cumulative amount of colchicine evaporated – small doses.
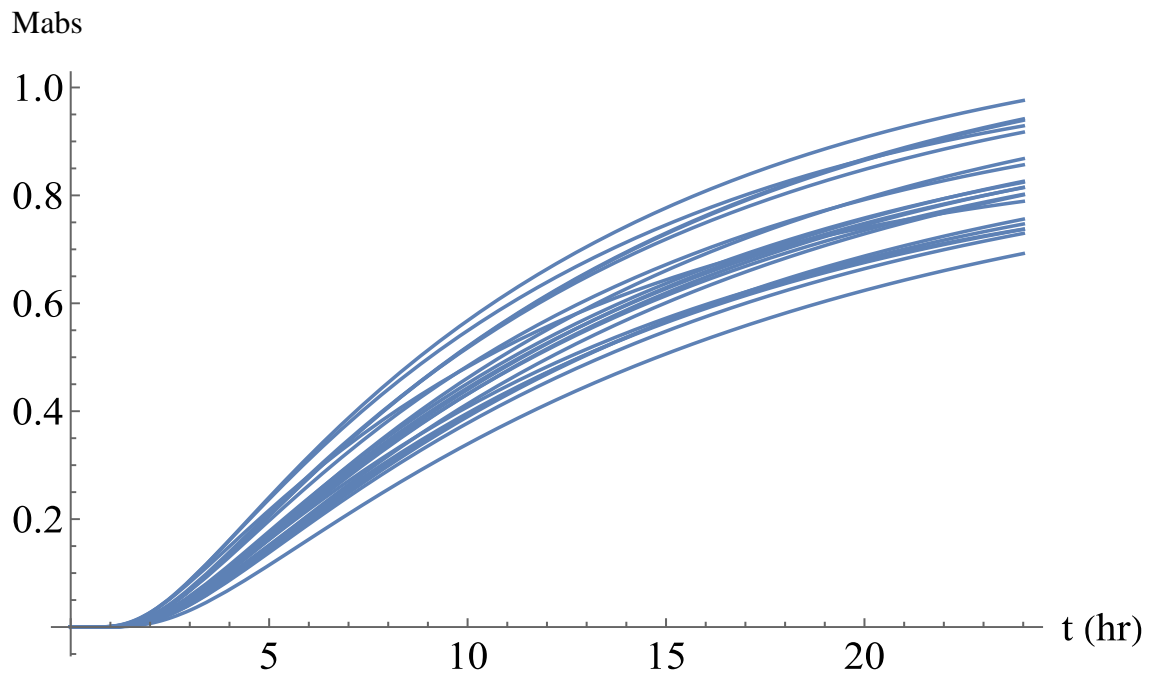
Figure 4.2.31 Effects of random changes on the cumulative amount of adamsite absorbed – large doses.
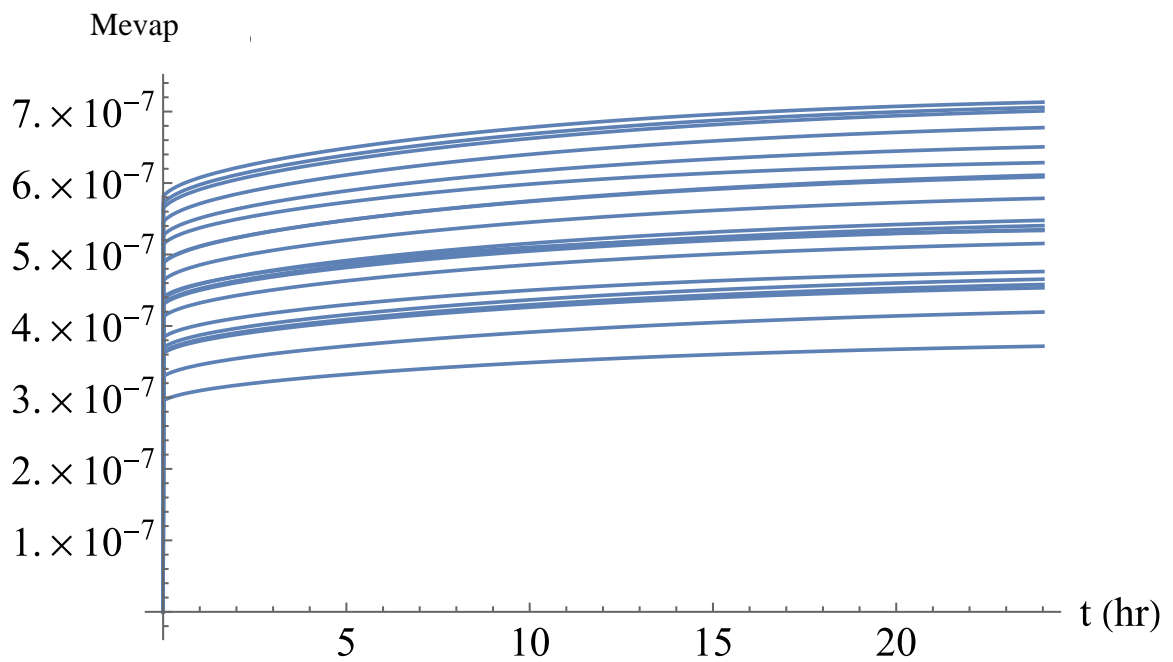
Figure 4.2.32 Effects of random changes on the cumulative amount of adamsite evaporated – large doses.
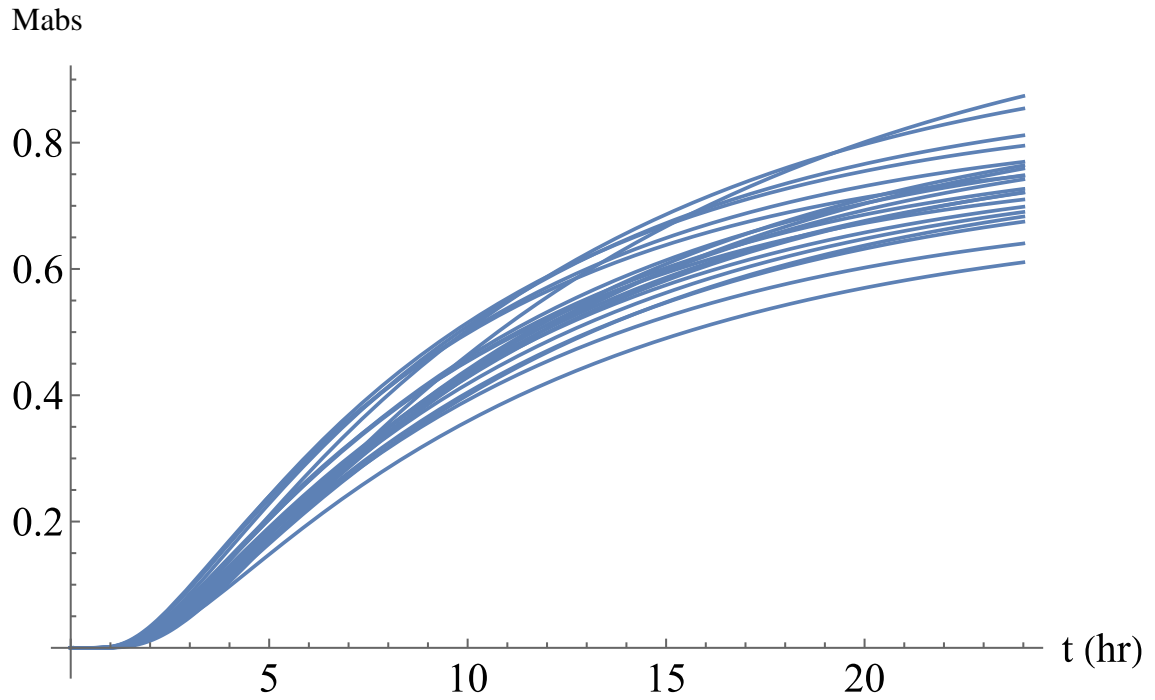
Figure 4.2.33 Effects of random changes on the cumulative amount of VX absorbed – large doses.
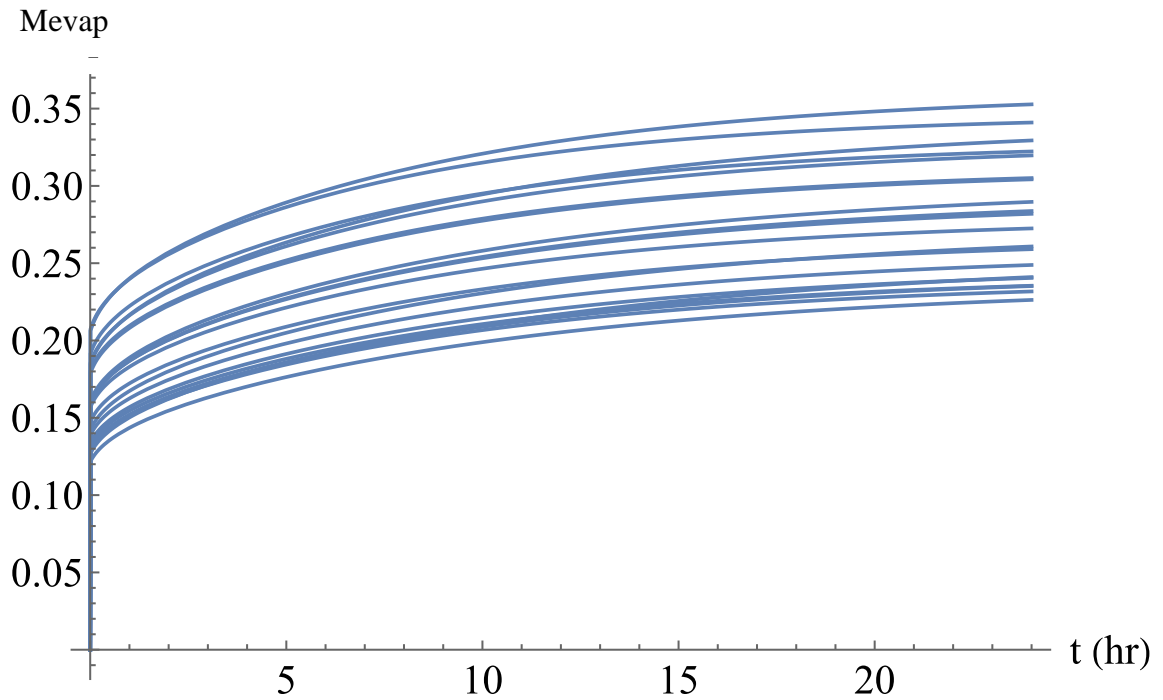
Figure 4.2.34 Effects of random changes on the cumulative amount of VX evaporated – large doses.
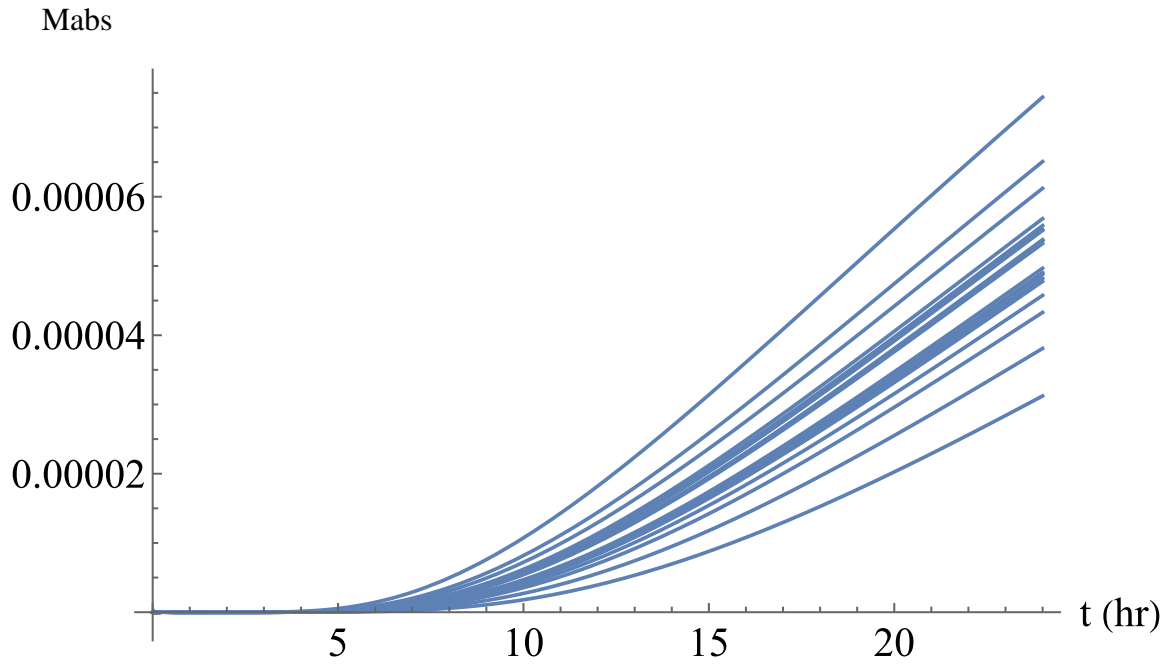
Figure 4.2.35 Effects of random changes on the cumulative amount of colchicine absorbed – large doses.
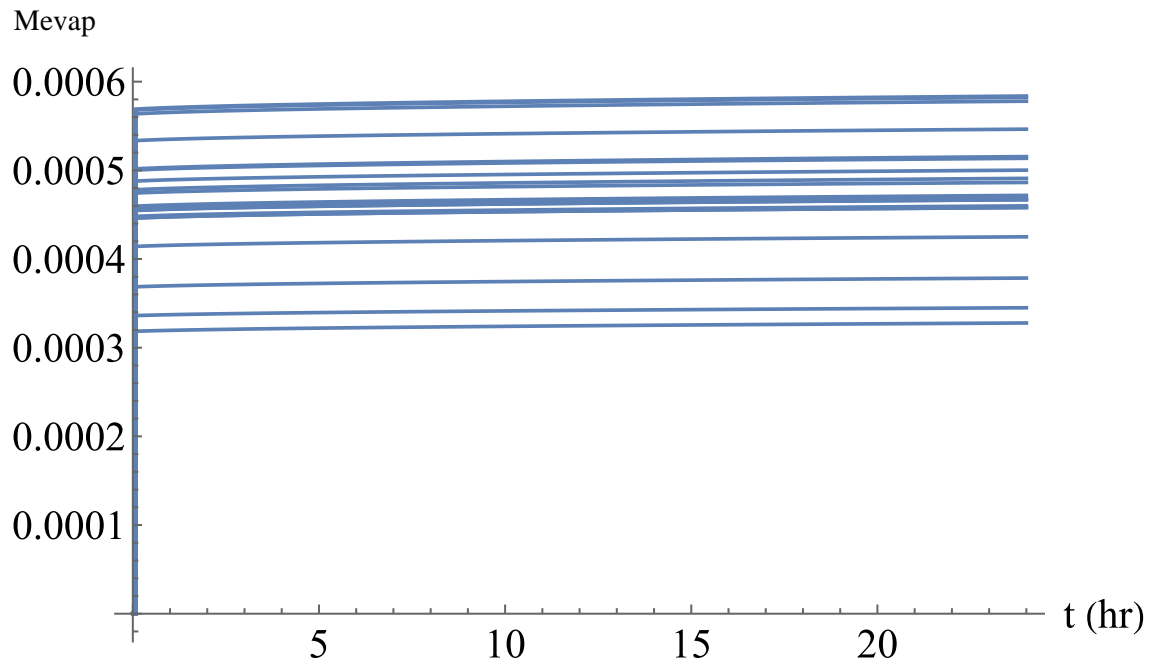
Figure 4.2.36 Effects of random changes on the cumulative amount of colchicine evaporated – large doses.

As shown with the techniques presented in our computational model, the parameter sensitivity of the values for κ, the diffusion coefficient, and the initial dose were assessed for their effects on the absorption or evaporation curves presented. The compounds studied were relative to their respected CWA classifications as to serve as representation for each unique type. With 10% around the mean value, the computational model is able to create a new set of random diffusion, κ, and initial dose values to compare how much the amount absorbed or evaporated could deviate as a result of the parameter uncertainty. VX, adamsite, and colchicine compounds were selected based upon their similar favorability to absorb into the skin. Figures 4.2.25-4.2.30 represent the "small dose model" where the initial dose was less than the saturated value. Figures 4.2.31-4.2.36 represent the "large dose model" where the initial dose was larger than the saturated value. Uncertainties in the parameters influence the absorption and evaporation profiles and, consequently, the exposure assessment. Due to the substantial change in the cumulative amount absorbed, the severity in side effects from exposure could prove to be deadly. In light of these results, toxicity studies and ensuing measures to prevent the spread of the CWAs into the organs and tissues should consider the implications of the parameter estimations.

4.3 Toxicity

From the analysis in 4.2., VX, colchicine, and adamsite have a proclivity to absorb into the skin. We can conclude that a significant risk is imposed on the skin barrier if coming into contact with these three compounds. Consulting Occupational Exposure Limits (OELs), taken in regard to inhalation, provide a baseline to compare the modeling data to toxicity levels in humans. The compounds' toxicity was accessed using the relationship to convert OELs to exposure dose as a dermal exposure benchmark (Keil, 2009). The daily Total

Weight Average permissible (TWA) value for the compound VX is 0.000003 mg/m^3 (Council, 2003). For males with an average ventilation of 17.22 m^3/day, the exposure dose should not exceed 5.17×10^{-5} mg/day. Likewise, for females with an average ventilation of 13.59 m^3/day, the exposure dose should not exceed 4.08×10^{-5} mg/day. The average hand areas of males and females are 448 and 392 cm^2, respectively (Lee et al., 2007). If only the hand is exposed while the rest of the body is protected, it can be assumed that the amount absorbed per time and area for males is 4.80×10^{-6} µg×cm^{-2}× hr^{-1} and for females 4.33×10^{-6} µg×cm^{-2}×hr^{-1}.

Figure 4.3.37 represents the plot of the flux of the compound VX with a concentration below saturation. The value used for the initial dose was 68 µg×cm^{-2}, which is the maximum amount without exceeding the saturated point. As seen, the toxicity is not reached, and can be assumed to not be lethal up to this concentration amount.
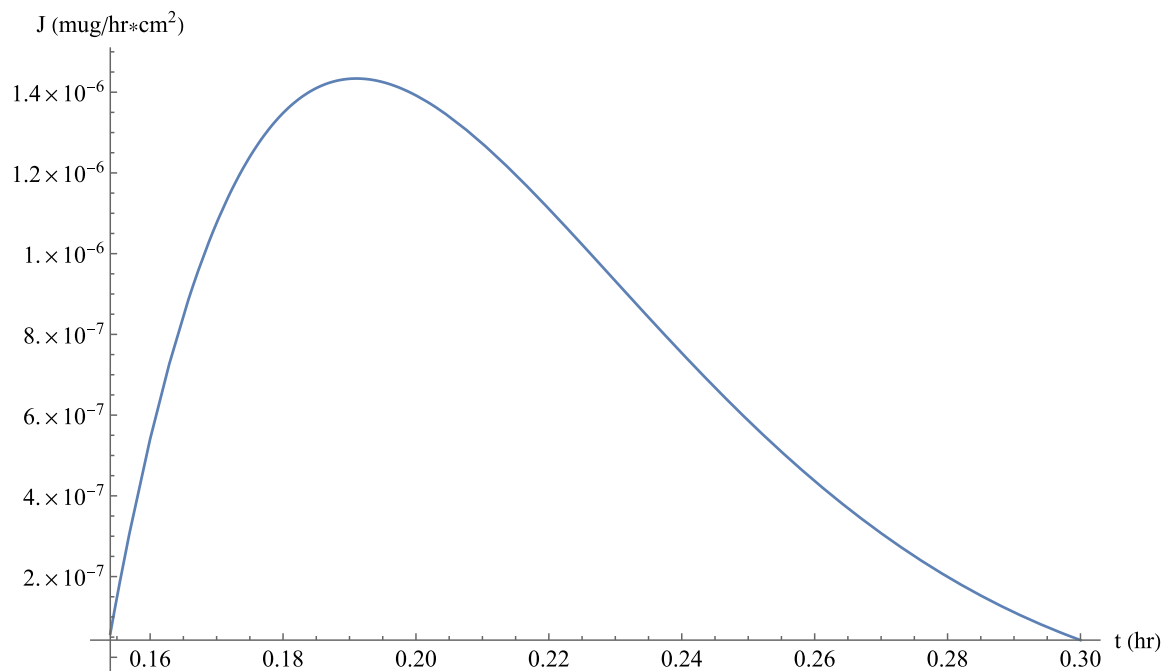
Figure 4.3.37 Flux graph of VX for small amount.
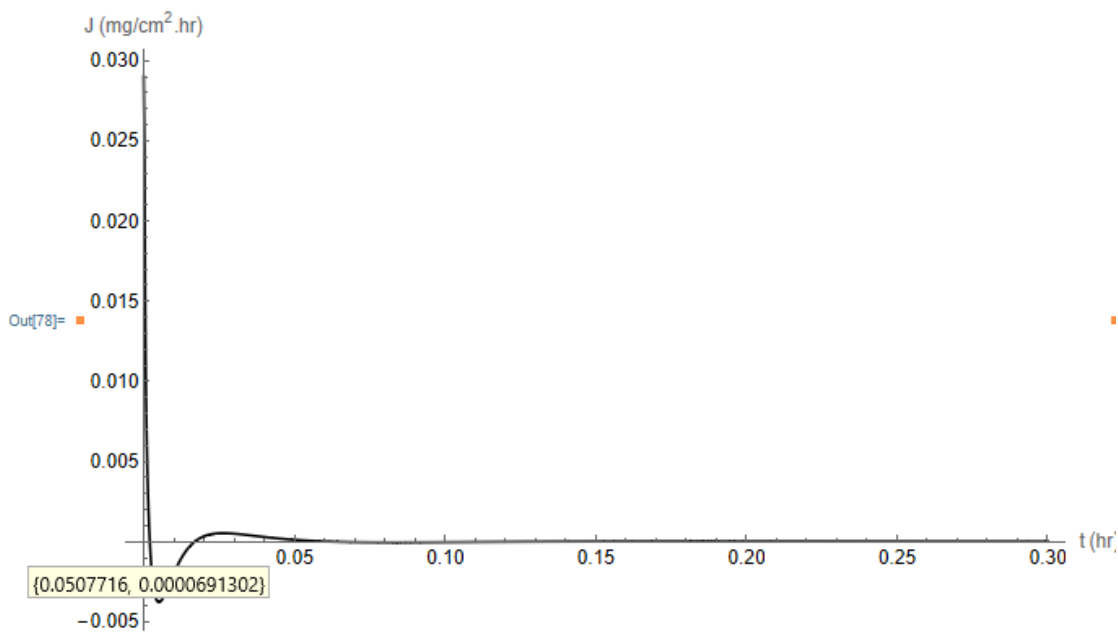
Figure 4.3.38 A representation of the OEL for VX at an initial concentration greater than saturation.
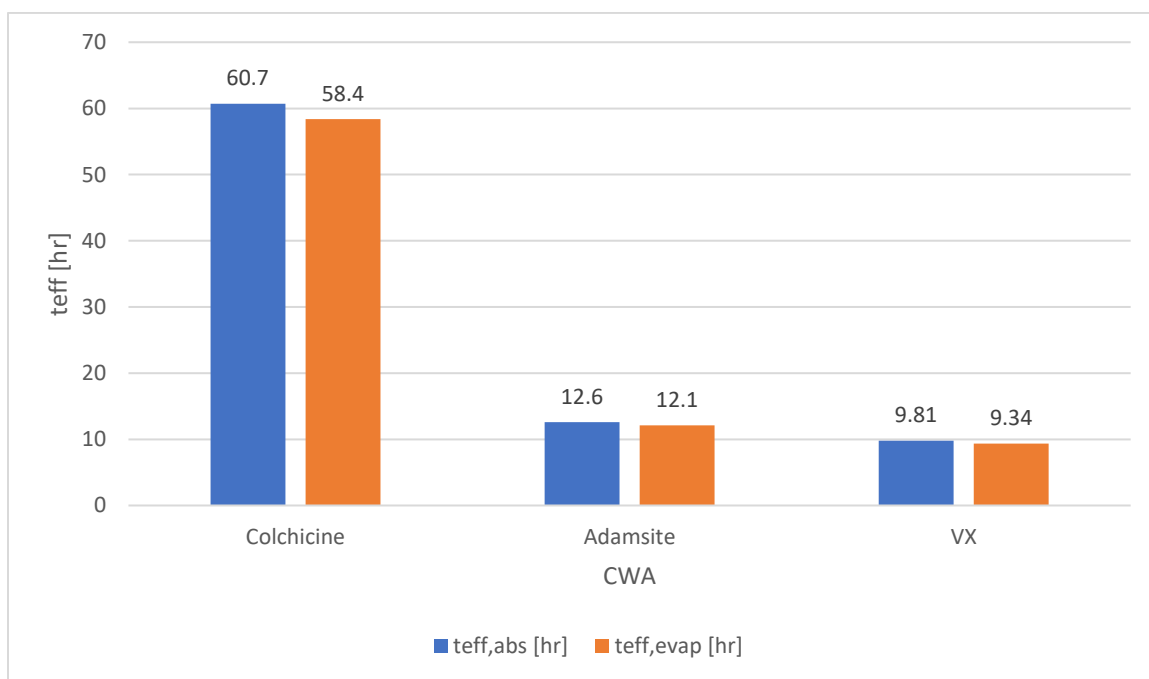
Figure 4.3.39 A representation of the effective time constants for absorption (blue) and evaporation (orange) for the compounds colchicine, adamsite, and VX.

However, as seen in Figure 4.3.38, for an initial concentration larger than the saturation, the OEL for both sexes are exceeded at about 3 minutes at a flux of about 6.91×10^{-5} $\mu g \times cm^{-2} \times hr^{-1}$. The flux was simulated with a 10% increase of Msat for the initial concentration which resulted in 0.761 mg/cm^2. The cumulative amount absorbed at this time period was about 1.73×10^{-6} mg/cm^2. Figure A.100 in the Appendix shows the graphical representation of this amount. It can be assumed that the risk of VX lethality would increase with a larger concentration and the window of time to react and decontaminate the affected skin would decrease. Figure 4.3.39 shows the effective time constants for both absorption and evaporation for the three compounds. VX's molecular weight, vapor pressure, $logK_{ow}$, and water solubility had contributed to causing the lowest effective time constants.

CHAPTER 5

CONCLUSION

Two computational models from Frasch and Kasting were developed and simulated in the Wolfram Mathematica environment. Small and large concentrations were analyzed for the transdermal permeability of CWAs. A large ratio of κ favored the evaporation of CWAs. A rise in the diffusion coefficient increased the absorption and evaporation of CWAs from the skin. Parameter uncertainty can have an appreciable impact on the dynamic profiles and the development of protocols to reduce the risk of contamination. The procedure outlined can be combined with occupational exposure limit data for inhalation to better understand toxicity due to dermal absorption.

APPENDIX

CWA Tables with Captions:

Table A.1 Nerve Agents with Parameter Values Estimated by the Procedure Outlined in the Text

Compound	MW [g/mol]	LogKow	k_p [cm/hr]	P_{vap} [torr]	S_w [mg/mL]	k_g [cm/hr]	κ	D_{sc} [cm²/s] 10^{-11}	Ksc	C_{sat} [mg/cm³]	M_{sat} [μg/cm²]	M_0 [μg/cm²]	t_{effabs} [hr]	$t_{effevap}$ [hr]	$M_{abs\infty}$	$M_{evap\infty}$
Sarin	140.09	0.3	4.11×10^{-4}	2.86	46.38	875.85	991.25	9.69	5.32	246.64	33.05	29.74	0.600	0.377	0.0510	0.949
Soman	182.17	1.78	2.26×10^{-3}	0.410	21.00	583.04	49.31	5.63	13.7	288.42	38.65	34.78	1.07	0.689	0.0689	0.931
Tabun	162.13	0.38	3.49×10^{-4}	0.0700	98.00	625.64	11.17	7.29	5.58	546.68	73.26	65.93	0.935	0.659	0.128	0.872
VX	267.37	2.09	1.21×10^{-3}	8.78×10^{-4}	30.00	500.17	0.170	1.88	17.2	516.24	69.18	62.26	9.81	9.34	0.862	0.138
Cyclosarin, GF	180.16	1.67	1.96×10^{-3}	0.0440	3.70	587.72	34.48	5.78	12.7	47.06	6.31	5.68	1.06	0.691	0.0768	0.923
GV	159.27	-0.78	6.21×10^{-5}	0.0682	1000	554.96	5.22	7.57	2.87	2866.41	384.1	345.69	1.04	0.802	0.203	0.797
O,O-diisopropyl fluorophosphate	184.15	1.13	8.21×10^{-4}	0.580	15.40	600.06	272.60	5.49	8.88	136.73	18.32	16.49	1.07	0.670	0.0535	0.947
Amiton	269.34	1.7	6.51×10^{-4}	4.48×10^{-4}	65.92	509.72	0.0800	1.83	12.99	855.98	114.7	103.23	10.70	10.24	0.930	0.0704

Table A.2 Vesicants with Parameter Values Estimated by the Procedure Outlined in the Text

Compound	MW [g/mol]	$LogK_{ow}$	k_p [cm/hr]	P_{vap} [torr]	S_w [mg/mL]	k_g [cm/hr]	κ	D_{sc} [cm²/s] 10^{-11}	Ksc	C_{sat} [mg/cm³]	M_{sat} [μg/cm²]	M_0 [μg/cm²]	t_{effabs} [hr]	$t_{effevap}$ [hr]	$M_{abs\infty}$	$M_{evap\infty}$
Sulfur Mustard, HD	159.08	2.14	0.00527	0.110	0.609	707.92	208.00	7.58	17.9	10.88	1.46	1.31	0.773	0.487	0.0545	0.945
Lewisite	207.32	2.56	0.00535	0.395	0.500	859.30	1415	4.07	25	12.51	1.68	1.51	1.43	0.896	0.0507	0.896
HN-3	204.53	2.27	0.00357	0.0110	0.160	616.46	131.00	4.22	19.8	3.16	0.42	0.38	1.40	0.882	0.0572	0.943
HN-1	170.08	2.02	0.00381	0.250	0.160	618.84	2320	6.58	16.3	2.61	0.35	0.32	0.883	0.554	0.0504	0.950
HN-2	156.05	0.91	0.00085	0.170	121.40	652.66	9.08	7.89	7.72	937.3	89.1651	113.04	0.892	0.643	0.144	0.856
Phosgene oxime	113.93	0.73	0.00111	11.2	25.00	935.52	2320	13.6	6.9	172.56	23.12	20.81	0.427	0.268	0.0504	0.950
Ethyldichloroarsine	174.89	2.34	0.00582	2.29	0.588	834.42	5260	6.19	20.9	12.27	1.64	1.48	0.938	0.589	0.0502	0.950
Methyldichloroarsine	160.86	1.85	0.00331	0.0544	1.80	977.74	77.40	7.41	14.4	25.92	3.47	3.13	0.804	0.511	0.0621	0.938
Phenyldichloroarsine	222.93	3.1	0.00994	0.0330	0.0804	682.09	338.00	3.33	41.2	3.31	0.44	0.4	1.75	1.10	0.0528	0.947

Table A.3 Blood Agents with Parameter Values Estimated by the Procedure Outlined in the Text

Compound	MW [g/mol]	LogK$_{ow}$	k$_p$ [cm/hr]	P$_{vap}$ [torr]	S$_w$ [mg/mL]	k$_g$ [cm/hr]	κ	D$_{sc}$ [cm^2/s] 10^{-11}	Ksc	C$_{sat}$ [mg/cm^3]	M$_{sat}$ [µg/cm^2]	M$_0$ [µg/cm^2]	t$_{effabs}$ [hr]	t$_{effevap}$ [hr]	M$_{abs\infty}$	M$_{evap\infty}$
HCN	27.025	-0.25	0.000765	742	95.40	1159.91	1.71x10^4	41.6	3.86	367.97	49.31	44.38	0.140	0.088	0.0501	0.950
Cyanogen chloride	61.46	-0.38	0.000403	1230	0.0275	1126.27	4.14x10^8	26.7	3.58	0.100	0.1	0.012	0.217	0.136	0.0500	0.950
Hydrogen sulfide	34.08	-1.38	0.000125	13600	3.98	1591.82	7.95x10^7	38.0	2.08	8.29	1.11	1.00	0.153	0.0958	0.0500	0.950

Table A.4 Lung Injurants with Parameter Values Estimated by the Procedure Outlined in the Text

Compound	MW [g/mol]	LogK$_{ow}$	k$_p$ [cm/hr]	P$_{vap}$ [torr]	S$_w$ [mg/mL]	k$_g$ [cm/hr]	κ	D$_{sc}$ [cm^2/s] 10^{-11}	Ksc	C$_{sat}$ [mg/cm^3]	M$_{sat}$ [µg/cm^2]	M$_0$ [µg/cm^2]	t$_{effabs}$ [hr]	t$_{effevap}$ [hr]	M$_{abs\infty}$	M$_{evap\infty}$
Phosgene	98.91	-0.71	0.000150	1420	475.10	1012.71	1.07x10^5	16.5	2.98	1415.24	189.64	170.68	0.352	0.221	0.0500	0.950
Diphosgene	197.8	1.49	0.00119	10.0	2.39	824.75	3.09x10^4	4.6	11.3	26.87	3.60	3.24	1.26	0.792	0.0500	0.950
Chlorine	70.9	0.85	0.00231	5830	6.30	2678.97	4.09x10^6	23.6	7.44	46.85	6.28	5.65	0.246	0.154	0.0500	0.950
Perfluoroisobutene	200.03	3.03	0.0120	1740	0.113	742.19	1.03x10^7	4.47	38.4	4.34	0.48	0.52	1.30	0.815	0.0500	0.950

Table A.5 Riot-control Agents with Parameter Values Estimated by the Procedure Outlined in the Text

Compound	MW [g/mol]	LogK$_{ow}$	k$_p$ [cm/hr]	P$_{vap}$ [torr]	S$_w$ [mg/mL]	k$_g$ [cm/hr]	κ	D$_{sc}$ [cm^2/s] 10^{-11}	Ksc	C$_{sat}$ [mg/cm^3]	M$_{sat}$ [µg/cm^2]	M$_0$ [µg/cm^2]	t$_{effabs}$ [hr]	t$_{effevap}$ [hr]	M$_{abs\infty}$	M$_{evap\infty}$
Chloropicrin	164.37	2.09	0.00456	24.0	1.62	891.62	2.56x10^4	7.08	17.2	27.88	3.74	3.36	0.820	0.514	0.0500	0.950
Bromobenzyl cyanide	196.04	1.83	0.00204	0.0120	0.678	616.29	56.30	4.71	14.2	9.65	1.29	1.16	1.28	0.817	0.0666	0.933
1-Chloroacetophenone	154.59	1.93	0.00406	0.00540	1.81	682.04	4.18	8.04	15.3	27.6	3.7	3.33	1.03	0.821	0.233	0.767
2-chlorobenzilidene malononitrile	188.61	2.76	0.00923	3.40x10^{-5}	0.119	573.73	0.180	5.18	29.8	3.55	0.48	0.43	3.54	3.365	0.855	0.145
Xylyl bromide	185.06	3.43	0.0268	0.153	0.0611	617.51	576.00	5.43	58.6	3.58	0.48	0.43	1.07	0.674	0.0516	0.948
Bromoacetone	136.98	0.11	0.00032	90.0	69.63	759.78	2.26x10^4	10.1	4.75	330.9	44.34	39.91	0.575	0.361	0.0500	0.950
Ethyl iodoacetate	214	1.62	0.00118	0.640	1.52	678.73	2790	3.74	12.3	18.71	2.51	2.26	1.55	0.975	0.0503	0.950

Table A.6 Psychomimetic Agents with Parameter Values Estimated by the Procedure Outlined in the Text

Compound	MW [g/mol]	LogK$_{ow}$	k$_p$ [cm/hr]	P$_{vap}$ [torr]	S$_w$ [mg/mL]	k$_g$ [cm/hr]	κ	D$_{sc}$ [cm^2/s] 10^{-11}	Ksc	C$_{sat}$ [mg/cm^3]	M$_{sat}$ [µg/cm^2]	M$_0$ [ug/cm^2]	t$_{effabs}$ [hr]	t$_{effevap}$ [hr]	M$_{abs∞}$	M$_{evap∞}$
3-quinuclidinyl benzilate	337.4	3.01	0.00198	2.38x10^{-10}	0.2	437.17	4.76x10^{-6}	0.761	37.7	7.54	1.01	0.91	27.3	26.2	1.00	4.52x10^{-6}

Table A.7 Toxins with Parameter Values Estimated by the Procedure Outlined in the Text

Compound	MW [g/mol]	LogK$_{ow}$	k$_p$ [cm/hr]	P$_{vap}$ [torr]	S$_w$ [mg/mL]	k$_g$ [cm/hr]	κ	D$_{sc}$ [cm^2/s] 10^{-11}	Ksc	C$_{sat}$ [mg/cm^3]	M$_{sat}$ [µg/cm^2]	M$_0$ [µg/cm^2]	t$_{effabs}$ [hr]	t$_{effevap}$ [hr]	M$_{abs∞}$	M$_{evap∞}$
Colchicine	399.4	1.03	4.40x10^{-5}	3.20x10^{-11}	0.24	429.26	2.80x10^{-5}	0.342	8.33	2.00	0.27	0.240	60.7	58.4	1.00	.70x10^{-5}

Table A.8 Vomiting Agents with Parameter Values Estimated by the Procedure Outlined in the Text

Compound	MW [g/mol]	LogK$_{ow}$	k$_p$ [cm/hr]	P$_{vap}$ [torr]	S$_w$ [mg/mL]	k$_g$ [cm/hr]	κ	D$_{sc}$ [cm^2/s] 10^{-11}	Ksc	C$_{sat}$ [mg/cm^3]	M$_{sat}$ [µg/cm^2]	M$_0$ [µg/cm^2]	t$_{effabs}$ [hr]	t$_{effevap}$ [hr]	M$_{abs∞}$	M$_{evap∞}$
Trifluoronitrosomethane	99.012	1.06	0.00221	7460	14.58	960.45	1.18x10^6	16.5	8.49	123.78	16.59	14.93	0.352	0.221	0.0500	0.950
Adamsite	277.58	4.05	0.0208	2.00x10^{-13}	0.00065	570.77	1.26x10^{-7}	1.65	127	0.0800	0.0110	0.0100	12.6	12.1	1.000	1.20x10^{-7}
Diphenylchloroarsine	264.58	0.00045	5.23x10^{-5}	4.50x10^{-4}	0.00272	555.28	2.50x10^4	1.95	4.46	0.0121	0.0016	1.46x10^{-3}	2.98	1.87	0.0500	0.950
Diphenylcyanoarsine	255.15	3.29	0.00876	7.16x10^{-6}	0.01882	536.55	0.320	2.2	50.22	0.9500	0.1300	0.1100	7.68	7.25	0.770	0.230

Effects of Model Parameters for Small Dose:
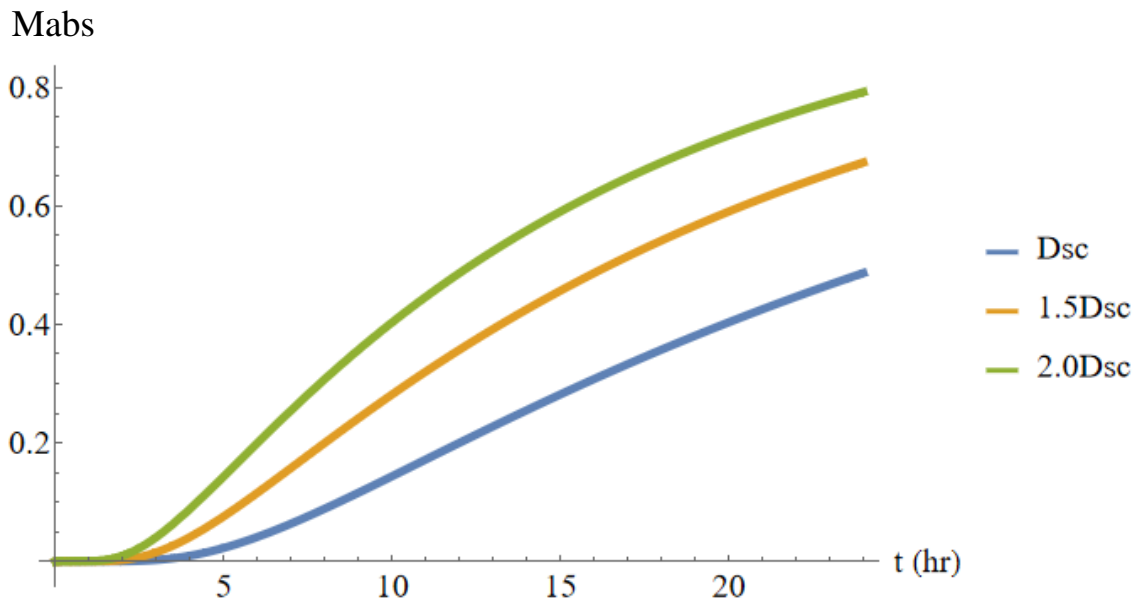
Figure A.40 Graphical representation of the effect of the diffusion coefficient for the absorption profile using 3-quinuclidinyl benzilate as a reference compound.
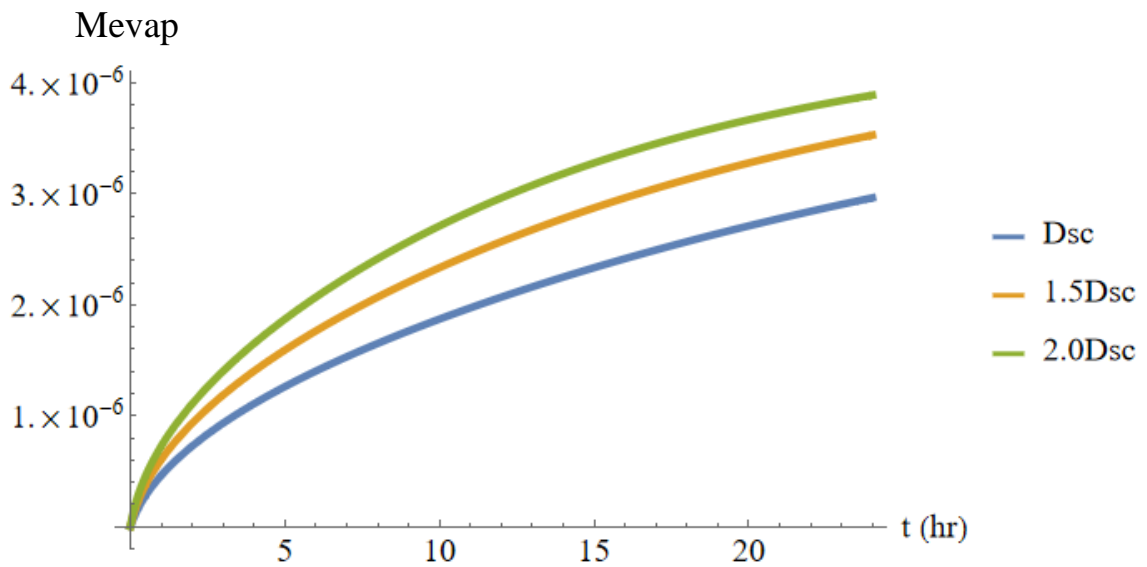
Figure A.41 Graphical representation of the effect of the diffusion coefficient for the evaporation profile using 3-quinuclidinyl benzilate as a reference compound.

Mabs
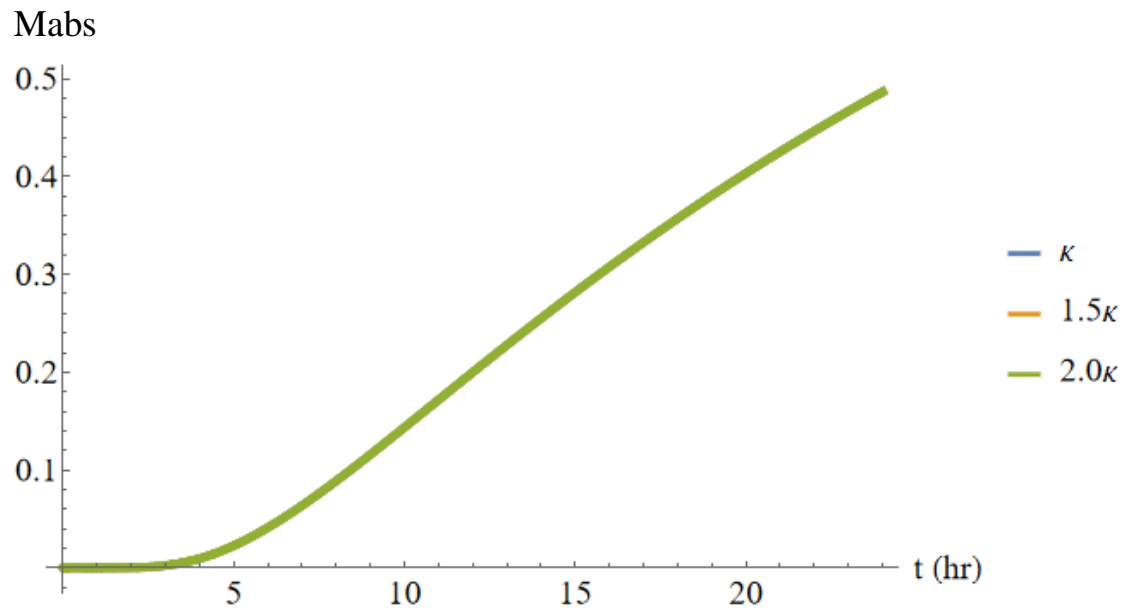
Figure A.42 Graphical representation of the effect of the ratio κ for the absorption profile using 3-quinuclidinyl benzilate as a reference compound.

Mevap
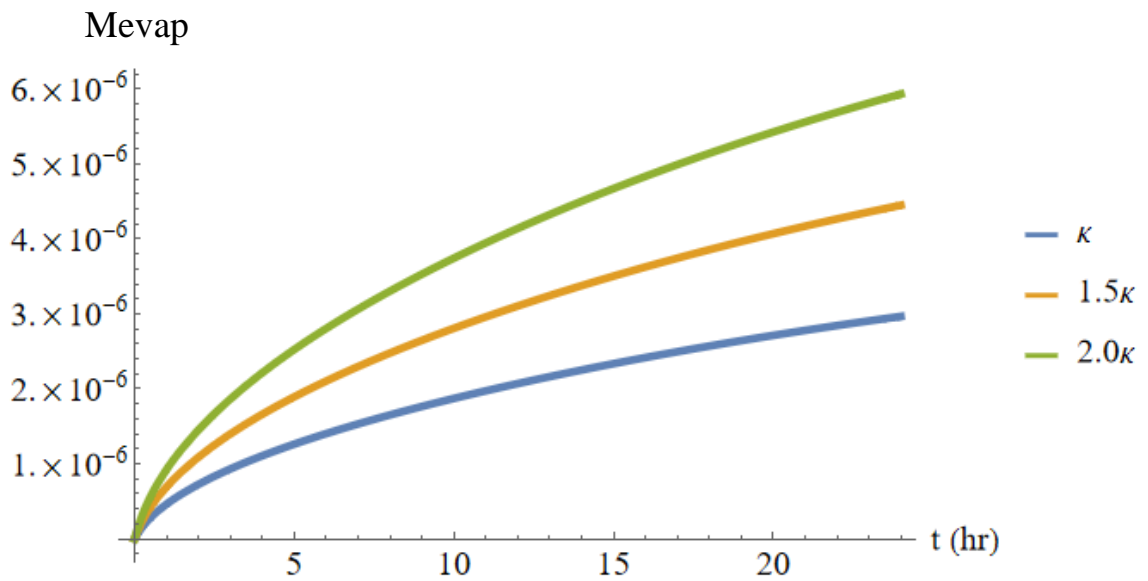
Figure A.43 Graphical representation of the effect of the ratio κ for the evaporation profile using 3-quinuclidinyl benzilate as a reference compound.
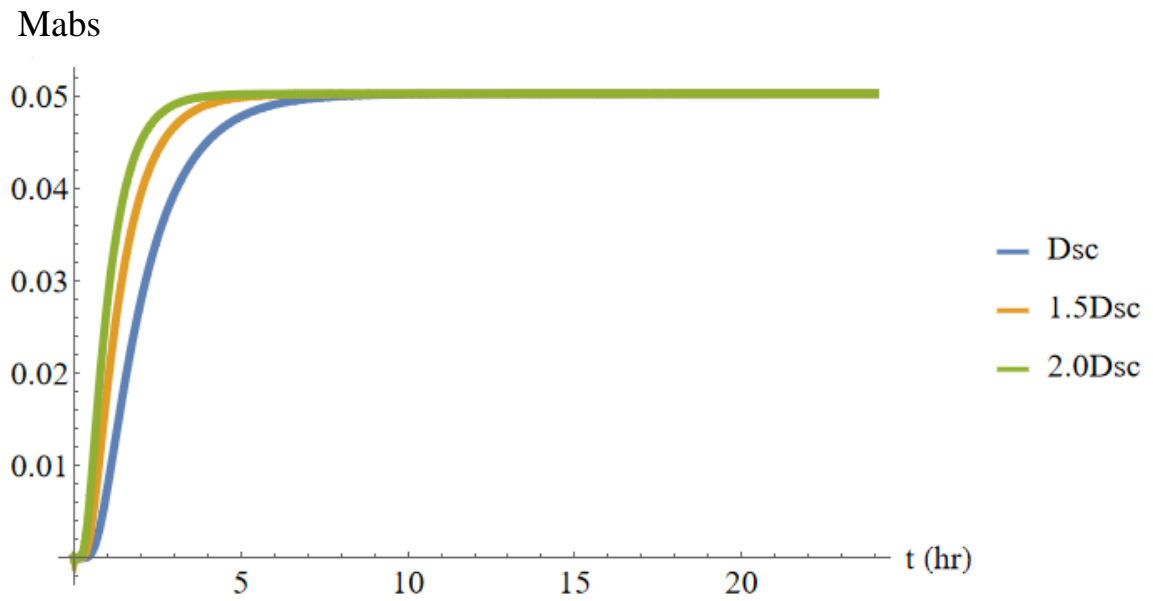
Figure A.44 Graphical representation of the effect of the diffusion coefficient for the absorption profile using ethyl iodoacetate as a reference compound.
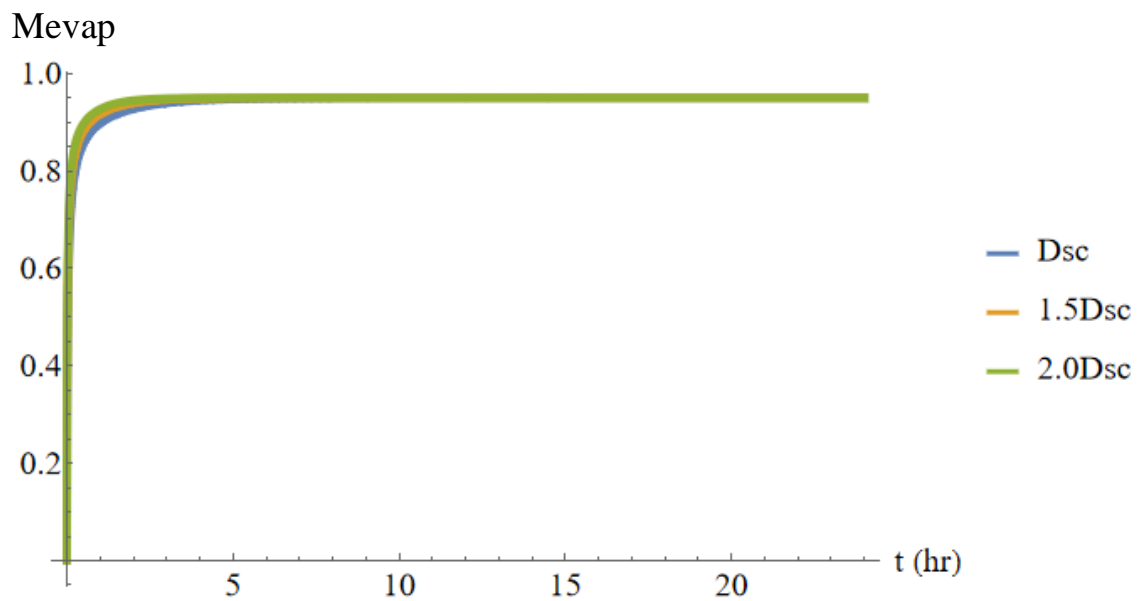
Figure A.45 Graphical representation of the effect of the diffusion coefficient for the evaporation profile using ethyl iodoacetate as a reference compound.
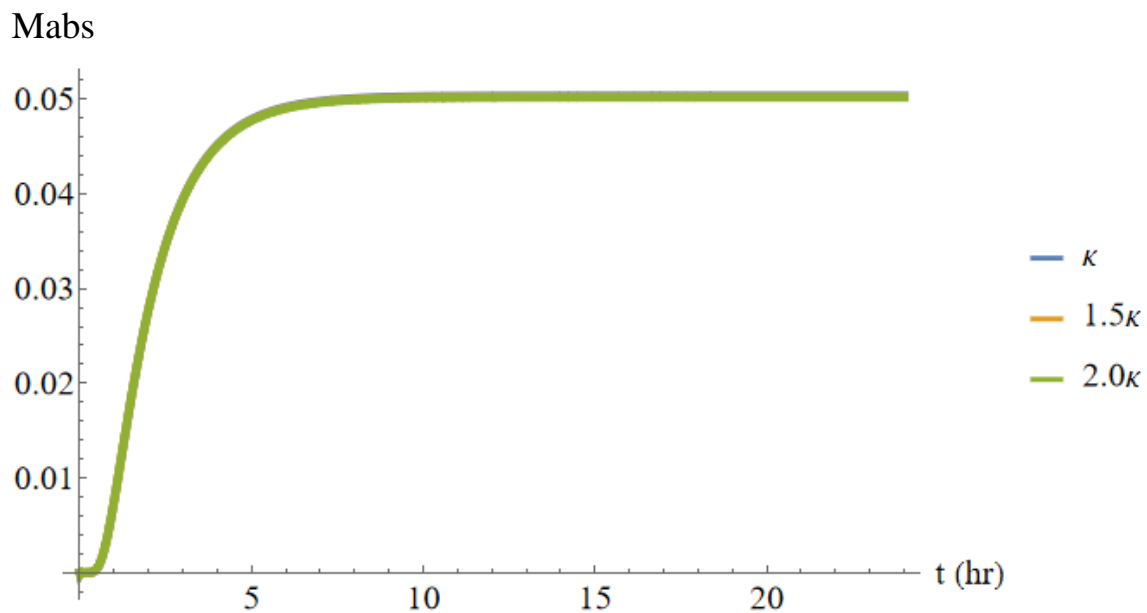
Figure A.46 Graphical representation of the effect of the ratio κ for the absorption profile using ethyl iodoacetate as a reference compound.
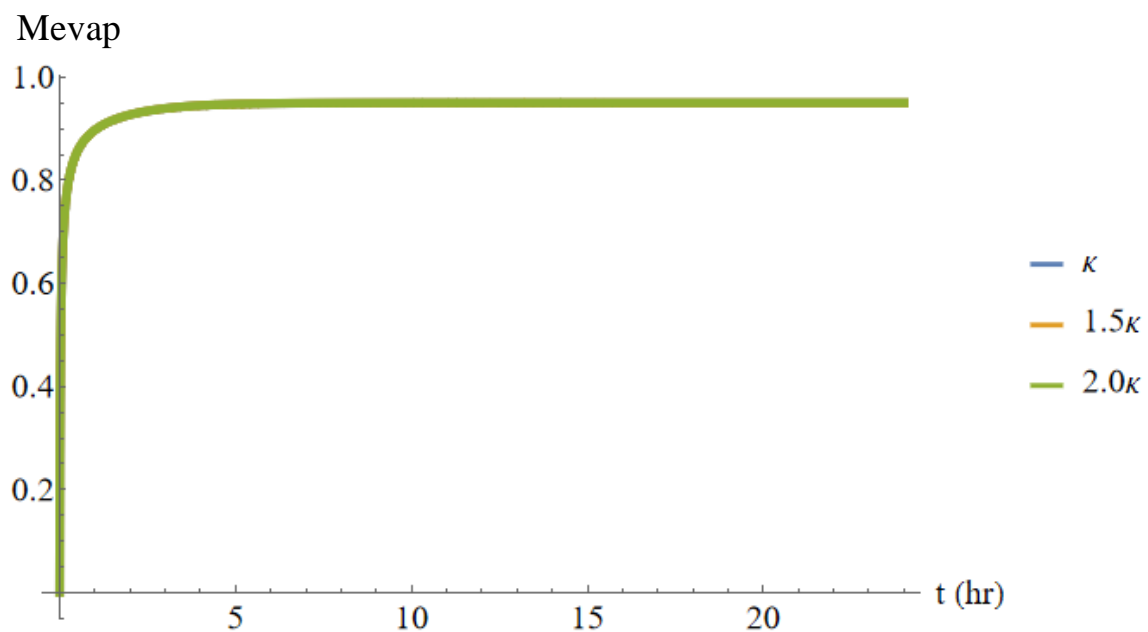
Figure A.47 Graphical representation of the effect of the ratio κ for the evaporation profile using ethyl iodoacetate as a reference compound.
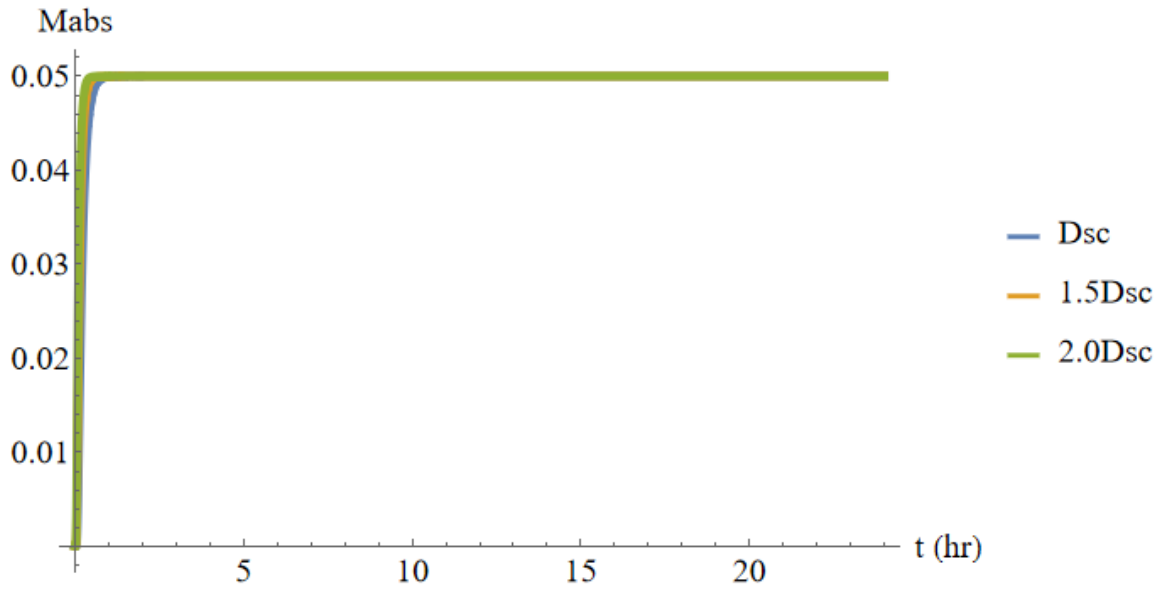
Figure A.48 Graphical representation of the effect of the diffusion coefficient for the absorption profile using hydrogen sulfide as a reference compound.
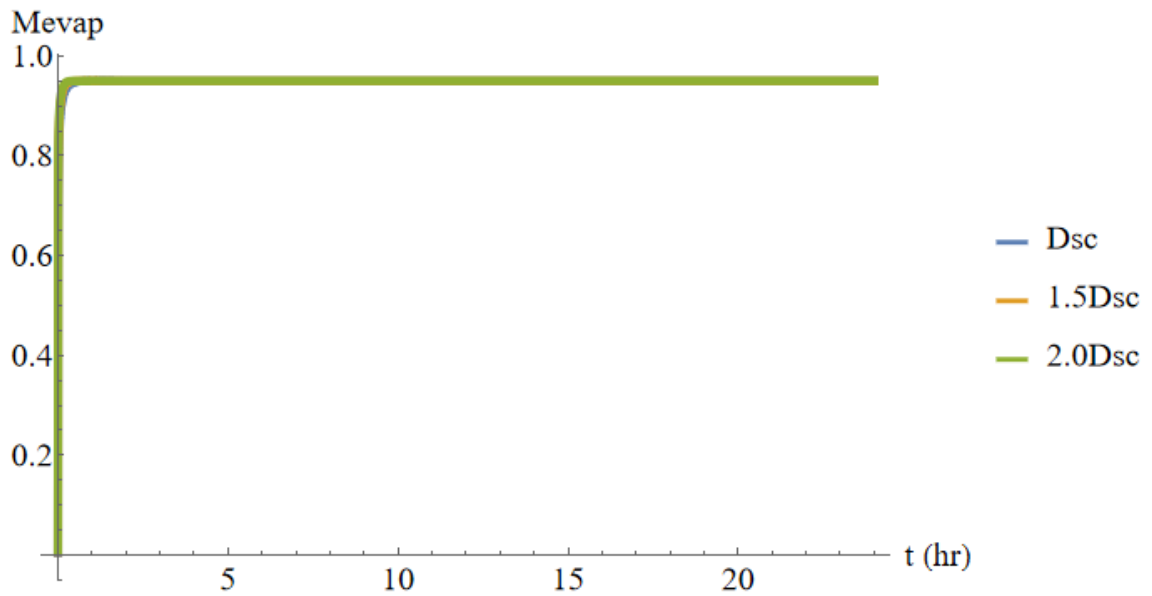
Figure A.49 Graphical representation of the effect of the diffusion coefficient for the evaporation profile using hydrogen sulfide as a reference compound.
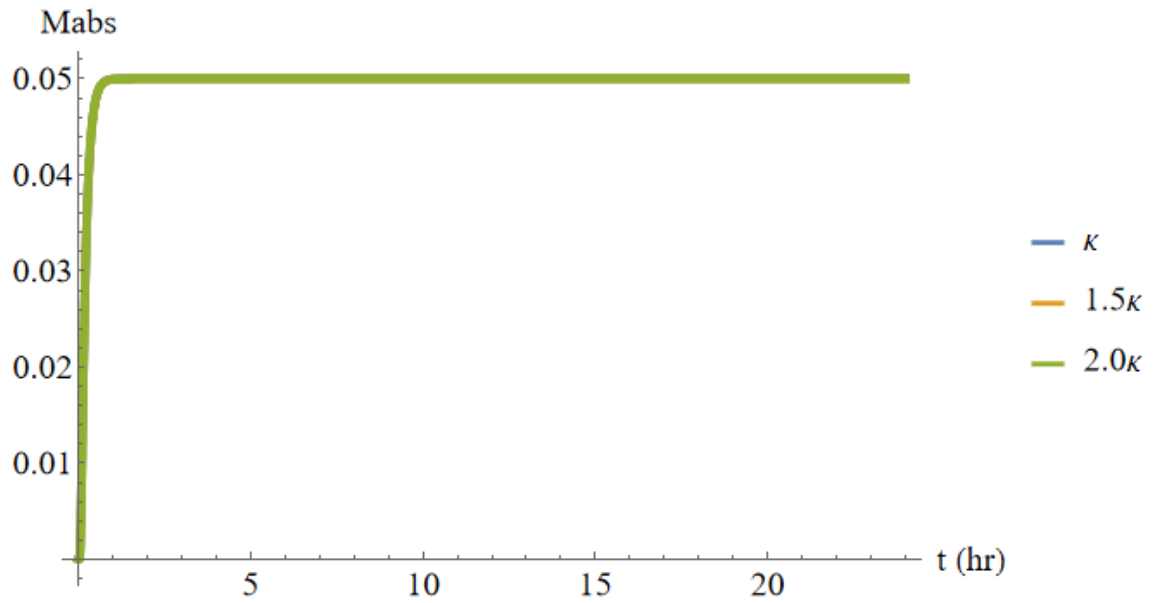
Figure A.50 Graphical representation of the effect of the ratio κ for the absorption profile using hydrogen sulfide as a reference compound.
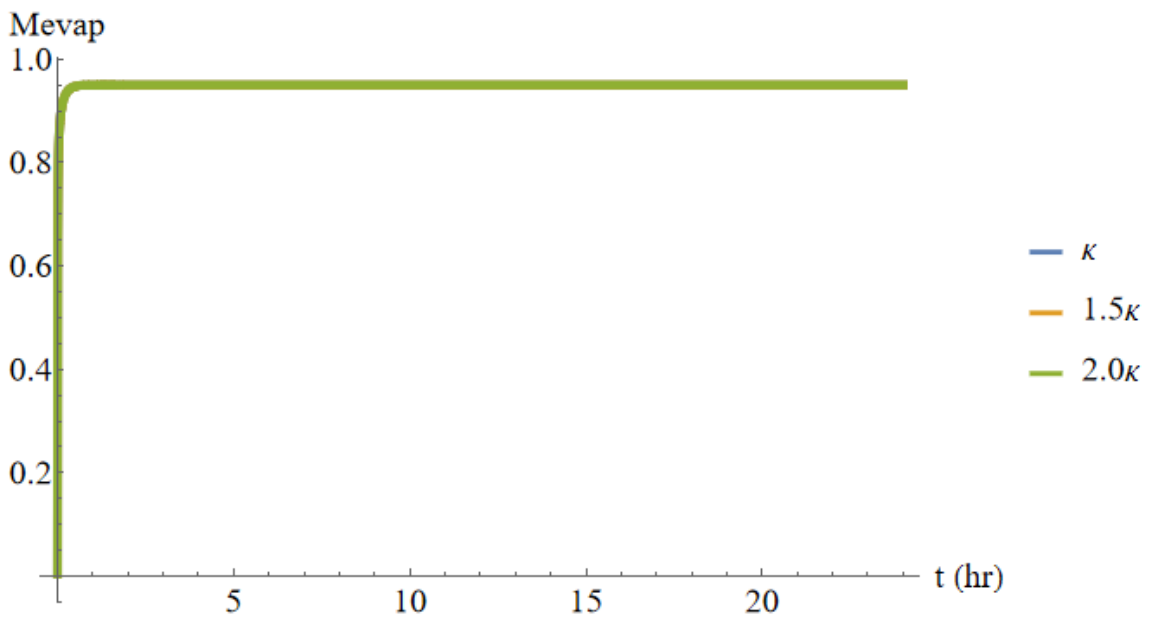
Figure A.51 Graphical representation of the effect of the ratio κ for the evaporation profile using hydrogen sulfide as a reference compound.
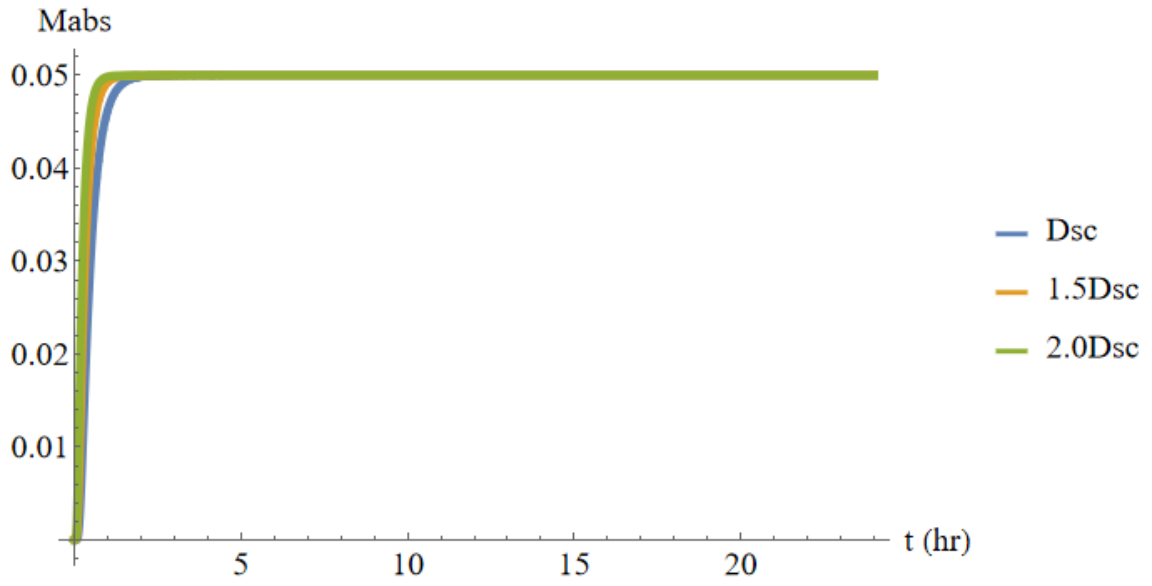
Figure A.52 Graphical representation of the effect of the diffusion coefficient for the absorption profile using phosgene as a reference compound.
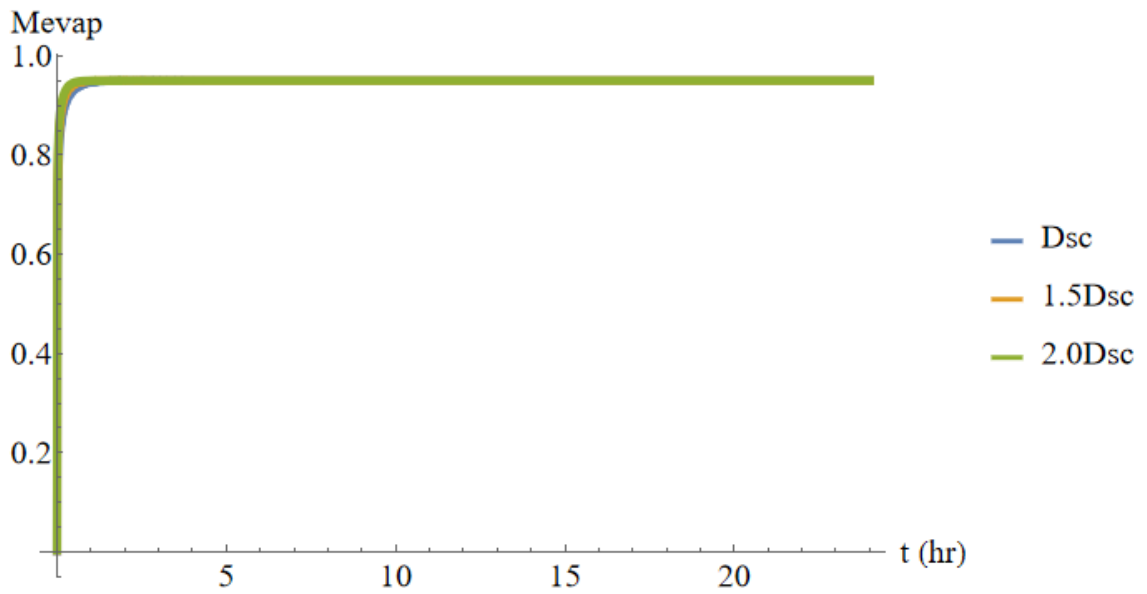
Figure A.53 Graphical representation of the effect of the diffusion coefficient for the evaporation profile using phosgene as a reference compound.
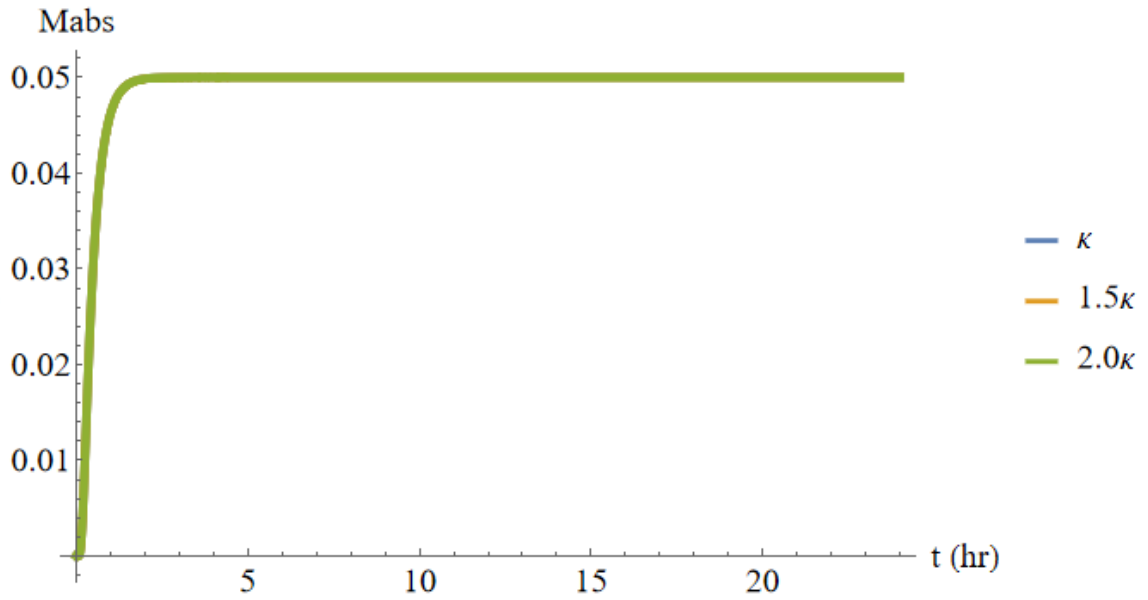
Figure A.54 Graphical representation of the effect of the ratio κ for the absorption profile using phosgene as a reference compound.
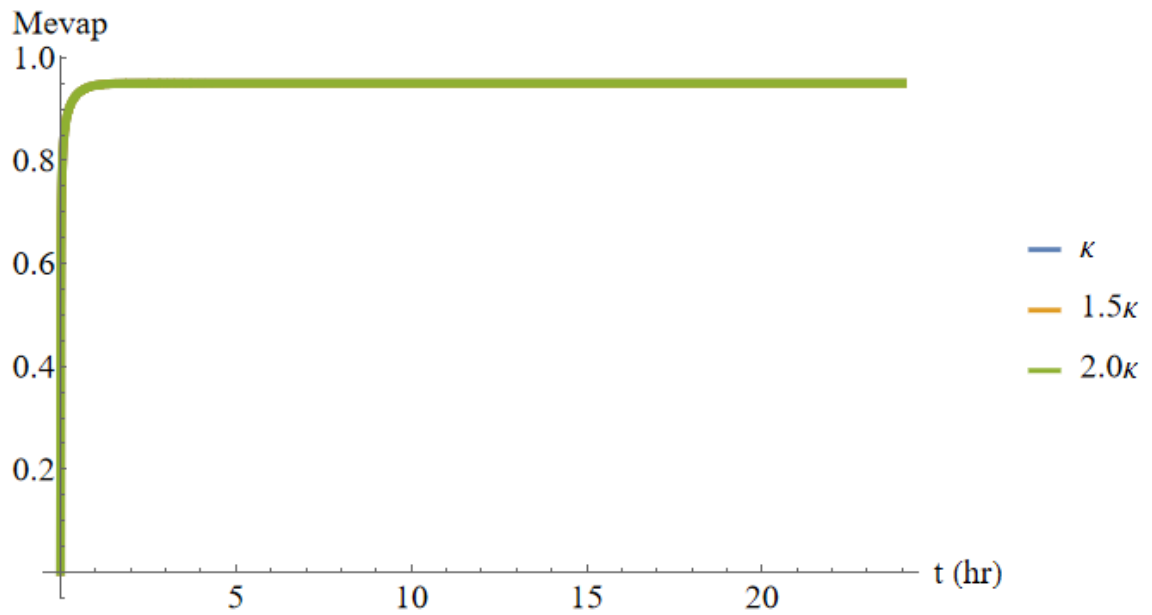
Figure A.55 Graphical representation of the effect of the ratio κ for the evaporation profile using phosgene as a reference compound.
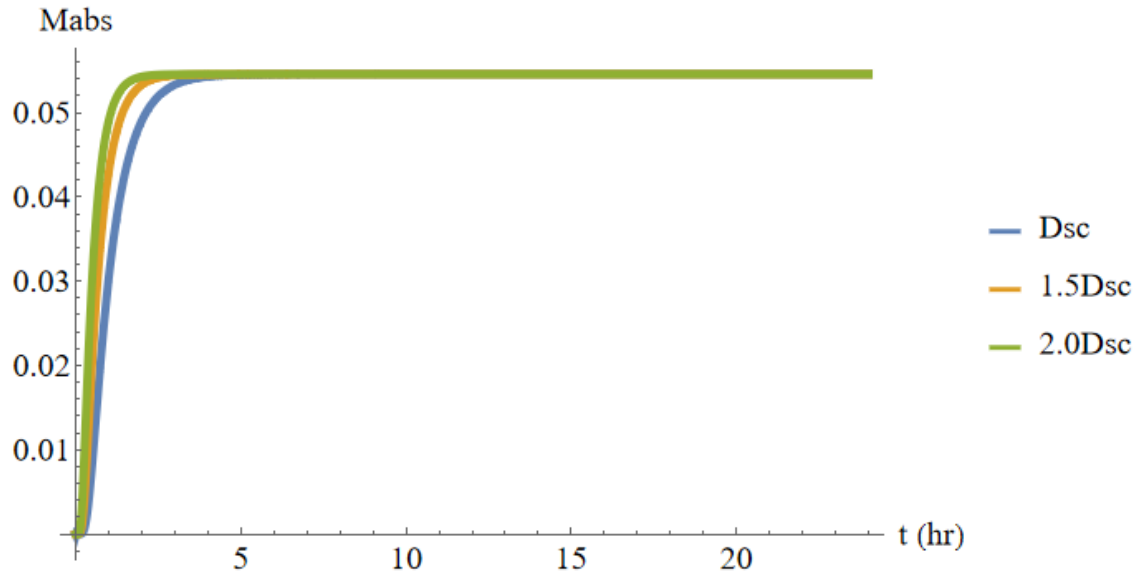
Figure A.56 Graphical representation of the effect of the diffusion coefficient for the absorption profile using sulfur mustard as a reference compound.
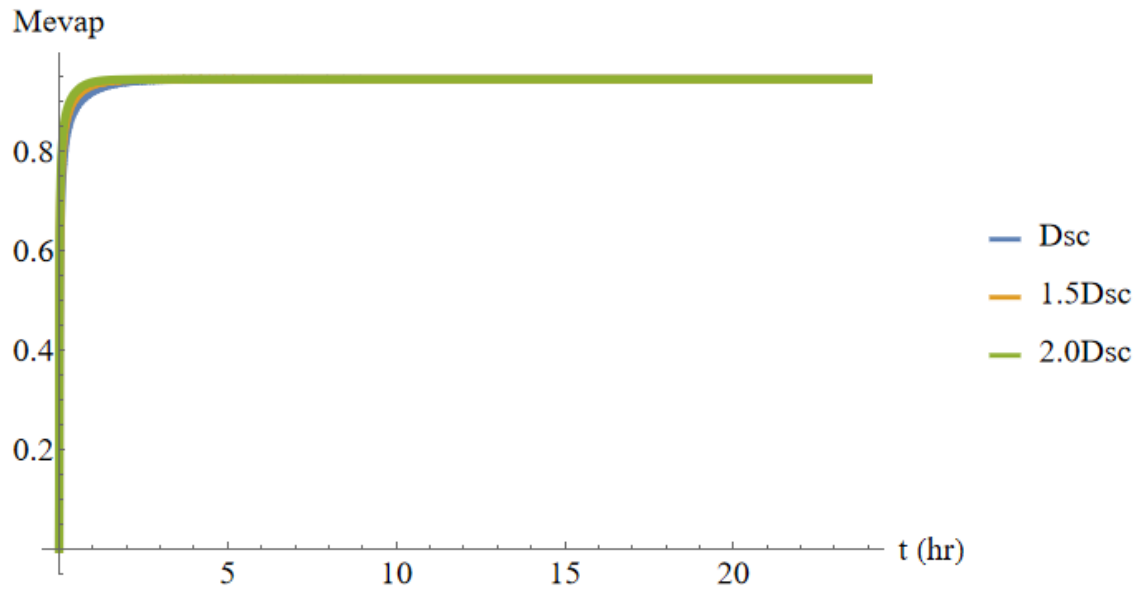
Figure A.57 Graphical representation of the effect of the diffusion coefficient for the evaporation profile using sulfur mustard as a reference compound.
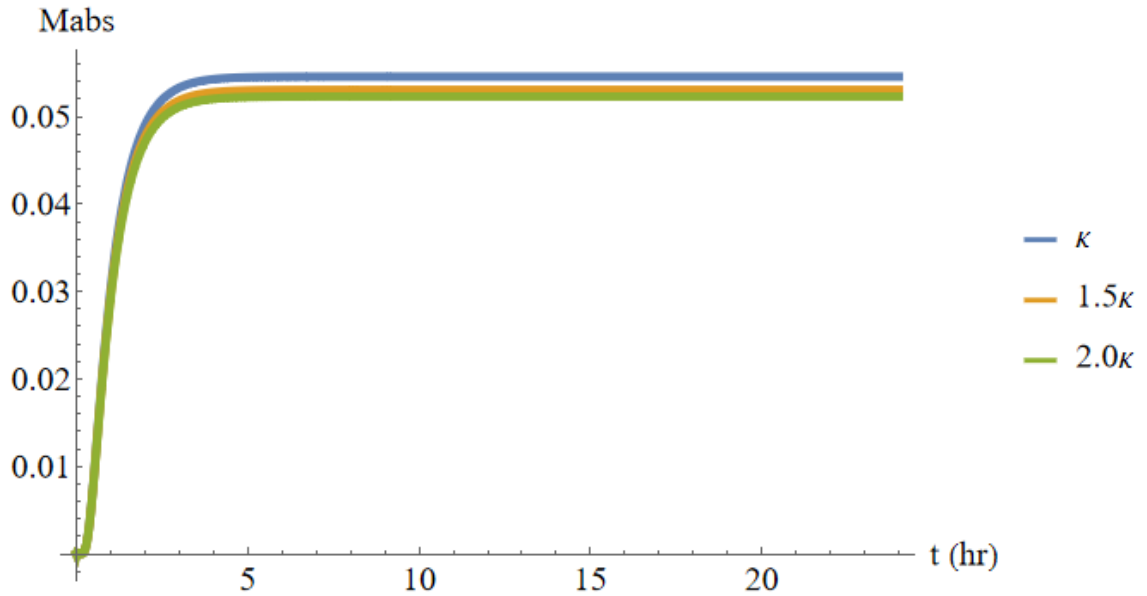
Figure A.58 Graphical representation of the effect of the ratio κ for the absorption profile using sulfur mustard as a reference compound.
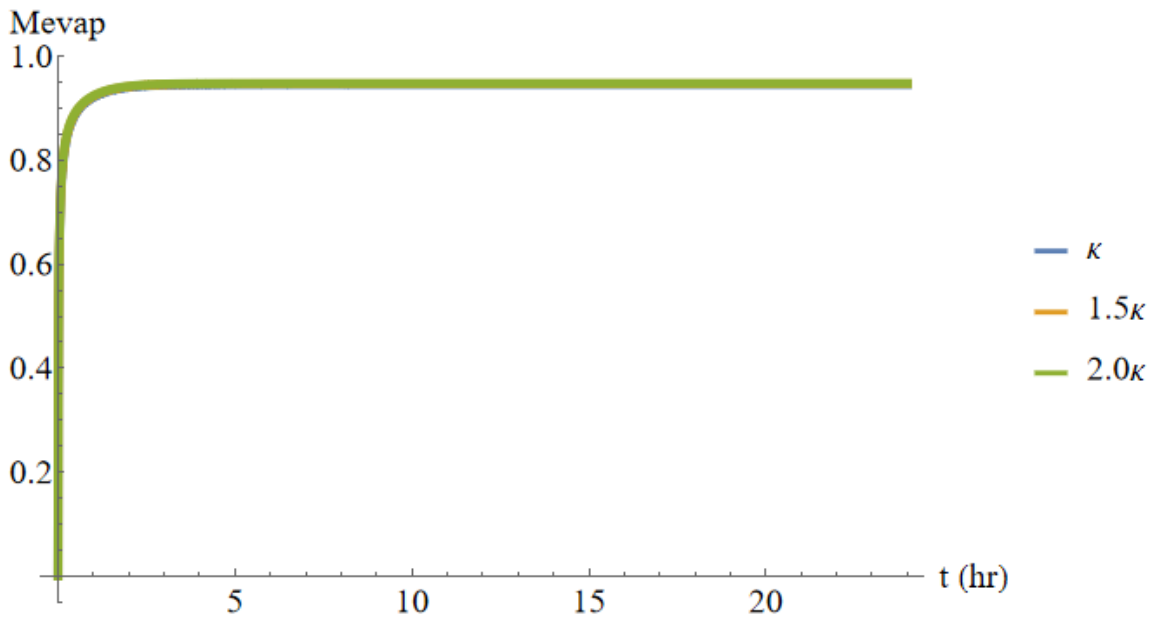
Figure A.59 Graphical representation of the effect of the ratio κ for the evaporation profile using sulfur mustard as a reference compound.

Effects of Model Parameters Large Dose:
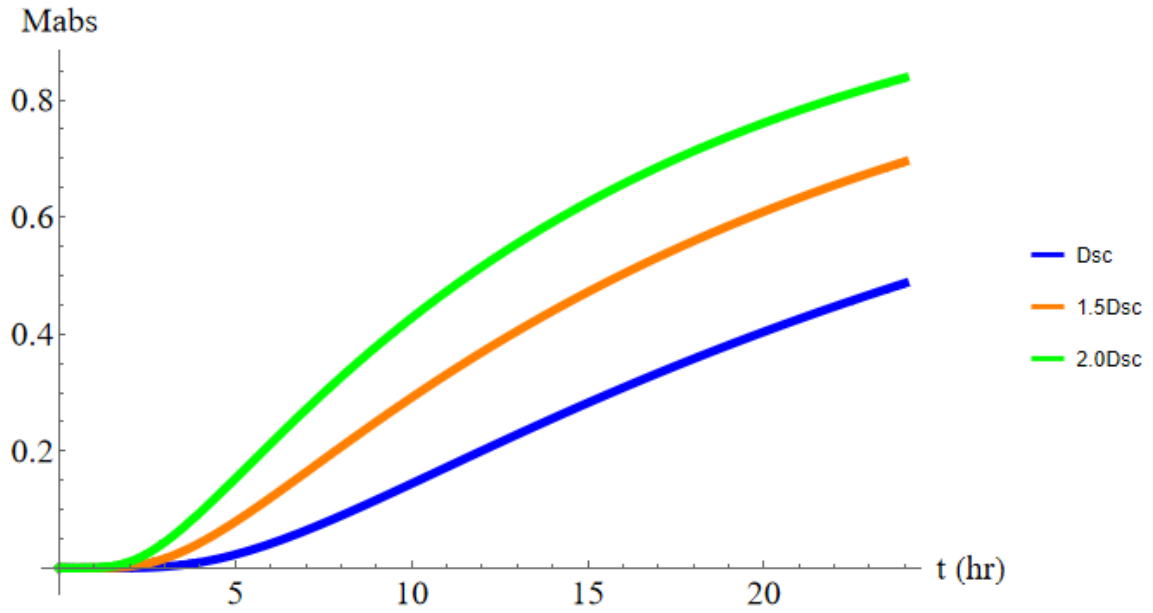
Figure A.60 Graphical representation of the effect of the diffusion coefficient for the absorption profile using 3-quinuclidinyl benzilate as a reference compound.
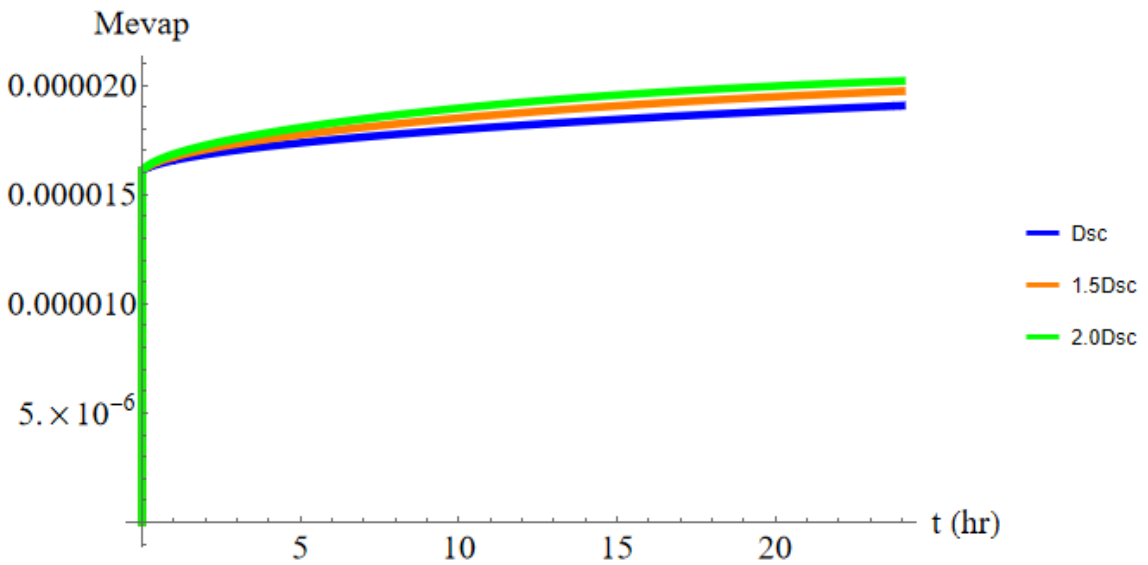
Figure A.61 Graphical representation of the effect of the diffusion coefficient for the evaporation profile using 3-quinuclidinyl benzilate as a reference compound.
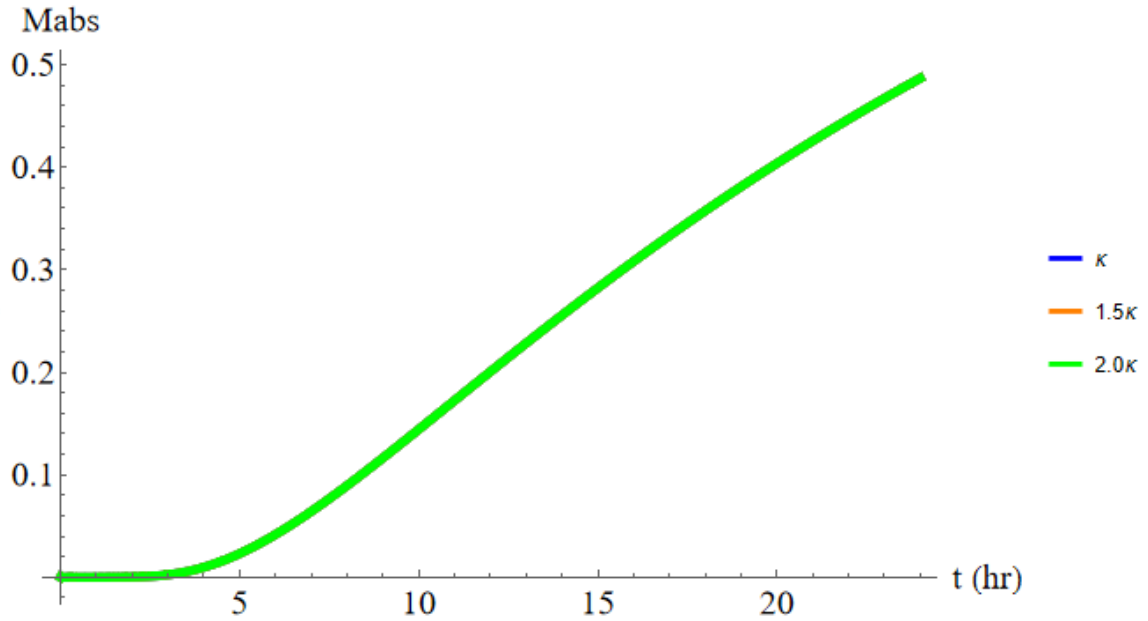
Figure A.62 Graphical representation of the effect of the ratio κ for the absorption profile using 3-quinuclidinyl benzilate as a reference compound.
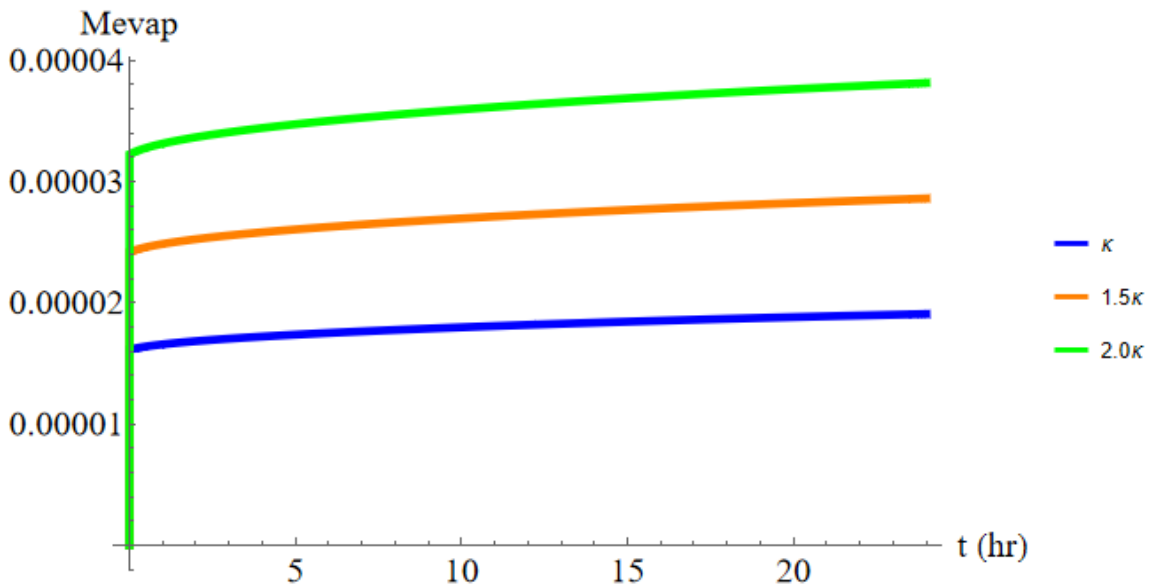
Figure A.63 Graphical representation of the effect of the ratio κ for the evaporation profile using 3-quinuclidinyl benzilate as a reference compound.
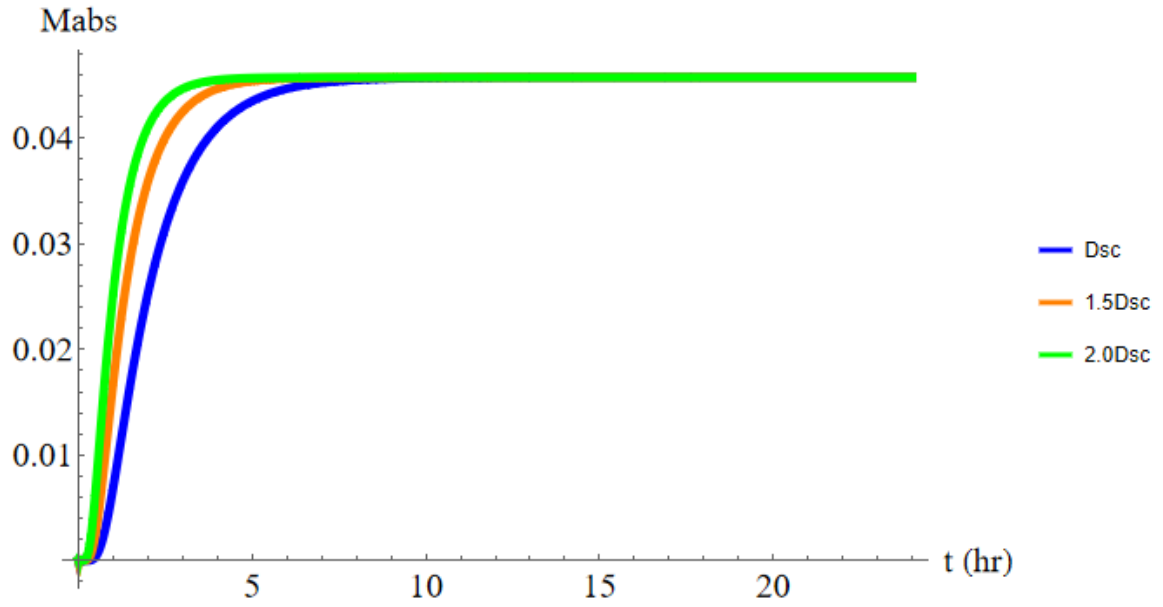
Figure A.64 Graphical representation of the effect of the diffusion coefficient for the absorption profile using ethyl iodoacetate as a reference compound.
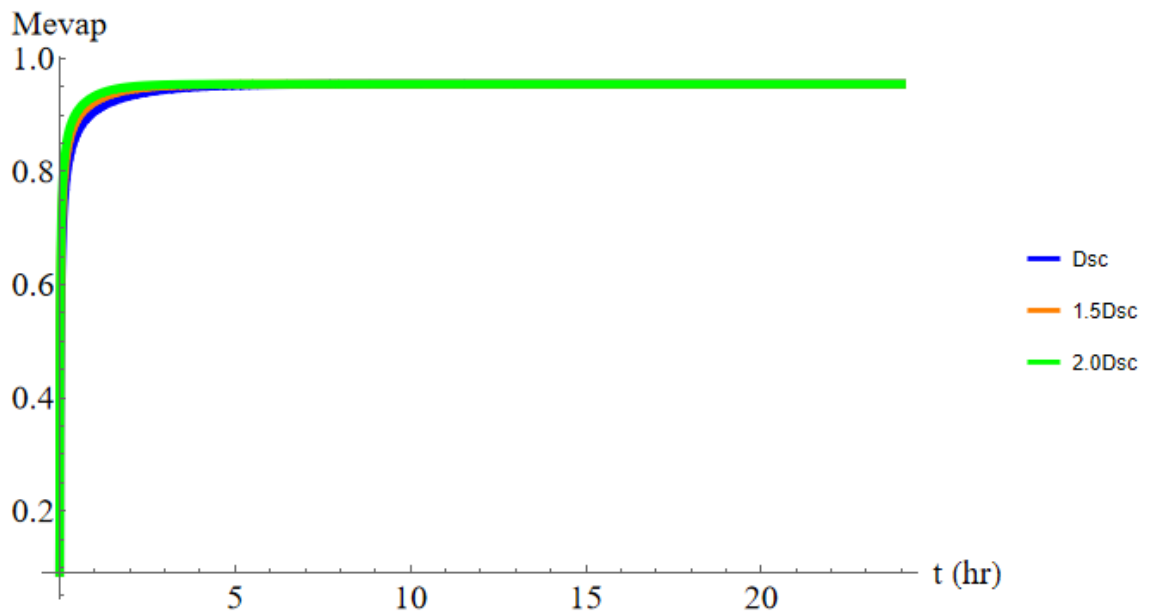
Figure A.65 Graphical representation of the effect of the diffusion coefficient for the evaporation profile using ethyl iodoacetate as a reference compound.
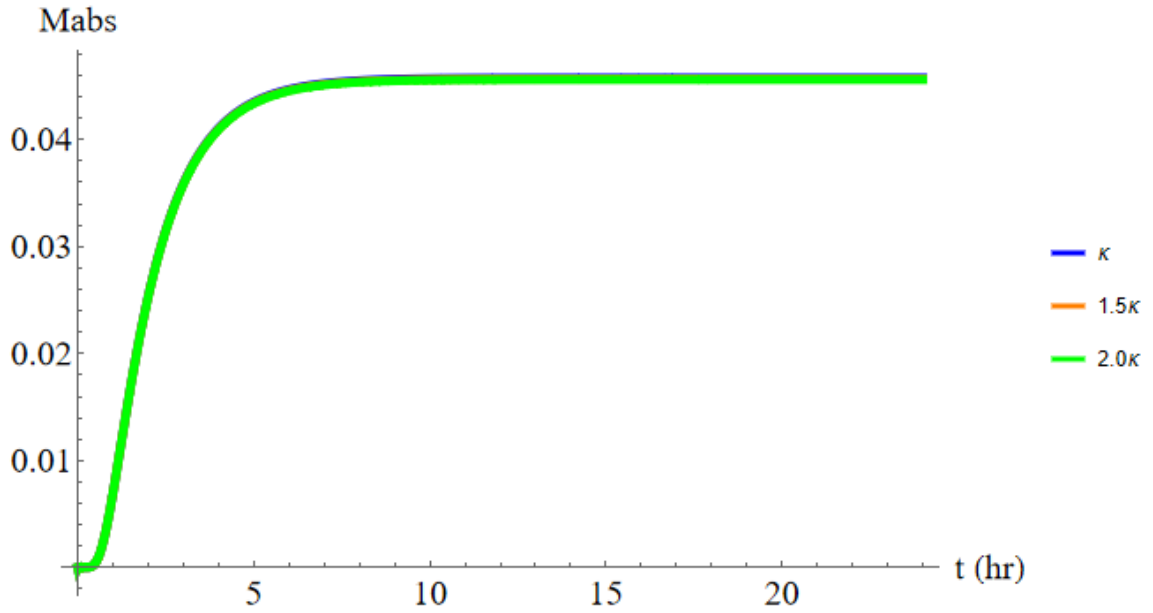
Figure A.66 Graphical representation of the effect of the ratio κ for the absorption profile using ethyl iodoacetate as a reference compound.
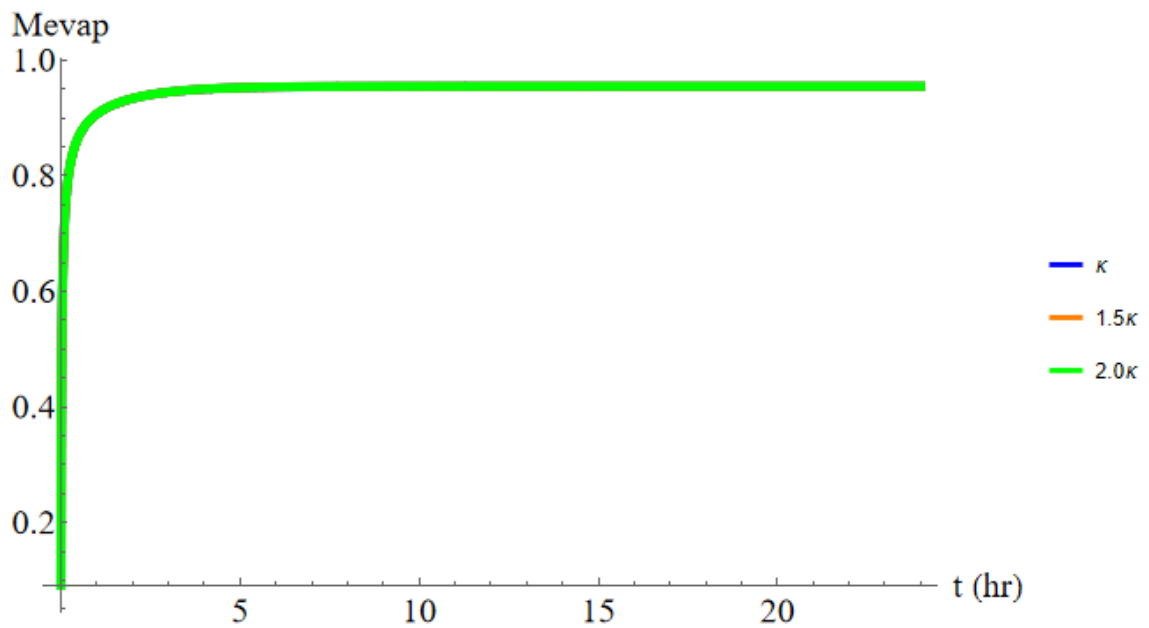
Figure A.67 Graphical representation of the effect of the ratio κ for the evaporation profile using ethyl iodoacetate as a reference compound.
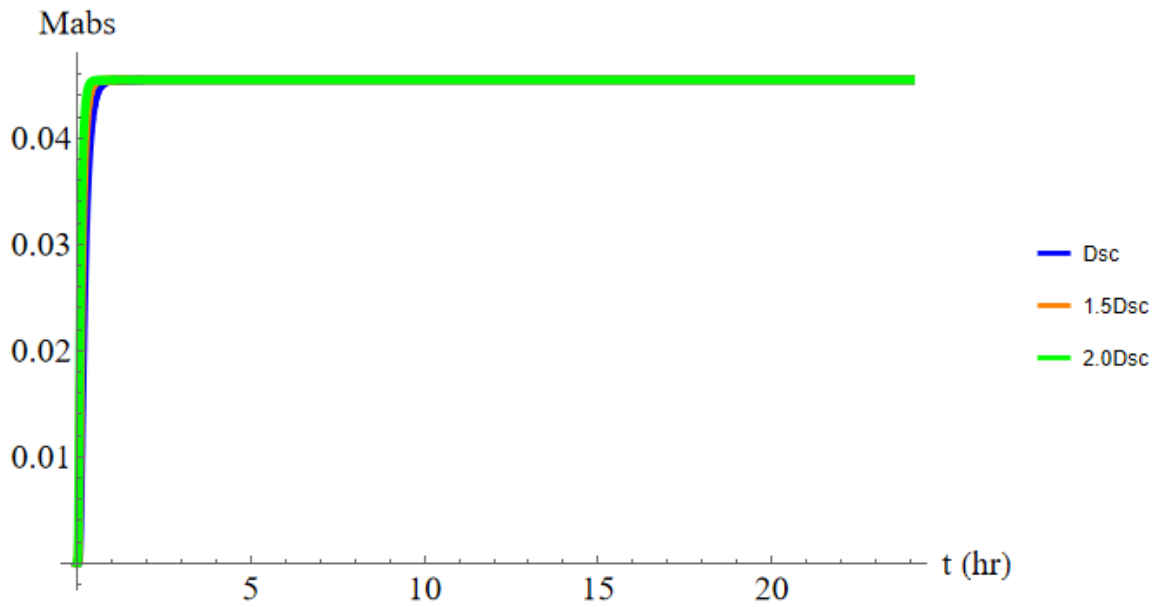
Figure A.68 Graphical representation of the effect of the diffusion coefficient for the absorption profile using hydrogen sulfide as a reference compound.
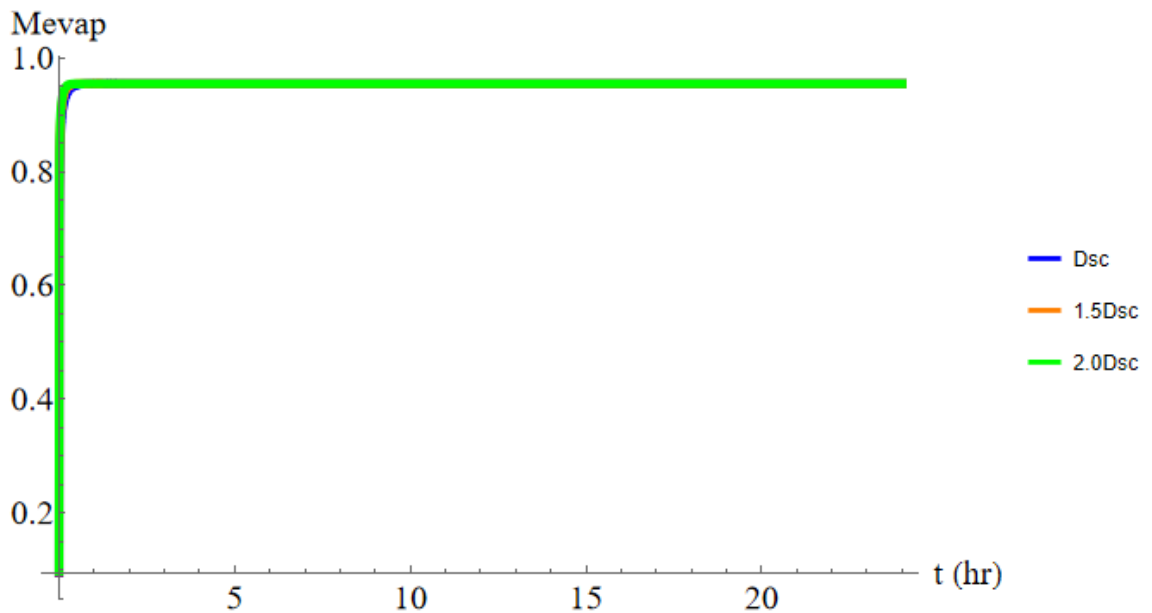
Figure A.69 Graphical representation of the effect of the diffusion coefficient for the evaporation profile using hydrogen sulfide as a reference compound.
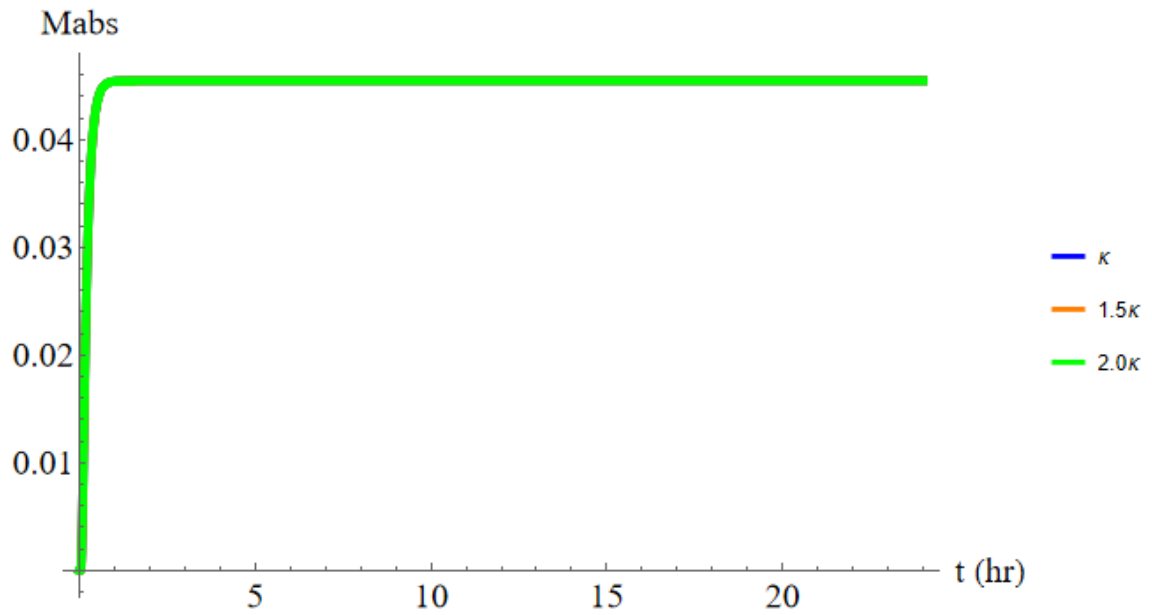
Figure A.70 Graphical representation of the effect of the ratio κ for the absorption profile using hydrogen sulfide as a reference compound.
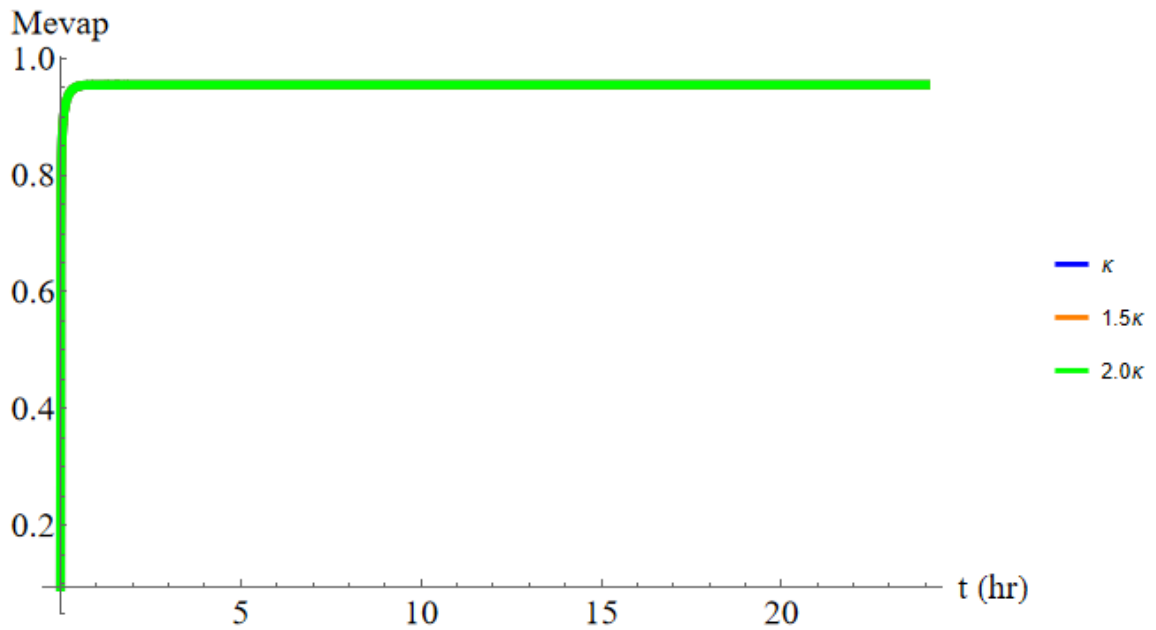
Figure A.71 Graphical representation of the effect of the ratio κ for the evaporation profile using hydrogen sulfide as a reference compound.
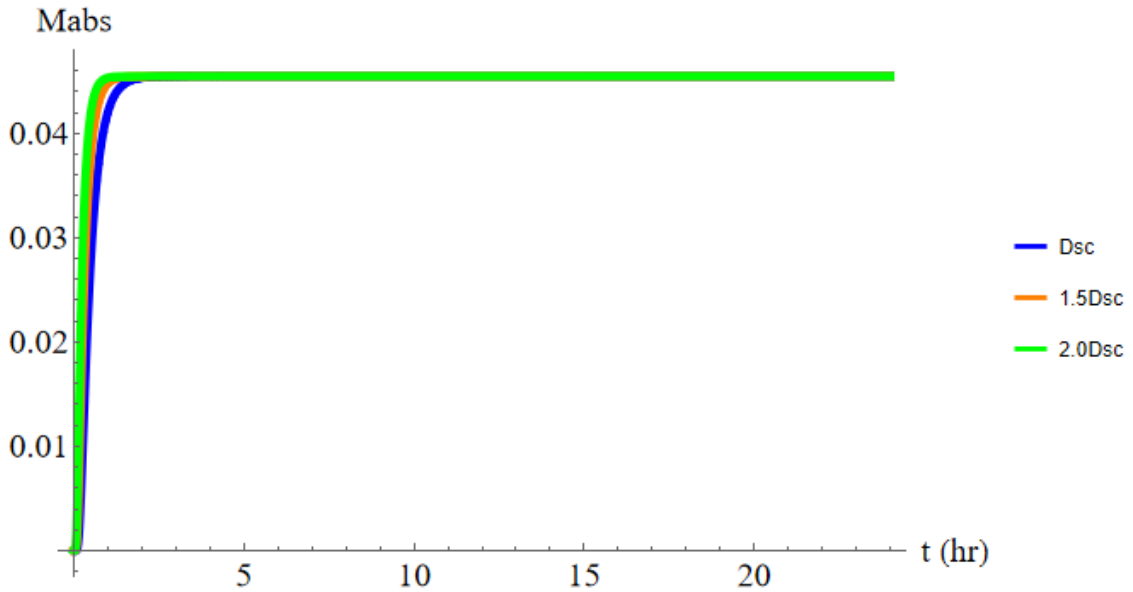
Figure A.72 Graphical representation of the effect of the diffusion coefficient for the absorption profile using phosgene as a reference compound.
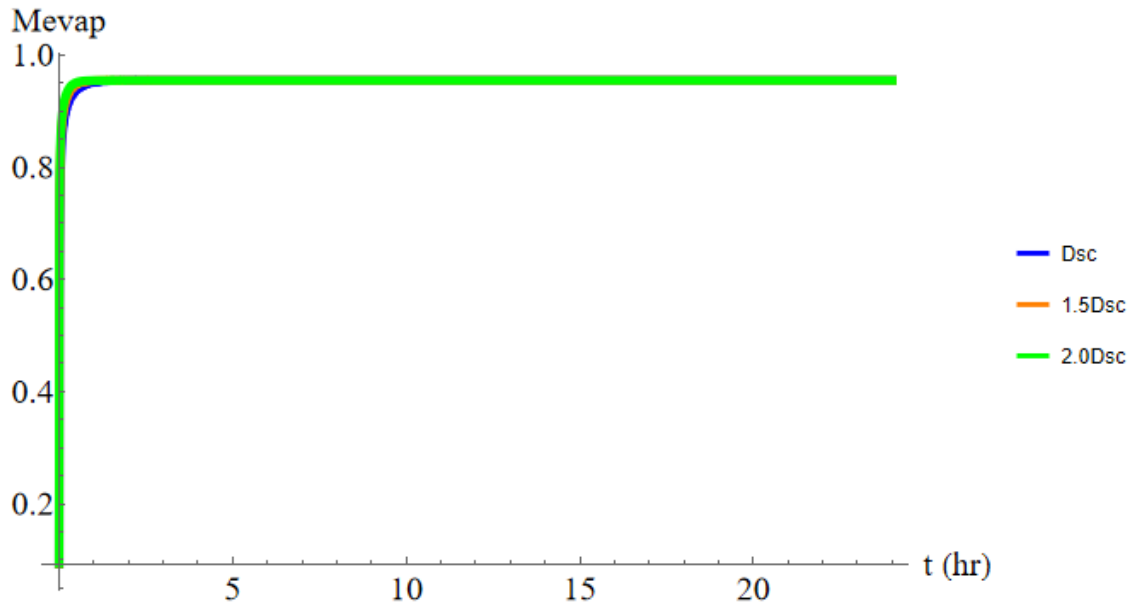
Figure A.73 Graphical representation of the effect of the diffusion coefficient for the evaporation profile using phosgene as a reference compound.
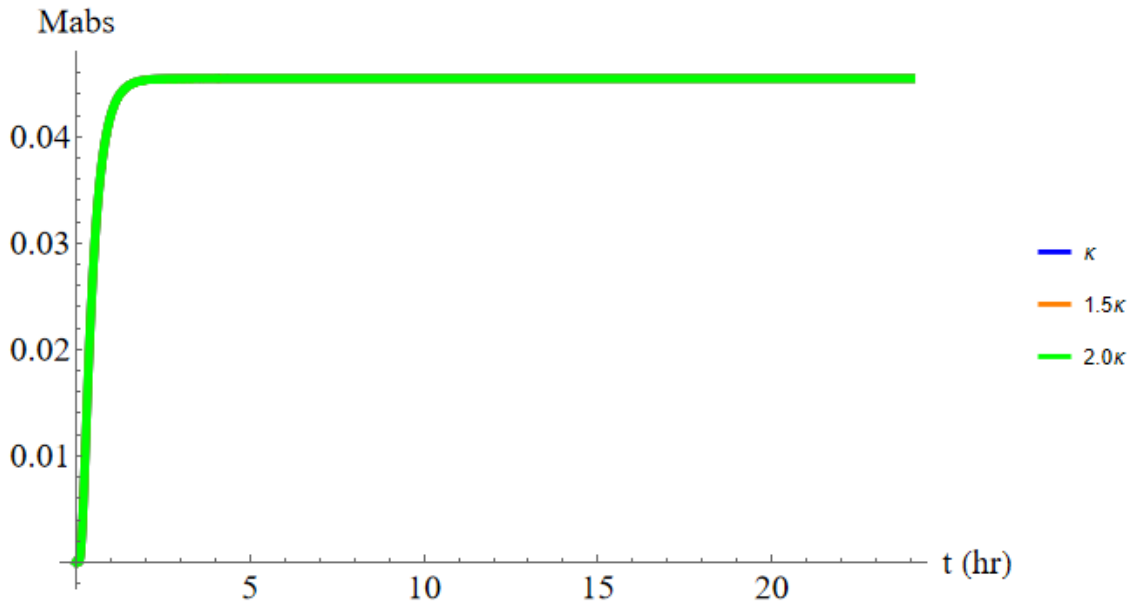
Figure A.74 Graphical representation of the effect of the ratio κ for the absorption profile using phosgene as a reference compound.
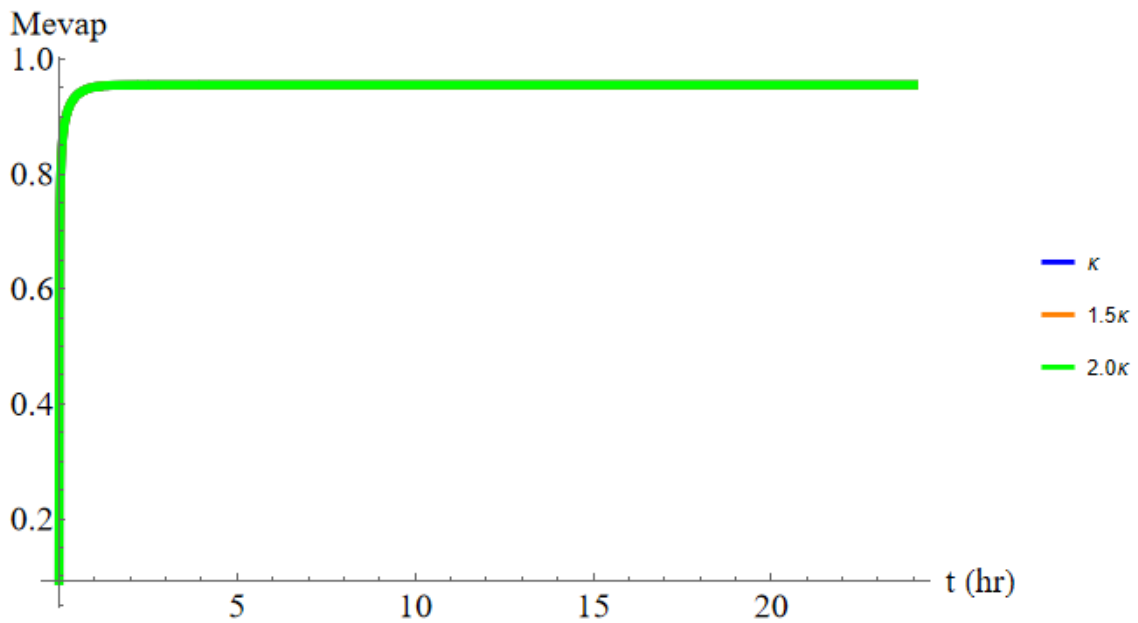
Figure A.75 Graphical representation of the effect of the ratio κ for the evaporation profile using phosgene as a reference compound.
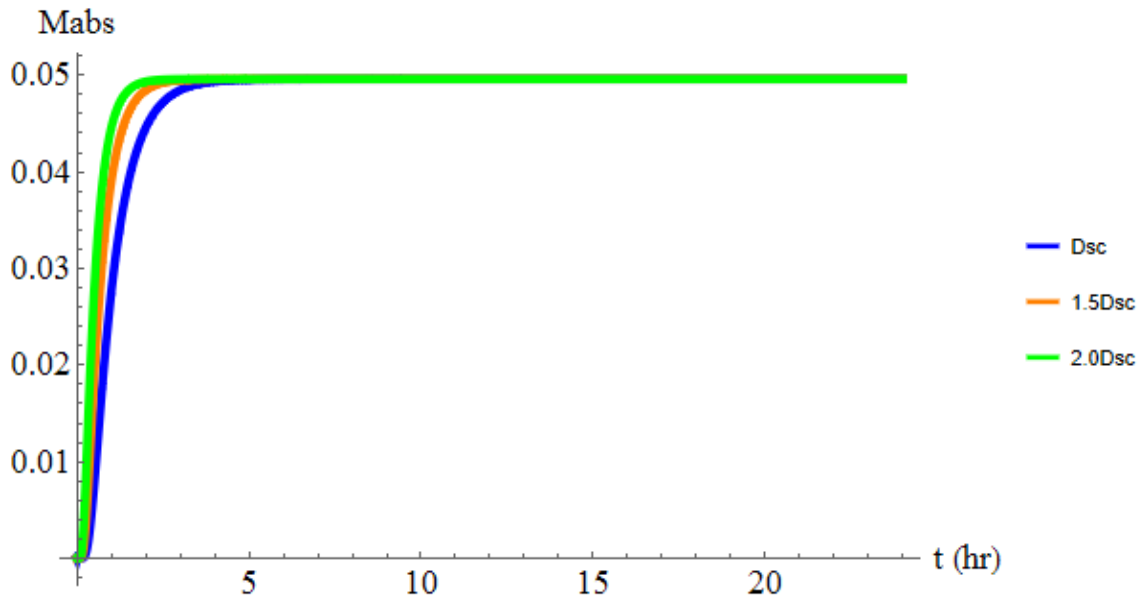
Figure A.76 Graphical representation of the effect of the diffusion coefficient for the absorption profile using sulfur mustard as a reference compound.
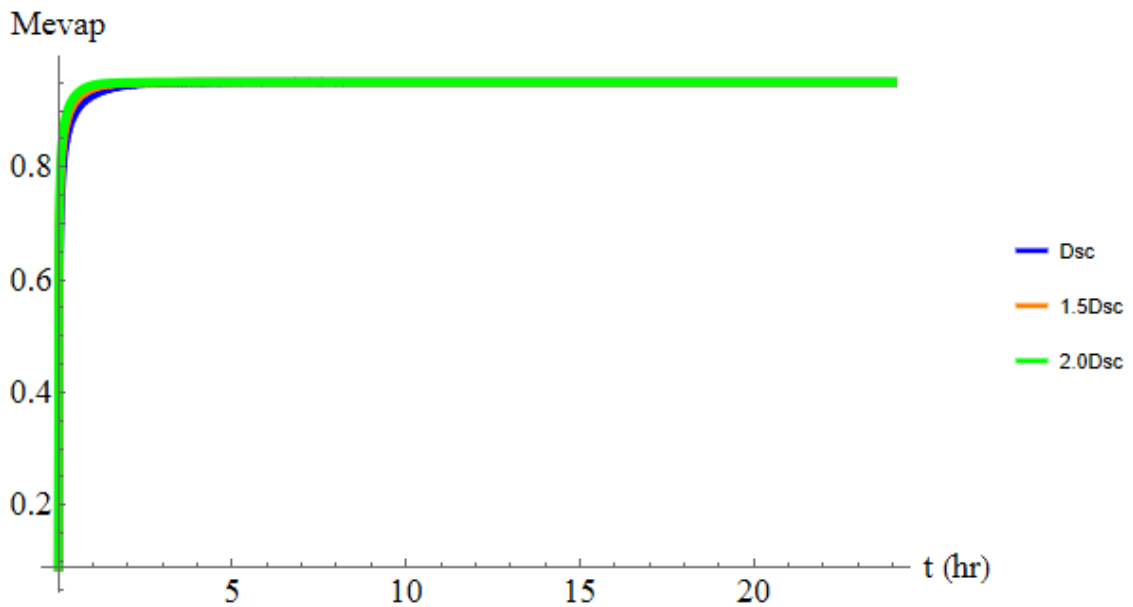
Figure A.77 Graphical representation of the effect of the diffusion coefficient for the evaporation profile using sulfur mustard as a reference compound.
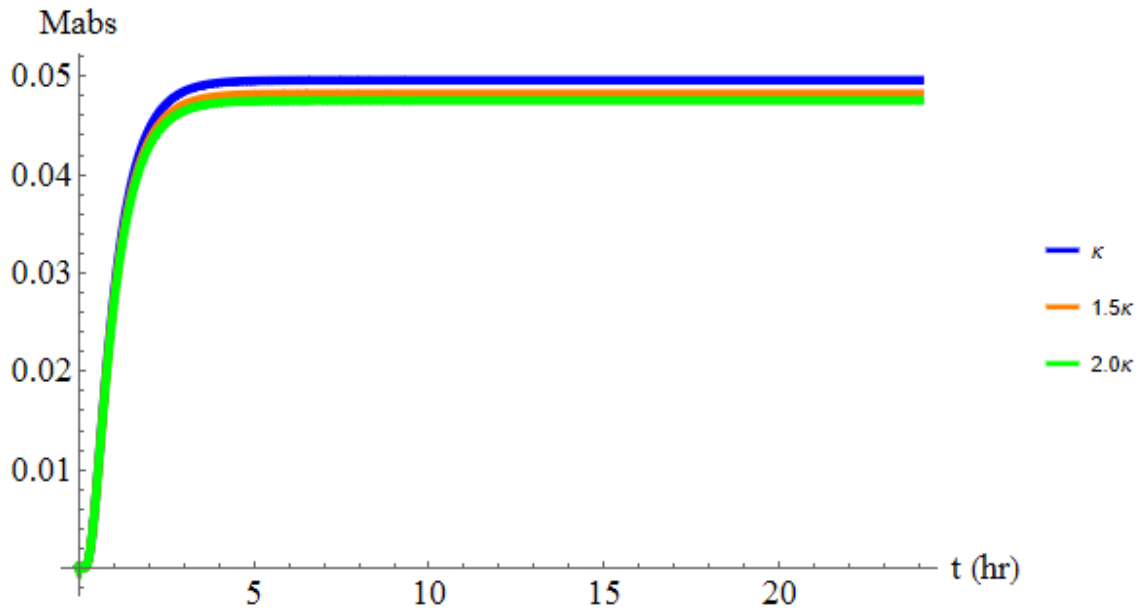
Figure A.78 Graphical representation of the effect of the ratio κ for the absorption profile using sulfur mustard as a reference compound.
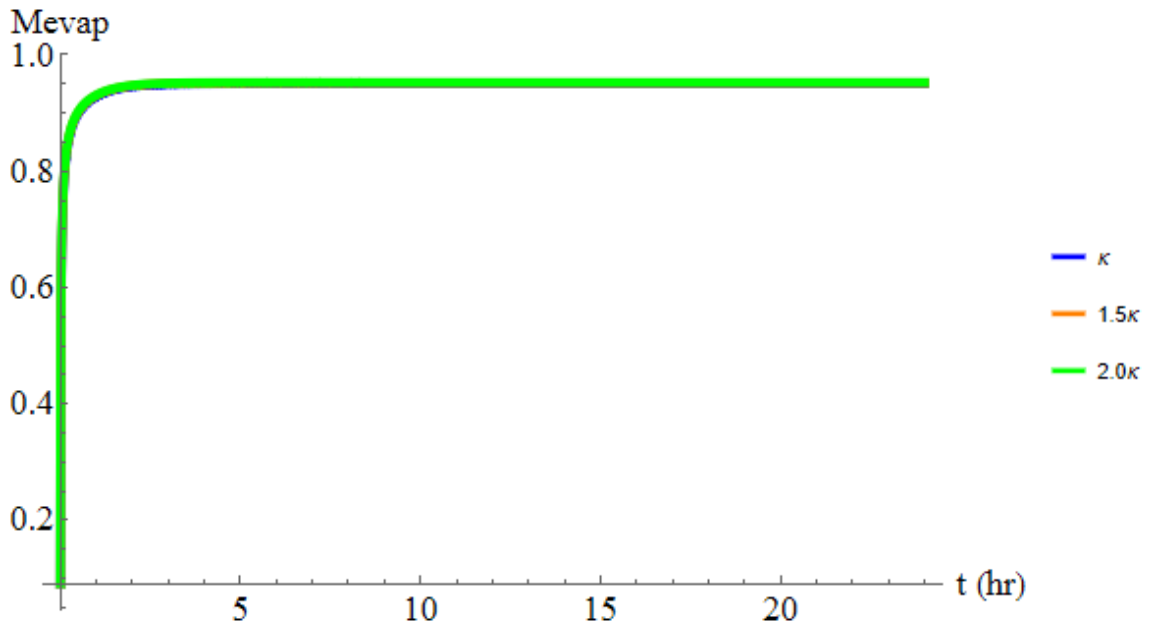
Figure A.79 Graphical representation of the effect of the ratio κ for the evaporation profile using sulfur mustard as a reference compound.

Small Dose Parameter Sensitivity:
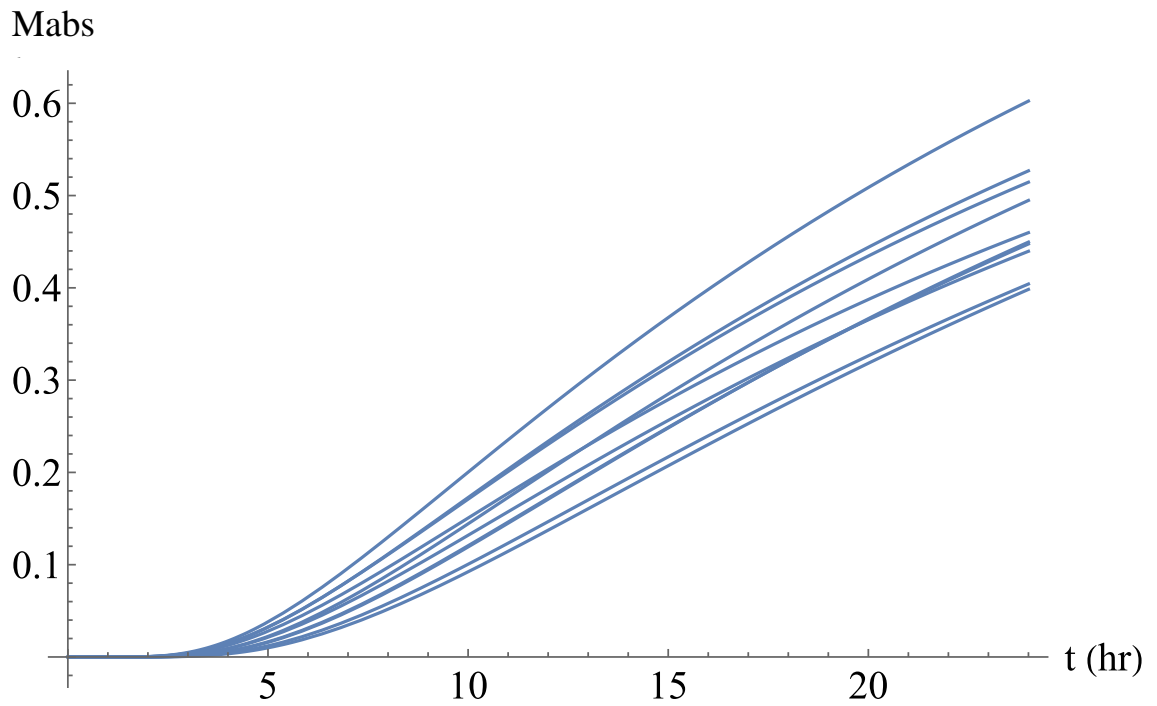
Figure A.80 Effects of random changes on the cumulative amount of 3-quinuclidinyl benzilate absorbed – small doses.
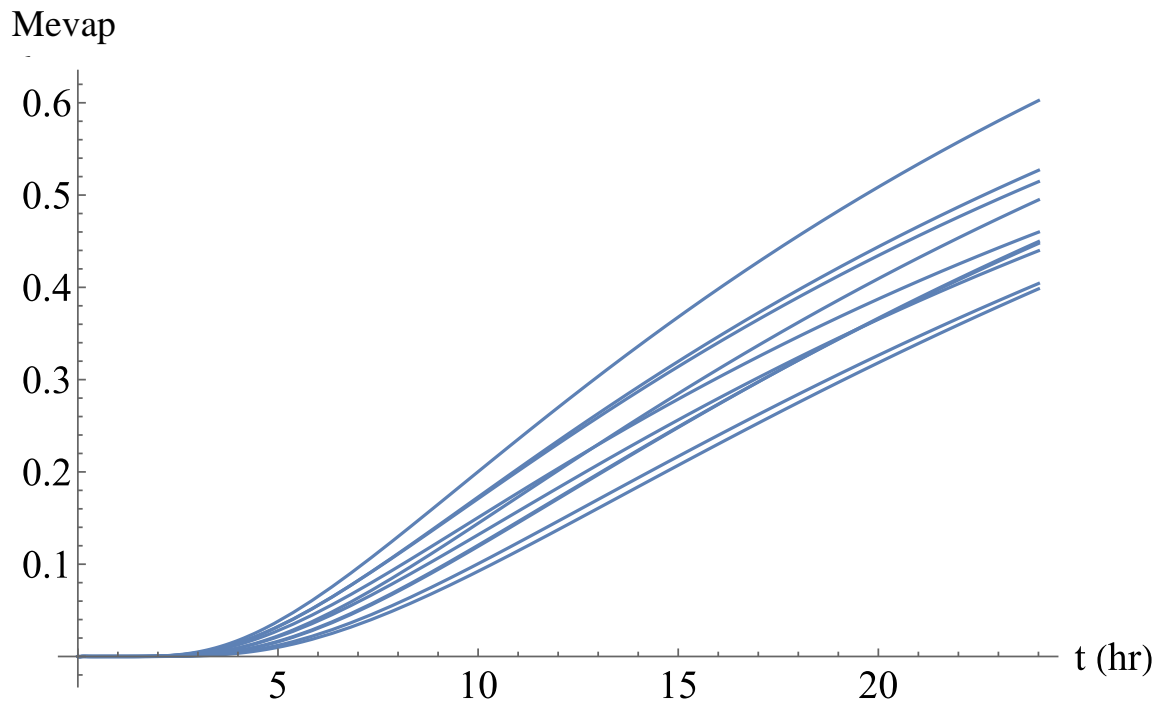
Figure A.81 Effects of random changes on the cumulative amount of 3-quinuclidinyl benzilate evaporated – small doses.
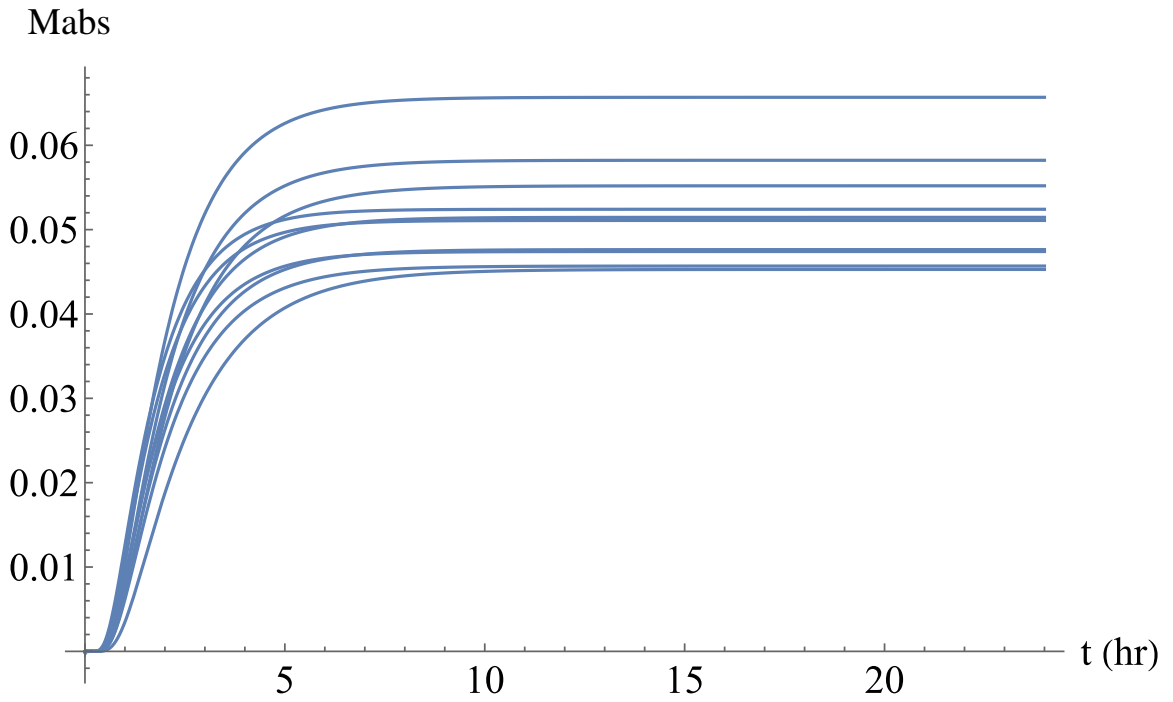
Figure A.82 Effects of random changes on the cumulative amount of ethyl iodoacetate absorbed – small doses.
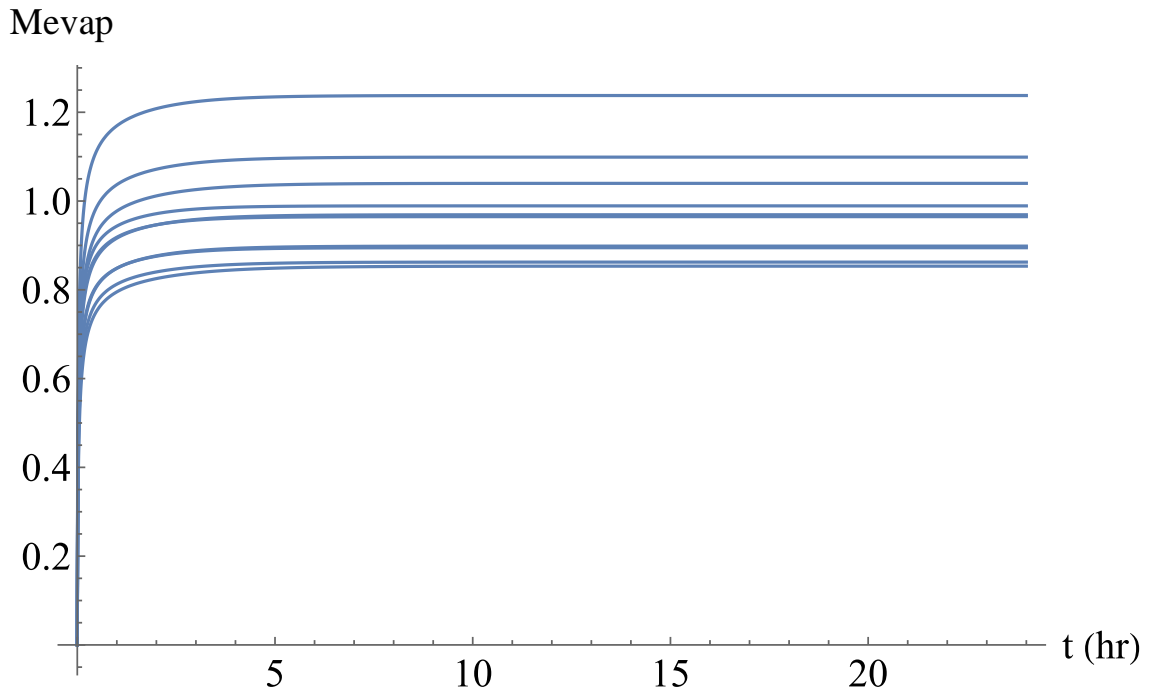
Figure A.83 Effects of random changes on the cumulative amount of ethyl iodoacetate evaporated–small doses.
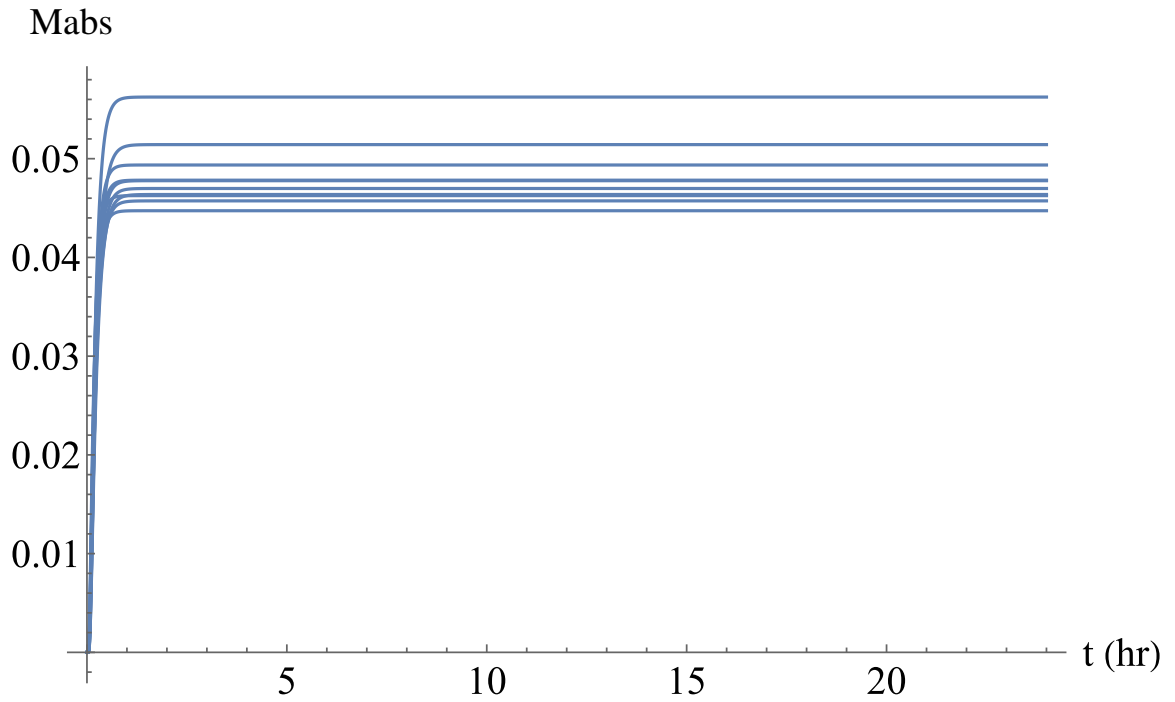
Figure A.84 Effects of random changes on the cumulative amount of hydrogen sulfide absorbed–small doses.
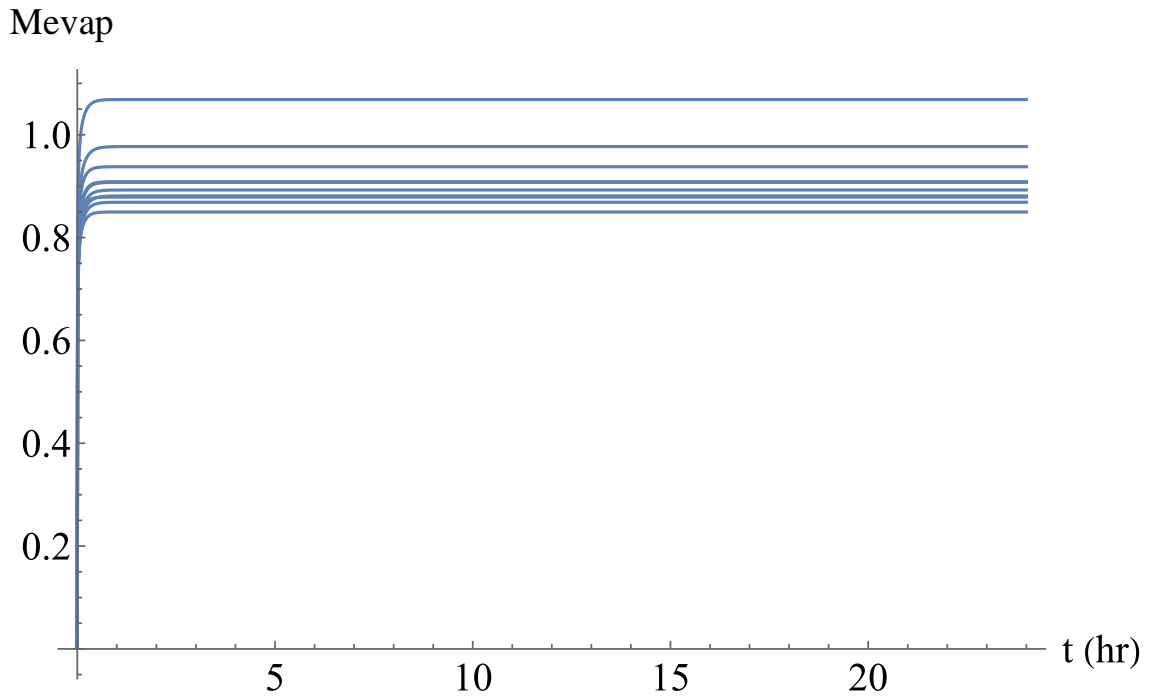
Figure A.85 Effects of random changes on the cumulative amount of hydrogen sulfide evaporated–small doses.
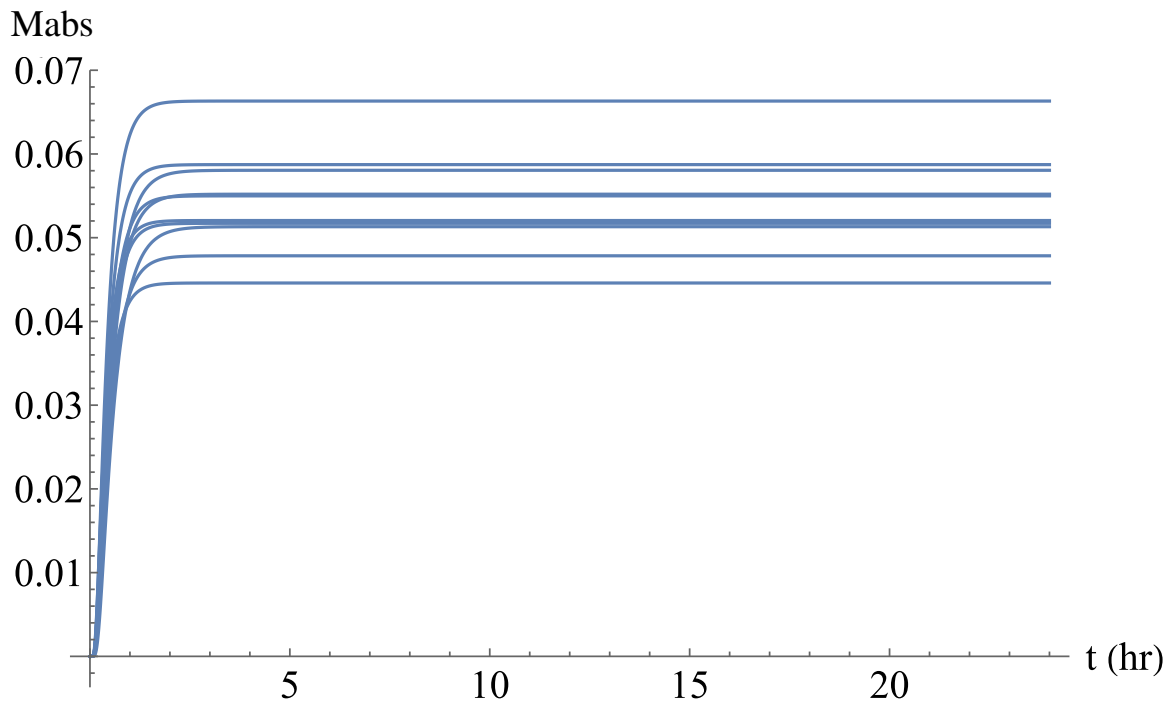
Figure A.86 Effects of random changes on the cumulative amount of phosgene absorbed–small doses.
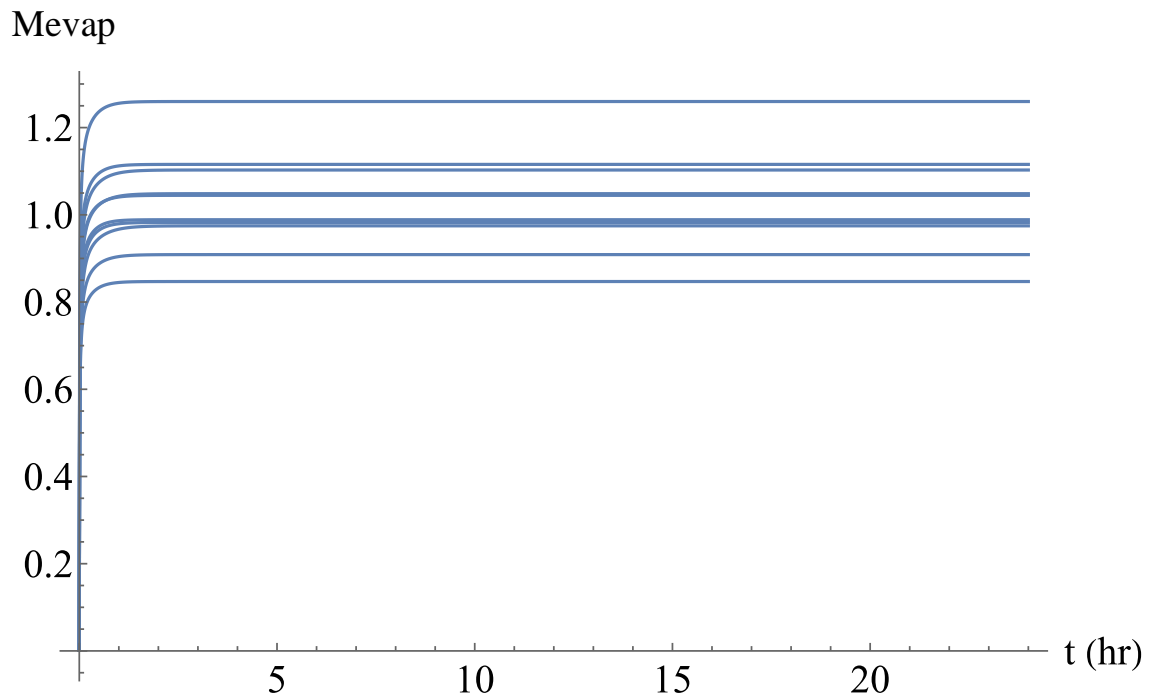
Figure A.87 Effects of random changes on the cumulative amount of phosgene evaporated–small doses.
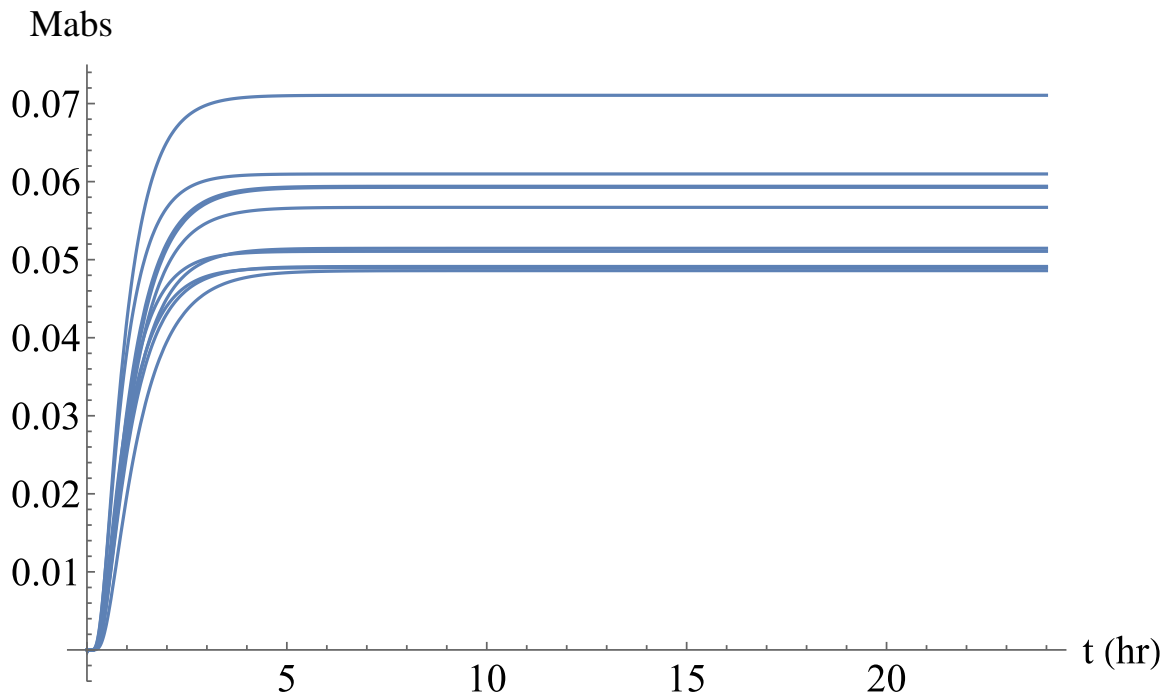
Figure A.88 Effects of random changes on the cumulative amount of sulfur mustard absorbed–small doses.
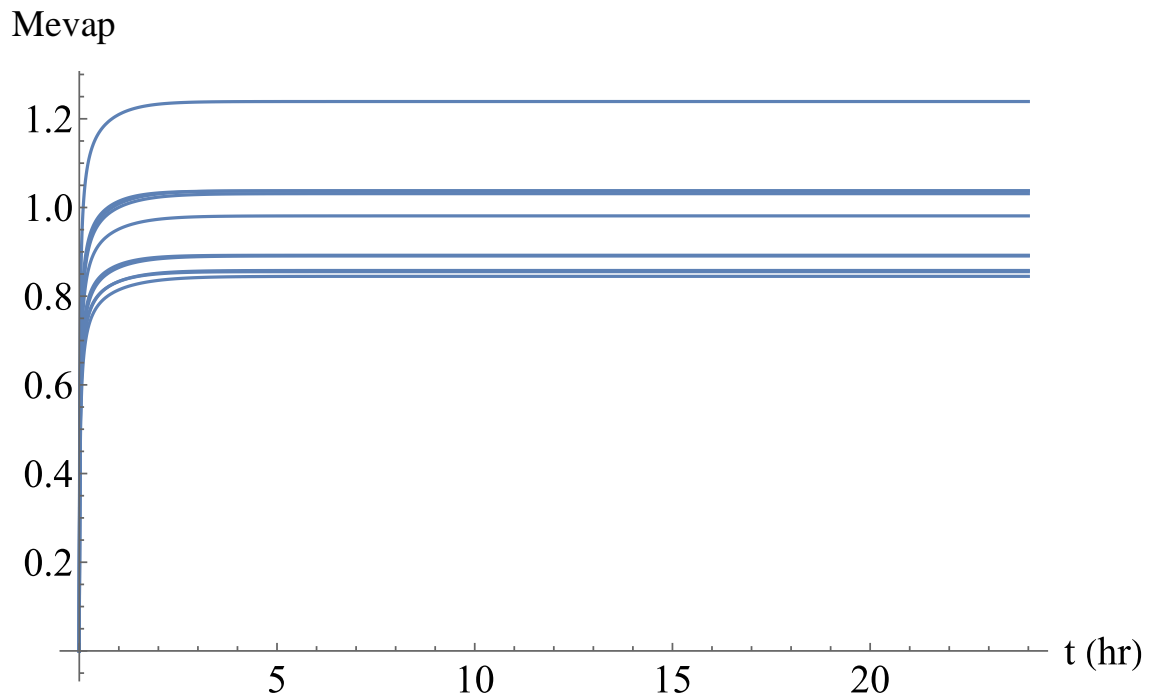
Figure A.89 Effects of random changes on the cumulative amount of sulfur mustard evaporated–small doses.

Large Dose Parameter Sensitivity:
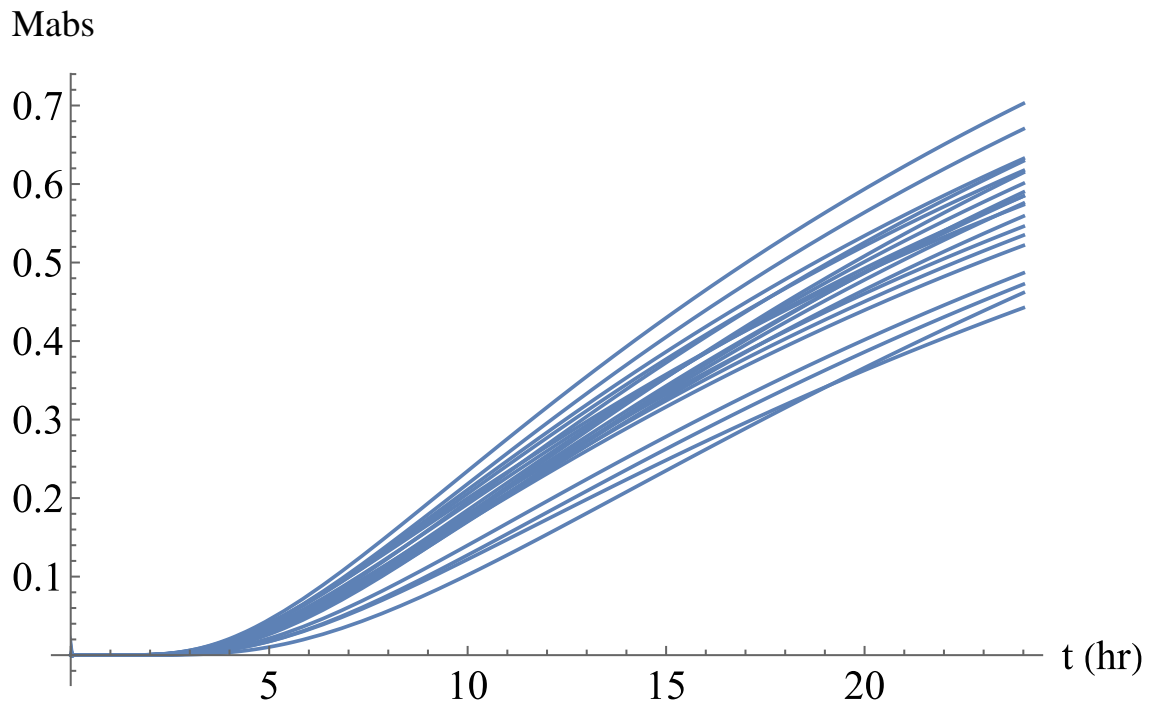
Figure A.90 Effects of random changes on the cumulative amount of 3-quinuclidinyl benzilate absorbed – large doses.
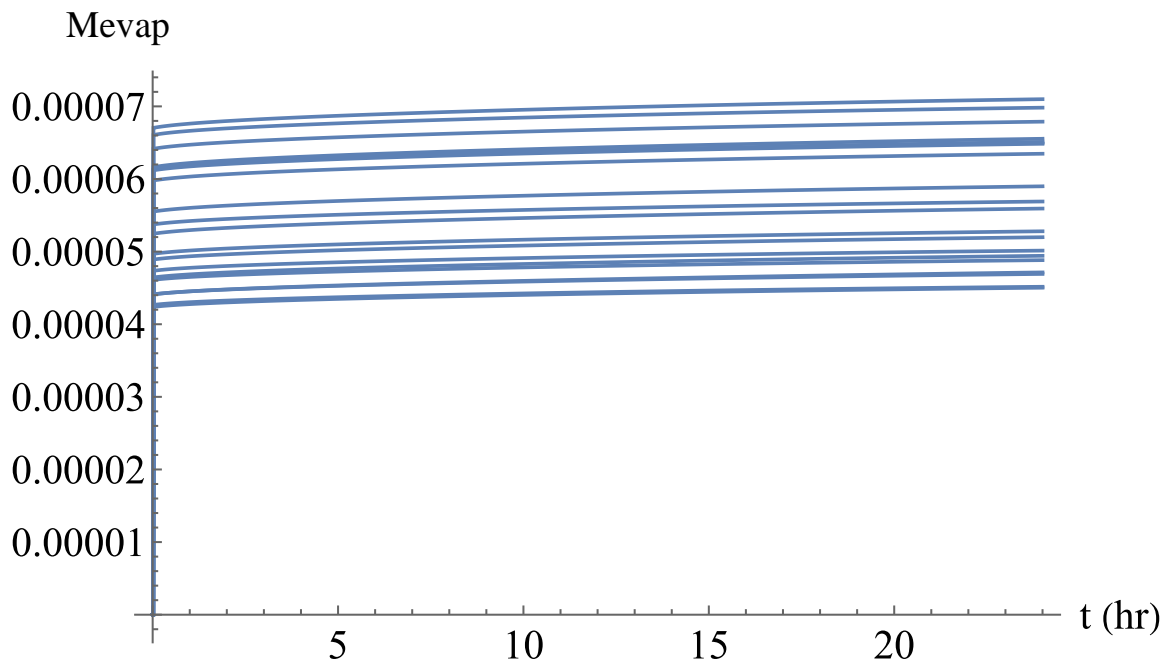
Figure A.91 Effects of random changes on the cumulative amount of 3-quinuclidinyl benzilate evaporated – large doses.
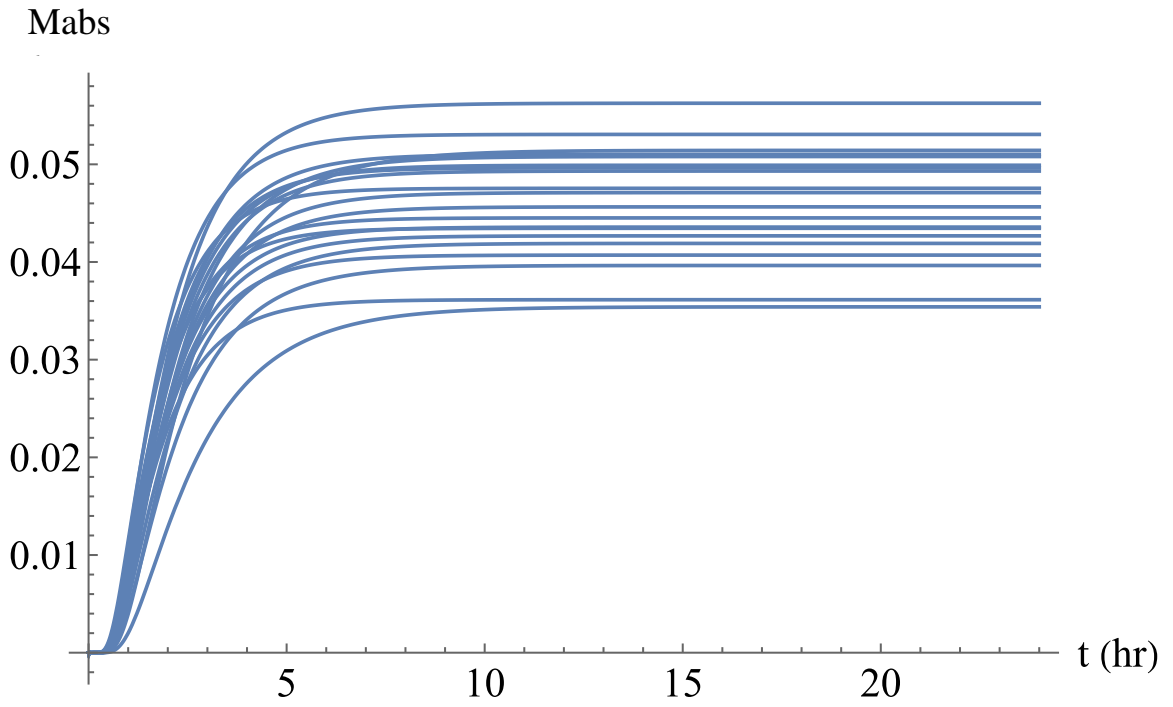
Figure A.92 Effects of random changes on the cumulative amount of ethyl iodoacetate absorbed – large doses.
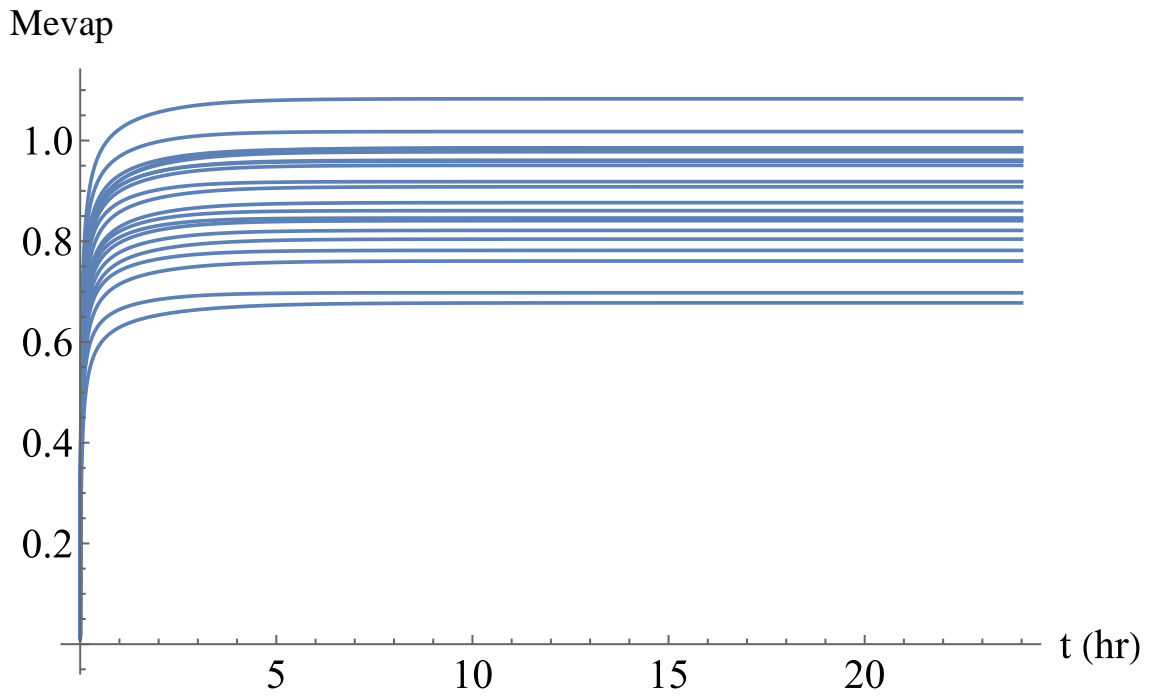
Figure A.93 Effects of random changes on the cumulative amount of ethyl iodoacetate evaporated – large doses.
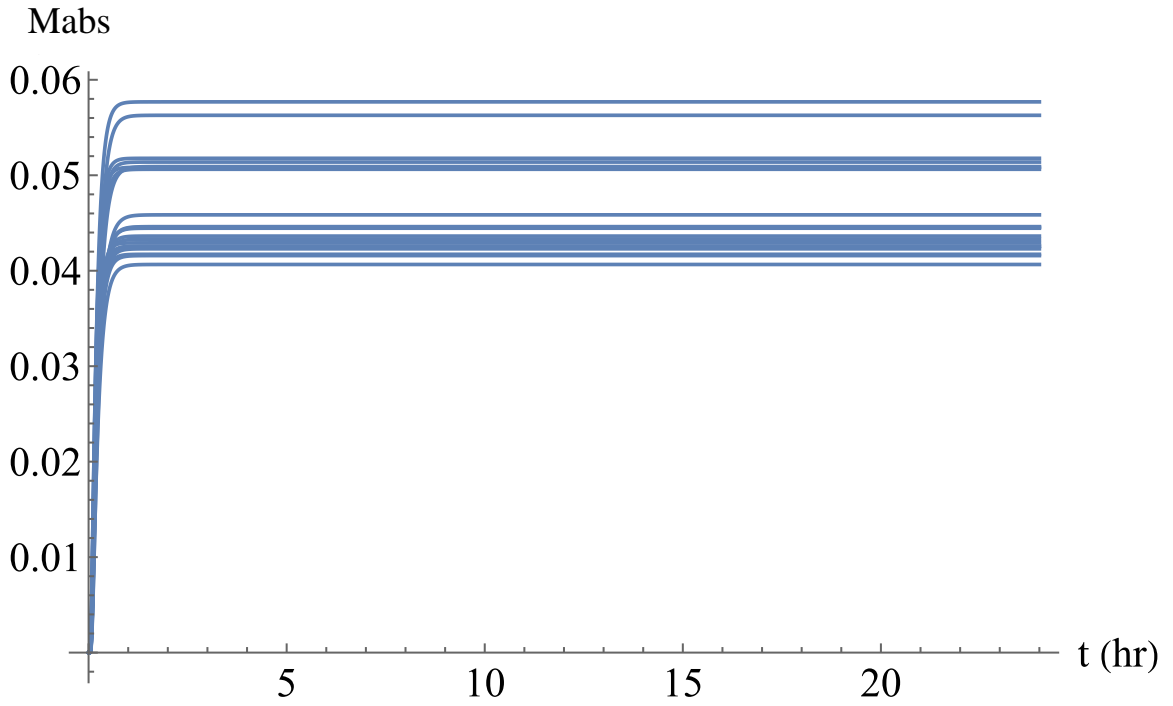
Figure A.94 Effects of random changes on the cumulative amount of hydrogen sulfide absorbed – large doses.
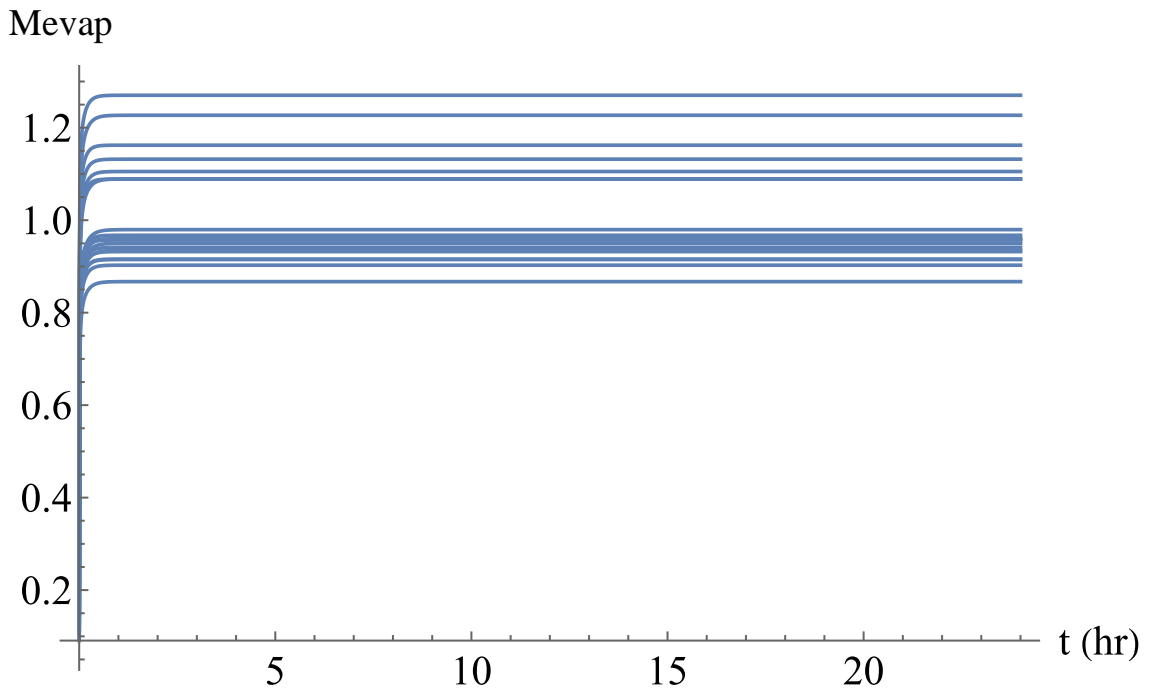
Figure A.95 Effects of random changes on the cumulative amount of hydrogen sulfide evaporated – large doses.
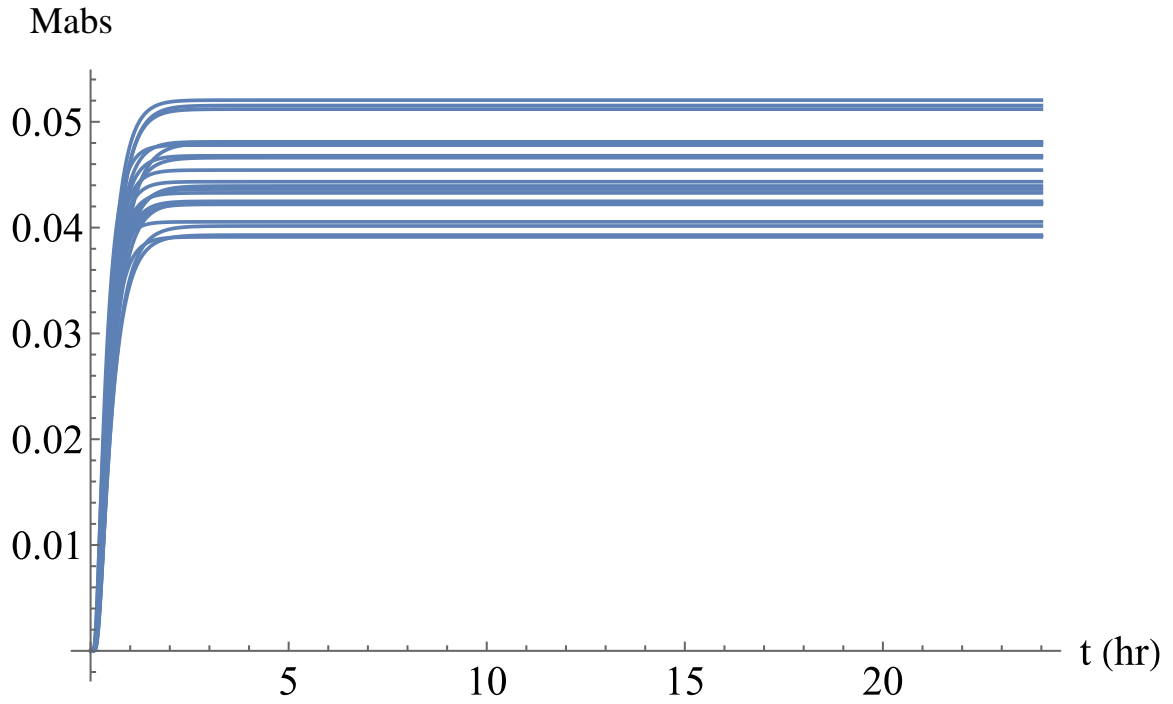
Figure A.96 Effects of random changes on the cumulative amount of phosgene absorbed – large doses.
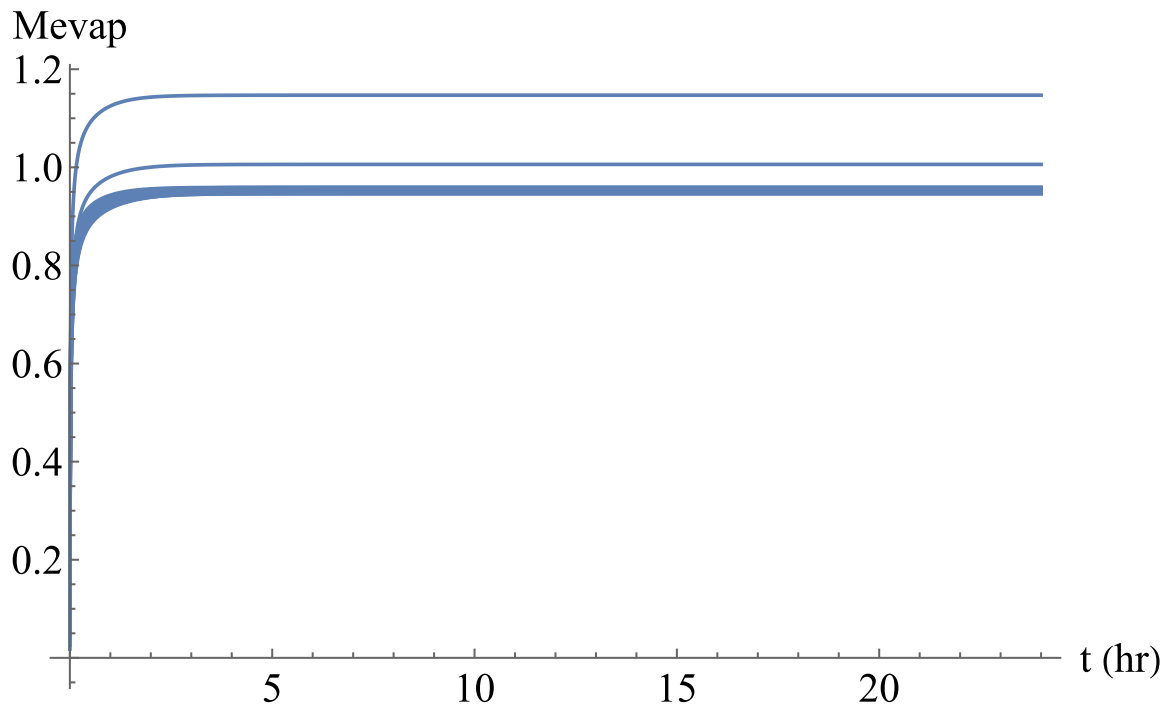
Figure A.97 Effects of random changes on the cumulative amount of phosgene evaporated – large doses.
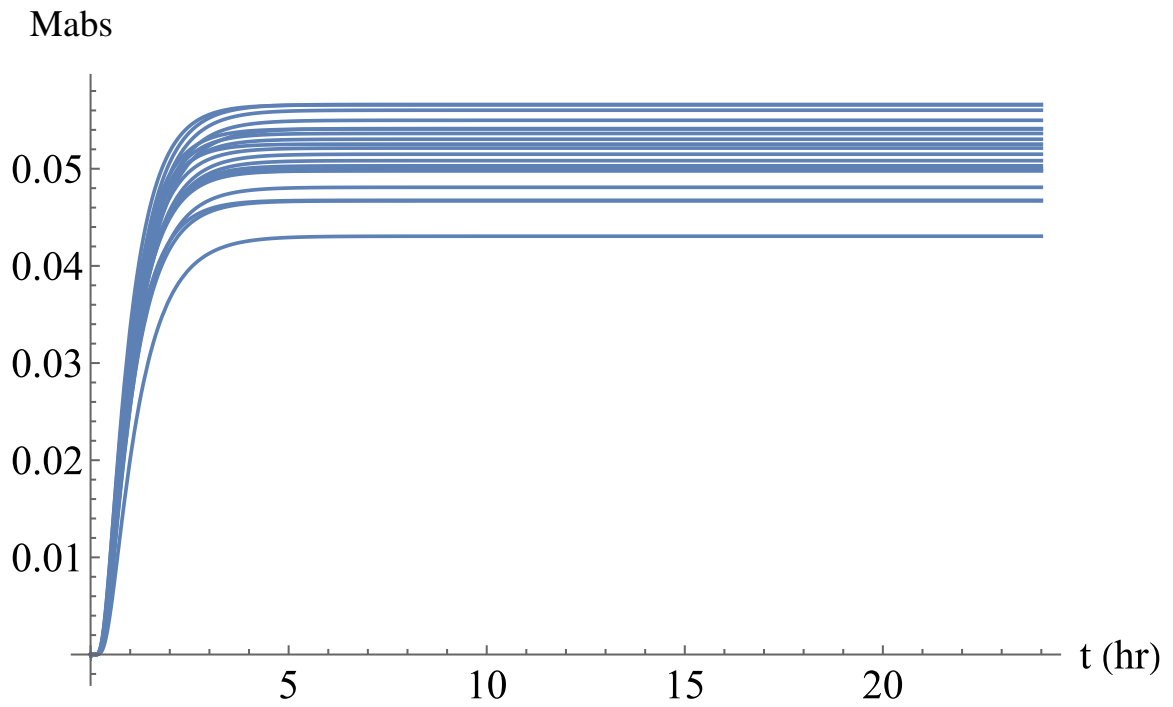
Figure A.98 Effects of random changes on the cumulative amount of sulfur mustard absorbed – large doses.
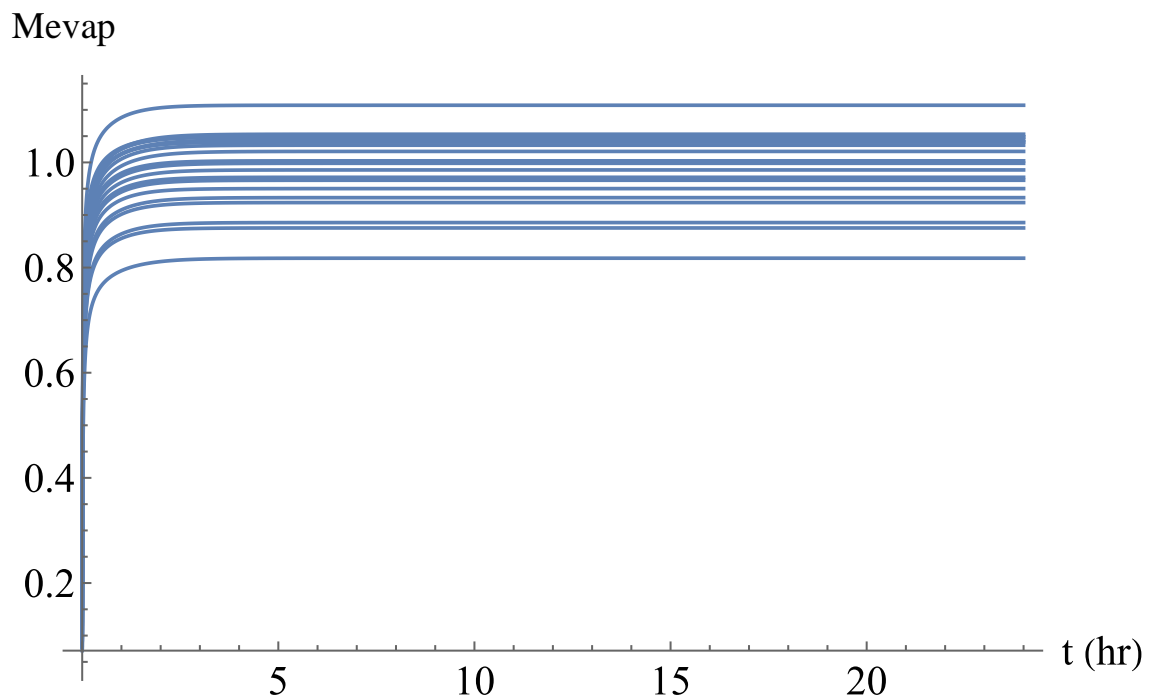
Figure A.99 Effects of random changes on the cumulative amount of sulfur mustard evaporated – large doses.
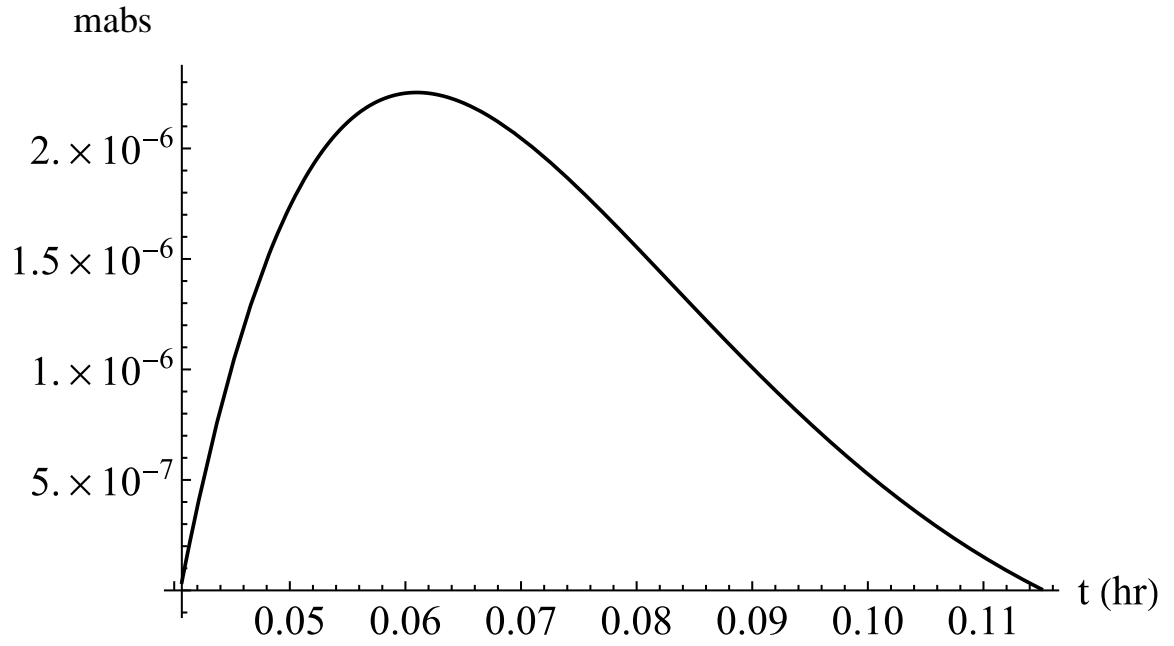
Figure A.100 The cumulative amount of VX absorbed when the dermal OEL limit has been exceeded.

REFERENCES

Alkilani, A. Z., McCrudden, M. T. C., & Donnelly, R. F. (2015). Transdermal Drug Delivery: Innovative Pharmaceutical Developments Based on Disruption of the Barrier Properties of the stratum corneum. *Pharmaceutics*, *7*(4), 438-470. https://doi.org/10.3390/pharmaceutics7040438

Andrews, S. N., Jeong, E., & Prausnitz, M. R. (2013). Transdermal delivery of molecules is limited by full epidermis, not just stratum corneum. *Pharmaceutical research*, *30*(4), 1099-1109. https://doi.org/10.1007/s11095-012-0946-7

Bakshi, K. S., Pang, S. N., & Snyder, R. (2000). Review of the US Army's health risk assessments for oral exposure to six chemical-warfare agents. *Review of the US Army's health risk assessments for oral exposure to six chemical-warfare agents.*, *59*(5/6).

Black, R. (2016). Development, historical use and properties of chemical warfare agents.

Blank, I. H. (1952). Factors Which Influence the Water Content of the Stratum Corneum. *Journal of Investigative Dermatology*, *18*(6), 433-440. https://doi.org/https://doi.org/10.1038/jid.1952.52

Boderke, P., Schittkowski, K., Wolf, M., & Merkle, H. P. (2000). Modeling of diffusion and concurrent metabolism in cutaneous tissue. *Journal of Theoretical Biology*, *204*(3), 393-407.

Boireau-Adamezyk, E., Baillet-Guffroy, A., & Stamatas, G. (2014). Age-dependent changes in stratum corneum barrier function. *Skin Research and Technology*, *20*(4), 409-415.

Cao, Y., Elmahdy, A., Zhu, H., Hui, X., & Maibach, H. I. (2020). Binding Affinity and Decontamination of Dermal Decontamination Gel (DDGel) to Model Chemical Warfare Agent (CWA) Simulants. In *Skin Decontamination* (pp. 163-181). Springer.

Capoun, T., & Krykorkova, J. (2019). Study of Decomposition of Chemical Warfare Agents using Solid Decontamination Substances. *Toxics*, *7*(4), 63. https://doi.org/10.3390/toxics7040063

Chauhan, S., D'cruz, R., Faruqi, S., Singh, K., Varma, S., Singh, M., & Karthik, V. (2008). Chemical warfare agents. *Environmental Toxicology and Pharmacology*, *26*(2), 113-122.

Colchicine. (2015). https://static.cymitquimica.com/products/45/pdf/sds-1146006.pdf

Coleman, K. (2005). Historical Precedents? In *A History of Chemical Warfare* (pp. 1-10). Springer.

Council, N. R. (2003). Acute Exposure Guideline Levels for Selected Airborne Chemicals: Volume 3.

Couto, A., Fernandes, R., Cordeiro, M. N. S., Reis, S. S., Ribeiro, R. T., & Pessoa, A. M. (2014). Dermic diffusion and stratum corneum: a state of the art review of mathematical models. *Journal of Controlled Release*, *177*, 74-83.

Dancik, Y., Miller Ma Fau - Jaworska, J., Jaworska J Fau - Kasting, G. B., & Kasting, G. B. Design and performance of a spreadsheet-based model for estimating bioavailability of chemicals from dermal exposure. (1872-8294 (Electronic)).

Denda, M., Sato, J., Masuda, Y., Tsuchiya, T., Koyama, J., Kuramoto, M., Elias, P. M., & Feingold, K. R. (1998). Exposure to a Dry Environment Enhances Epidermal Permeability Barrier Function. *Journal of Investigative Dermatology*, *111*(5), 858-863. https://doi.org/https://doi.org/10.1046/j.1523-1747.1998.00333.x

Frasch, H. (2012). Dermal absorption of finite doses of volatile compounds. *Journal of pharmaceutical sciences*, *101 7*, 2616-2619.

Frasch, H. F. (2012). Dermal absorption of finite doses of volatile compounds. *Journal of pharmaceutical sciences*, *101*(7), 2616-2619.

Frasch, H. F., & Bunge, A. L. (2015). The transient dermal exposure II: post-exposure absorption and evaporation of volatile compounds. *Journal of pharmaceutical sciences*, *104*(4), 1499-1507.

Freemantle, M. (2015). *The Chemists' War: 1914-1918*. Royal Society of Chemistry.

Ganesan, K., Raza, S., & Vijayaraghavan, R. (2010). Chemical warfare agents. *Journal of pharmacy and bioallied sciences*, *2*(3), 166.

Ganesan, K., Raza, S. K., & Vijayaraghavan, R. (2010). Chemical warfare agents. *J Pharm Bioallied Sci*, *2*(3), 166-178. https://doi.org/10.4103/0975-7406.68498

Geankoplis, C. J. (2018). *Transport processes and separation process principles* (Fifth edition. ed.). Prentice Hall.

Gorzelanny, C., Mess, C., Schneider, S. W., Huck, V., & Brandner, J. M. (2020). Skin barriers in dermal drug delivery: Which barriers have to be overcome and how can we measure them? *Pharmaceutics*, *12*(7), 684.

Goswami, D. G., Agarwal, R., & Tewari-Singh, N. (2018). Phosgene oxime: Injury and associated mechanisms compared to vesicating agents sulfur mustard and lewisite. *Toxicol Lett*, *293*, 112-119. https://doi.org/10.1016/j.toxlet.2017.11.011

Hilmas, E., & Hilmas, C. J. (2009). CHAPTER 61 - Medical Management of Chemical Toxicity in Pediatrics. In R. C. Gupta (Ed.), *Handbook of Toxicology of Chemical Warfare Agents* (pp. 919-950). Academic Press. https://doi.org/https://doi.org/10.1016/B978-012374484-5.00061-4

Janik, E., Ceremuga, M., Saluk-Bijak, J., & Bijak, M. (2019). Biological Toxins as the Potential Tools for Bioterrorism. *International journal of molecular sciences*, *20*(5), 1181. https://doi.org/10.3390/ijms20051181

Kasting, G. B., & Miller, M. A. (2006). Kinetics of finite dose absorption through skin 2: volatile compounds. *Journal of pharmaceutical sciences*, *95*(2), 268-280.

Kasting, G. B., Miller, M. A., & Bhatt, V. D. (2008). A spreadsheet-based method for estimating the skin disposition of volatile compounds: application to N,N-diethyl-m-toluamide (DEET). *J Occup Environ Hyg*, *5*(10), 633-644. https://doi.org/10.1080/15459620802304245

Keil, C. B. C. C. E. A. T. R. e. (2009). *Mathematical models for estimating occupational exposure to chemicals*.

Kydonieus, A. F. (2017). *Treatise on controlled drug delivery: fundamentals-optimization-applications*. CRC Press.

Lee, J. Y., Choi Jw Fau - Kim, H., & Kim, H. (2007). Determination of hand surface area by sex and body shape using alginate. (1880-6791 (Print)).

Moshiri, M., Darchini-Maragheh, E., & Balali-Mood, M. (2012). Advances in toxicology and medical treatment of chemical warfare nerve agents. *Daru : journal of Faculty of Pharmacy, Tehran University of Medical Sciences*, *20*(1), 81-81. https://doi.org/10.1186/2008-2231-20-81

Mueller, A. (2017). *Biomimetic Nanotechnology*. De Gruyter.

Tojo, K. (1987). Mathematical modeling of transdermal drug delivery. *Journal of chemical engineering of Japan*, *20*(3), 300-308.

van Smeden, J., & Bouwstra, J. A. (2016). Stratum Corneum Lipids: Their Role for the Skin Barrier Function in Healthy Subjects and Atopic Dermatitis Patients. *Curr Probl Dermatol*, *49*, 8-26. https://doi.org/10.1159/000441540

Wartell, M. A., Kleinman, M. T., Huey, B. M., & Duffy, L. M. (1999). Strategies to protect the health of deployed US forces: force protection and decontamination.

Wexler, P., & Anderson, B. D. (2005). *Encyclopedia of toxicology* (2nd ed.). Elsevier. Book review (E-STREAMS) http://www.e-streams.com/es0911/es0911_4525.html

Publisher description
http://www.loc.gov/catdir/enhancements/fy0726/2005920934-d.html

Wexler, P., & Anderson, B. D. (2014). *Encyclopedia of toxicology* (Third edition. ed.). Elsevier/AP, Academic Press is an imprint of Elsevier.

Ye, W., Pan, Y., He, L., Chen, B., Liu, J., Gao, J., Wang, Y., & Yang, Y. (2021). Chapter 3 - Design with modeling techniques. In H. D. Goodfellow & Y. Wang (Eds.), *Industrial Ventilation Design Guidebook (Second Edition)* (pp. 109-183). Academic Press. https://doi.org/https://doi.org/10.1016/B978-0-12-816673-4.00008-0